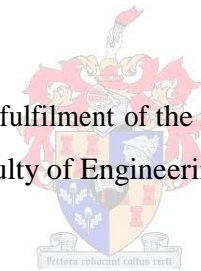# Validation of Computational Fluid Dynamics Model of a simple pump sump with vertical intake

by

Mark Mathew Hoppe

Thesis presented in partial fulfilment of the requirements for the degree

Master of Science in the Faculty of Engineering at Stellenbosch University

Supervisor: Mr Wageed Kamish

Faculty of Engineering

April 2014

DECLARATION

By submitting this thesis electronically, I declare that the entirety of the work contained therein is my own, original work, that I am the sole author thereof (save to the extent explicitly otherwise stated), that reproduction and publication thereof by Stellenbosch University will not infringe any third party rights and that I have not previously in its entirety or in part submitted it for obtaining any qualification.

_____   _____

Mark Mathew Hoppe   Date

SYNOPSIS

The designs of pump intake structures are generally verified by means of a hydraulic model study to ensure the structure will operate without large air or swirl entraining vortices. This is an expensive and time consuming process. The popularity of Computational Fluid Dynamics (CFD) is ever increasing in the engineering world and the use thereof in the modelling of flows in pump intake structures is just one of the many areas of focus. The use of a validated CFD model in the design phase of pump intakes would be beneficial, and ideally would reduce the frequency of requiring hydraulic model studies.

This study investigates the applicability of using a 3 dimensional CFD model as a design tool by validation with a physical model. A physical model of a simple pump intake was available and with a few modifications the flow conditions were significantly improved. The quantitative validation of the CFD model was carried out by means of comparing corresponding point velocity magnitudes. An Acoustic Doppler Velocimeter (ADV) was used in the physical model. The data obtained were successfully filtered to remove noise and other disturbances. The qualitative validation was done by means of photographs and observations. The photographs made use of illuminated tracer particles to identify flow patterns.

The CFD model compares well qualitatively, but the velocity magnitudes are not yet sufficiently reliable. It is recommended that the CFD model can be used for qualitative studies, but future research should focus on the accuracy of the CFD model. Using higher resolution velocity measurements in the physical model by means of other types of instruments, a better comparison can be made, as well as enabling validation of the ADV readings.

SINOPSIS (AFRIKAANS)

Die ontwerpe van die pomp inname strukture word gewoonlik bevestig deur middel van 'n hidrouliese model studie om lug-intrekking te minimeer. Dit is 'n duur en tydrowende proses . Die gebruik van Computational Fluid Dynamics (CFD), 'n tipe numeriese modelle neem toe in die ingenieurswese wêreld. Die gebruik daarvan in die modellering van vloei in pomp inname strukture is net een van die vele areas van toepassing . Die gebruik van 'n betroubare CFD model in die ontwerp fase van pomp innames sal voordelig wees , en ideaal sou die noodaaklikheid van fisiese hidrouliese model studies verminder.

Hierdie studie ondersoek die toepaslikheid van die gebruik van 'n 3 -dimensionele model CFD model as 'n ontwerp instrument deur bevestiging met 'n fisiese model . 'n Eenvoudige pomp-inname model was beskikbaar en het met 'n paar veranderinge die vloei toestande aansienlik verbeter . Die kwantitatiewe bevestiging van die CFD model is uitgevoer deur middel van vergelyking van korresponderende punt snelheid groottes. In die fisiese model is die snelhede met 'n Akoestiese Doppler Velocimeter (ADV) gemeet. Die data wat verkry is suksesvol gefiltreer om geraas en ander versteurings te verwyder . Die kwalitatiewe bevestiging is gedoen deur middel van foto's en waarnemings. In die foto's is gebruik gemaak van verligte spoor deeltjies om vloei patrone te identifiseer.

Die CFD model vergelyk kwalitatief goed, maar die snelheid groottes is nog nie voldoende betroubaar nie. Dit word aanbeveel dat die CFD model gebruik kan word vir kwalitatiewe studies, maar toekomstige navorsing behoort te fokus op die verbeteringe van dieakkuraatheid van die CFD model. Met behulp van 'n hoër resolusie snelheid metings van die fisiese model, deur middel van ander tipe instrumente, kan 'n beter vergelyking gemaak word , sowel as die geldigheid van die ADV lesings in staat te stel.

ACKNOWLEDGEMENTS

Table of Contents

LIST OF FIGURES

LIST OF TABLES

LIST OF ABBREVIATIONS

ADV	-	Acoustic Doppler Velocimeter
CFD	-	Computational Fluid Dynamics
FVM	-	Finite Volume Method
GRP	-	Glass Reinforced Plastics
LDA	-	Laser Doppler Anemometry
LDV	-	Laser Doppler Velocimetry
LED	-	Light Emitting Diode
LES	-	Large Eddy Study
LLS	-	Laser Light Sheet
OEM	-	Original Equipment Manufacturer
PISO	-	Pressure-Implicit Split-Operator
PIV	-	Particle Image Velocimetry
RANS	-	Reynolds Averaged Navier-Stokes
SNR	-	Signal-to-Noise Ratio
VOF	-	Volume of Fluid
VSD	-	Variable Speed Drive

LIST OF SYMBOLS

Symbols defined as below unless otherwise stated in the text.

a	-	Minor axis of ellipse	[m]
D	-	Bell mouth diameter	[m]
d	-	Suction pipe diameter	[m]
d_m	-	Model suction pipe diameter	[m]
d_p	-	Prototype suction pipe diameter	[m]
Fr	-	Froude number	-
Fr_m	-	Model Froude number	-
Fr_p	-	Prototype Froude number	-
g	-	Gravitational acceleration	$[m/s^2]$
h_{cr}	-	Level of critical submergence	[m]
k	-	Turbulent kinetic energy	$[m^2/s^2]$
Q_{air}	-	Volume flow of air	$[m^3/s]$
r	-	Radius of rounding of bell mouth entry	[m]
Re	-	Reynolds number	-
V	-	Velocity magnitude	[m/s]
V_{CFD}	-	Velocity magnitude calculated by CFD model	[m/s]
V_D	-	Velocity magnitude in bell mouth throat	[m/s]
V_m	-	Velocity magnitude in model	[m/s]
VMAC	-	Velocity Magnitude calculated from Averaged Components	[m/s]
VMAM	-	Velocity Magnitude calculated from individual Magnitudes	[m/s]
VOF_{air}	-	Volume fraction of air	-
V_p	-	Velocity magnitude in prototype	[m/s]
$V_{Physical}$	-	Velocity magnitude measured in physical model	[m/s]
We	-	Weber number	-

x_i	-	value of the ith sample in the dataset	-
Z	-	Bell mouth elevation w.r.t. sump floor	[m]
Γ	-	Average circulation over the depth, D/2 from the centre line	[m^2/s]
ε	-	Turbulent dissipation	[m^2/s^3]
μ	-	Dynamic viscosity of fluid	[kg/m.s]
$μ_s$	-	Mean of sample (Statistical)	-
ρ	-	Mass density of fluid	[kg/m^3]
σ	-	Surface tension of fluid	[N/m]
$σ_s$	-	Standard deviation of sample (Statistical)	-

LIST OF PLATES

DVD ROM   -   Images, videos and diagrams as referenced in text

1. INTRODUCTION

1.1   Background Information

A brief background of pump intakes and Computational Fluid Dynamics (CFD) will be given below, with the aim of introducing the reader to the general topics on which this thesis will be focusing.

Pump Intakes

Pump intakes are used to provide us with drinking water, sewerage pumping, power generation systems, cooling systems for power stations, river abstraction works, etc. They form an integral part of modern civilizations. The continuous operation of these systems without interruption is of high importance. Therefore the design of these structures is critical and an efficient method for prediction of design performance is greatly sought after.

Pump intakes are generally classified in one of two classes, relating to installation size. Knauss (1987:4) states that concerning the flow rate, pump intakes in sumps are generally classified as small or medium size installations whereas intake structures are classified as large size installations. The work in this thesis focuses on a vertically upward suction pipe in a rectangular pump sump and is therefore more applicable to small and medium sized prototype installations. However, the use of the methods presented in this report would apply similarly to large scale installations with the exception of a smaller scale ratio required for the physical model. Knauss (1987:53) points out that the scale ratio should be limited to no less than 1 to 20 for a Froude scale model to produce prototype vortex formation.

The generally accepted method of pump sump design is by use of rule-of-thumb design guidelines and empirical relationships that were developed using generalised physical model studies. The designs of larger scale installations typically include physical model tests to ensure satisfactory performance in terms of, among other things, reduced vortex action and reduction of air and swirl entrainment. Smaller installations often rely on the abovementioned design guidelines because physical model studies are too costly and time consuming to be of economic value to the projects. Common practice to solve air entrainment problems is by increasing the intake submergence, although this can lead to costly oversized structures.

Computational Fluid Dynamics

Versteeg and Malalasekera (2007:1) introduce CFD as the use of computer-based simulation to solve systems that include fluid flow, heat transfer and associated phenomena. They also list several applications of CFD including:

- Aerodynamics of aircraft
- Hydrodynamics of ships
- Combustion processes
- Turbo machinery
- Chemical processes
- Marine engineering
- Environmental engineering
- Hydrology and oceanography
- Meteorology
- Biomedical engineering

The popularity of CFD in design and development in numerous engineering fields has been ever increasing since the 1980's. With the advances in computer technology and the affordability of high end systems that are capable of running large simulations, the user base has been ever expanding and smaller firms are now able to make use thereof.

The ability of CFD to model various scenarios with quick turn-around time and low costs makes it an ideal tool for all areas of design and development. It does however have certain drawbacks. Current CFD modelling of ships provides results that show the correct trends, however the values obtained are often unreliable and insufficient as the only source of information for power calculation and hydrodynamic forces, therefore empirical formulae or scale model tests are still required for final design considerations. The general trend with previous CFD modelling of pump intakes follows a similar line as for ships, it shows good flow patterns and trends, but it is not an absolute design package. It can be used for qualitative comparison of various designs, but a physical model is generally required for final validation.

The pump intakes or sumps are generally geometrically simple and often misleading as the flow patterns that arise are highly complex. The complexity of the flow adds to the difficulties that CFD has in modelling these two-phase flows.

A general background of pump sumps and design thereof has been provided above. Additionally a brief introduction to the applications of CFD has been discussed. Problems relating to pump sump design and modelling will be discussed in section 1.2.

1.2   Problem Statement

The need for the continuous operation of pump intakes to serve our daily needs has been mentioned above and some of the problems relating to pump intakes will be discussed in this section. Air entrainment in pump intakes is one of the major problems that will be discussed in this thesis. Another critical factor that will be discussed is swirl entrainment.

The term critical submergence, which will be referred to often in this text, is an indicator of the submergence levels, above the intake, at which the amount of air and swirl entrainment is detrimental to operation, possibly leading to reduced flow rates and higher running costs.

Air and swirl entrainment due to vortex action in pump intakes is a considerable problem as it can lead to the increased probability of cavitation of the pump impeller which can damage the blade surface and reduce pump efficiency and head which in turn leads to service delivery failure. Additionally, vibrations due to pressure fluctuations on the impeller blades can lead to bearing and other structural component failure, thereby reducing the pump life cycle and increasing maintenance frequency and costs. The aforementioned problems generally result from operating the system at water levels below the level of critical submergence.

There are two easily applied solutions to overcome the above mentioned operational difficulties and they are either increasing the submergence levels, or by the reduction of pump speed to reduce vortex and swirl action in the sump. These two methods do however have their unfavourable impacts on sump size and cost as well as operating the pump outside of its range of highest efficiency, respectively.

An improved method of designing or aiding the design process of pump intake structures is required to replace or assist the ageing rule-of-thumb and empirical relationships as can be seen in the design guidelines such as the ANSI/HI 9.8-1998 and PD CEN/TR 13930:2009.

The ability of Computational Fluid Dynamics or CFD as a design tool, to accurately model the flow patterns and critical submergence levels in pump intakes would be of great value. It is therefore a core focal point in hydraulic research. Stellenbosch University is joining the research into this field with the end goal being a calibrated CFD model that can accurately model various scenarios without the need for future validation.

There are numerous approaches that can be taken for a CFD model, not all will provide adequate results, but the correct combination could prove to be an invaluable design tool. There are numerous solver algorithms, turbulence models and multiphase flow models that can be used during the set-up phase of CFD modelling. All assumptions made during the set-up of the CFD model need to be well documented.

The problems relating to pump intakes and the design thereof have been introduced above, thereby allowing the reader to see that the ultimate problem lies with the design of pump intakes and the search for an accurate design tool to enable more efficient designs which do not require physical model testing. Additionally, the ideal model would allow for the modelling of existing pump intakes that have the above mentioned problems and the design of modifications, be that in the form of vortex suppressor devices or revised bell mouth designs or other modifications. The objectives of the research contained in this thesis will be discussed in section 1.3.

1.3   Research Objectives

A brief background of pump intake design and CFD modelling has been given in section 1.1 and in section 2.2 the problems relating to the research has been given. The research objectives will now be presented in the ensuing paragraphs.

- To construct and set-up a physical model of a geometrically simple pump sump with a vertically upward suction outlet to be used for identification of critical areas, as well as a tool for validation of the CFD model which is to be set up.

- To set up a two-phase transient state CFD model of the physical model to be used for the modelling of the sump, with particular interest in the region surrounding the bell mouth and any other areas that are identified using the physical model.

- To investigate the applicability and accuracy of the CFD model to quantify the air entrainment which is required for the determination of critical submergence levels.

- To set up a method for the comparison of the physical and the CFD models using the available equipment. The available equipment for the physical model includes an Acoustic Doppler Velocimeter (ADV) which will be used for 3-dimensional point velocity measurements.

1.4   Thesis Statement

The thesis of this work is the validation of a 3D CFD model for use in the design phase of pump intakes with the aim of replacing or reducing the need for physical model studies, focusing on levels of critical submergence and the related air entrainment, for geometrically simple systems.

1.5   Delineation and Limitations

The various areas of interest for this study in the above mentioned thesis statement will be delineated here to ensure a precise overview of the work to be carried out is presented in this thesis.

The 3D CFD model has the following characteristics:

- Pressure-Based, transient state solver
- Implicit, Volume of Fluid (VOF) multiphase model unless otherwise stated
- Standard k-ε turbulence model

- Cut cell meshing technique
- ANSYS-Workbench, -Meshing and -Fluent 14.0 is the software used for geometry creation, meshing creation and solving respectively. (ANSYS, 2013)

The model used for the study is of the vertically upward inlet type only. Any inclination of the bell mouth, use of a horizontal intake or use of an elbow inlet was not considered. The bell mouth was of elliptical profile with a small edge radius on the inlet side. No other bell mouth configurations were considered.

The physical model used for validation is a 240 mm wide, 4000 mm long channel with a depth of 1000 mm. It has a head box for flow stilling and runs as a closed system between the head box, channel and suction inlet. The head box contains various flow stilling devices. The bell mouth has a diameter of 115 mm, and the suction pipe inner diameter is 72 mm giving a diameter ratio (D/d) of 1.6. More details of the physical model can be seen in the methodology and physical model chapters, chapters 3 and 4, respectively.

1.6 Chapter Overviews

Chapter 2 is the literature review which provides a good understanding of the current and past research relevant to this study.

Chapter 3 is the method, which includes the research design, methodology and limitations to enable the reader to gain further understanding of the methods used or reason why other methods were not used.

Chapter 4 provides results obtained specific to the physical model tests.

Chapter 5 provides results obtained specific to the CFD model.

Chapter 6 provides a comparison of the results obtained from the physical and CFD models, which is the main focus of this thesis.

Chapter 7 gives the authors conclusions regarding the research carried out.

Chapter 8 provides recommendations for future research.

2. LITERATURE REVIEW

2.1   Introduction

Vortex formation and the resulting air entrainment in pump intake structures is a considerable problem as it leads to ventilation and cavitation of the impeller blades which can damage the blade surface and reduce pump head and efficiency which can lead to service delivery failure. Pressure fluctuations over the impeller blades caused by ventilation and swirl reduces the life cycle of bearings and surrounding structural components thereby increasing maintenance costs and reducing overall pump life cycle. The vortices typically occur in different strengths. Knauss (1987:18) provides the classification of the vortices in levels from 1 to 6, namely surface swirl, surface dimple, dye core to intake, entrainment of floating debris, entrainment of air bubbles and a full air core vortex to the intake, of which levels 2 to 6 can be seen in order from left to right in Figure 2.1 below.

Pump intake design guidelines currently make use of rule-of-thumb dimensioning along with various empirical relationships, which has been found to oversize sumps and therefore lead to higher construction costs (Hoppe, 2010). One of the methods of dealing with air-entrainment is increasing the submergence, which in turn increases the size of the structure and therefore increases construction costs.

The generally accepted method of verification of a sump design is by means of a physical model. This is a costly and time-consuming process. The method under investigation in this study is the use of CFD (Computational Fluid Dynamics) to model and predict flows in pump sumps in order to optimize the design thereof. CFD is an ever expanding field and many engineering disciplines make use of it for design optimization. Examples such as formula 1 motor racing, design of aeroplanes, combustion processes, etc. The difficulty with accurate modelling of pump sumps when it comes to air entrainment is the use of a two phase model, which as in ship design, introduces complications and limitations which can limit the quality of the results.

In its current state, CFD still requires validation by a physical model to ensure the accuracy of the results. The ultimate solution would be a calibrated CFD model that would allow accurate modelling and flow prediction without the need for physical model verification. This

study aims to investigate the applicability of the use of commercial CFD codes, namely ANSYS Fluent 14.0, to model the flows in geometrically simple pump sumps.
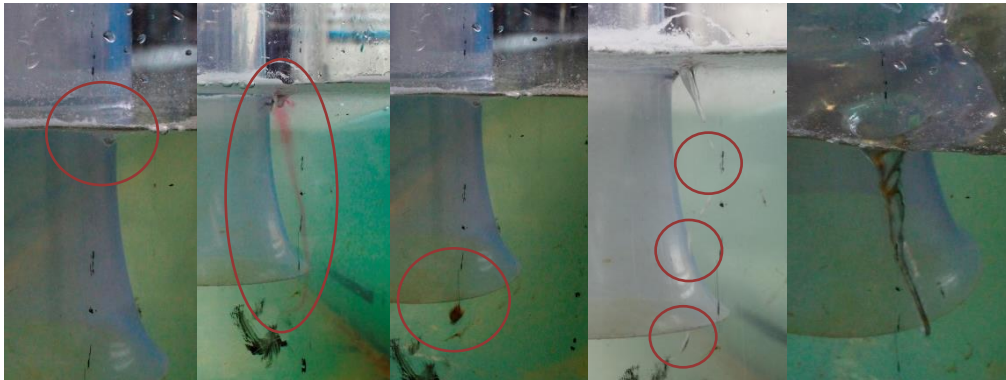
Figure 2.1 - Vortices level 2 to level 6 (left to right)

2.2   Basics of Pump Intake Design

A few critical parameters relating to the design of pump sumps and intakes will be discussed below, relating to the bell mouth design and specification, approach channel and the calculation of critical submergence.

Bell mouth design

Literature relating to the design of the bell mouth for the use in pump intakes is scarce. The only references found are in Prosser (1983:16) and the PD CEN/TR 13930:2009 standards (Rotodynamic pumps – Design of pump intakes – Recommendations for installation of pumps) where it defines an upper and lower limit for the diameter ratio between the bell mouth entrance and the suction pipe and specifies that the profile shape should be a quarter of an ellipse. Additionally, it can be concluded that the minor axis of the ellipse is defined as follows:

$$a = \frac{D - d}{2}$$

With *D* the bell mouth diameter and *d* the suction pipe diameter.

Blair and Melvin Cahoon (2006:34-41) made use of CFD to model the inflow of air in the intake of an internal combustion engine. They investigated various profile shapes and carried out a CFD simulation of the various designs and determined that the quarter ellipse profile

was best. The paper may seem out of context, but since the results are for Mach numbers below 0.25, the principles of fluid flow still hold, therefore the desired pressure distributions and potential flows remain similar.

Approach channel geometry

The approach channel plays an important part in a pump intake. The quality of the approach flow is dependent on this and Knauss (1987) states that vortex shedding from structures in the approach channel is a major cause of unwanted flow conditions in the sump, such as vortices and pre-rotation.

Approach flow profile

The approach flow profile should be kept symmetrical in shape and of constant velocity or accelerating as it is then less likely to cause rotation. Knauss (1987) recommends the use of screens and diffusers should deceleration of the flow be required.

Approach flow velocities

The velocity of the approach flow influences the generation of vortices in the sump. The velocity should be kept low and of uniform profile as mentioned above to ensure satisfactory flow conditions throughout the sump.

Prosser (1983) recommends an approach velocity which should be 0.3 m/s or less.

Cooper et al. (2008) recommends that the approach velocity be kept between 0.3 m/s and 0.4 m/s.

Inlet velocities

The bell mouth inlet velocities are of high importance when it comes to vortex formation in the surrounding regions.

The ANSI/HI 9.8-1998 Pump Intake Design standards recommend a design velocity at the inlet to the bell mouth of 1.7 m/s. It provides an acceptable range, depending on the flow which can be seen on page 21 of that document.

PD CEN/TR 13930:2009 recommends a bell mouth inlet velocity of 1.5 m/s.

Hydraulic prediction of Critical Submergence

The prediction of the level of critical submergence in a pump sump is of high importance to reduce increased maintenance and operational costs induced by higher submergence levels or running at reduced speeds to accommodate the resulting air and swirl entrainment if this level is breached. Knauss (1987) concludes that the use of an analytical calculation in the determination of the critical submergence yields unsatisfactory results and cannot be relied upon. Therefore physical model studies or empirical solutions are required for this purpose.

2.3   Physical modelling

Physical modelling has for long been the only reliable way of determining the operational success of pump intake design regarding, for example, air entrainment. The process is time consuming and costly. Physical modelling is used in many industries, for example aeronautical or marine, to determine the functionality of design. More recently, many industries are rapidly moving away from this type of testing and relying exclusively on the results from CFD simulations.

Some theory relating to modelling of fluid flows as well as that of pump intakes will be discussed below.

Physical Modelling of Pump Intakes

Knauss (1987) defines the critical submergence (h_{cr}) of a vertical intake arrangement as follows:

$$h_{cr} = f(V, d, D, r, Z, \Gamma, g, \sigma, \mu, \rho)$$

Where

V = average velocity of flow through intake pipe (diameter d);

d = intake pipe diameter;

D = bell mouth opening diameter (extreme diameter);

r = radius of rounding of bell mouth entry, if any;

Z = bell mouth elevation w.r.t. the sump floor;

Γ = average circulation over the depth at a distance D/2 from the centre line of the intake;

g = gravitational acceleration;

ρ = mass density of fluid;

σ = surface tension of fluid;

μ = dynamic viscosity of fluid.

He then carries out a dimensional analysis and reduces the equation to a function of five length ratios and the Froude (Fr), Weber (We) and Reynolds (Re) numbers. These three numbers are defined as follows:

$$Fr = \frac{V}{\sqrt{gd}}$$

$$We = V\sqrt{\frac{\rho d}{\sigma}}$$

$$Re = \frac{Vd\rho}{\mu}$$

Gravity remains constant for model and prototype and gravitational and inertial forces dominate modelling of intakes, therefore it makes sense to use Froude similitude when it comes to choosing a scaling law. As long as the Reynolds and Weber numbers are above a threshold value, Knauss (1987) concludes that the use of Froude similitude without other large adjustments, for Reynolds or Weber, can be used for reliable modelling of the vortex phenomenon. These thresholds are Re > 50 000 × Fr and the We > 11.

For Froude similitude, the following relationship holds true (with the subscripts p and m representing the prototype and model values respectively):

$$\frac{Fr_p}{Fr_m} = 1$$

Solving for the model velocity yields:

$$V_m = V_p \sqrt{\frac{d_m}{d_p}}$$

This is the governing equation that was used to calculate the various inlet velocities that can be seen in Figure 3.9.

2.4   Computational Fluid Dynamics (CFD) models

CFD is the numerical solution of the Navier-Stokes (N-S) equations, which are the fundamental partial differential equations that describe viscous fluid flow. (Versteeg and Malalasekera 2007) CFD software is generally supplied in packages, containing several components to handle geometry creation, meshing, solving and post processing, such as can be found in the ANSYS 14.0 software package. ANSYS Fluent makes use of the Finite Volume Method (FVM) to solve the N-S equations for each of the finite cells in the volume being modelled.

As CFD models are progressing, it is becoming increasingly powerful as physics algorithms improve and improved methods of turbulence modelling are found. The modelling of turbulence is a highly complex task, and some simplified details will be provided under the relevant subtitle below regarding the turbulence model used for this study.

CFD models have been transformed from in-house development codes to large scale, commercially available Graphical User Interface (GUI) software packages. These are easier for the non-expert to understand leading to the increased use of CFD models in industry.

It is known that CFD models can simulate flow phenomenon to very accurate levels when calibrated correctly. Calibration of the model is no easy task and requires extensive validation using a physical model as well as input sensitivity analysis.

The pressure-velocity coupling algorithm and turbulence model used for the study will be briefly explained in a simplified manner, followed by a brief discussion on validation of CFD results as well as the applicability of the use of CFD to model pump intakes.

Pressure-Velocity Coupling

The Pressure Implicit with Splitting of Operators (PISO) pressure-velocity coupling algorithm was used for this study. This algorithm can maintain stability in transient flow problems even when a large time-step is used. The PISO algorithm solves the flow field using one predictor step and two corrector steps, Versteeg and Malalasekera (2007) state that it can be seen as an extension of the SIMPLE algorithm, with an additional corrector step to improve it. A simplified flow diagram of the algorithm is shown in Figure 2.2 below.
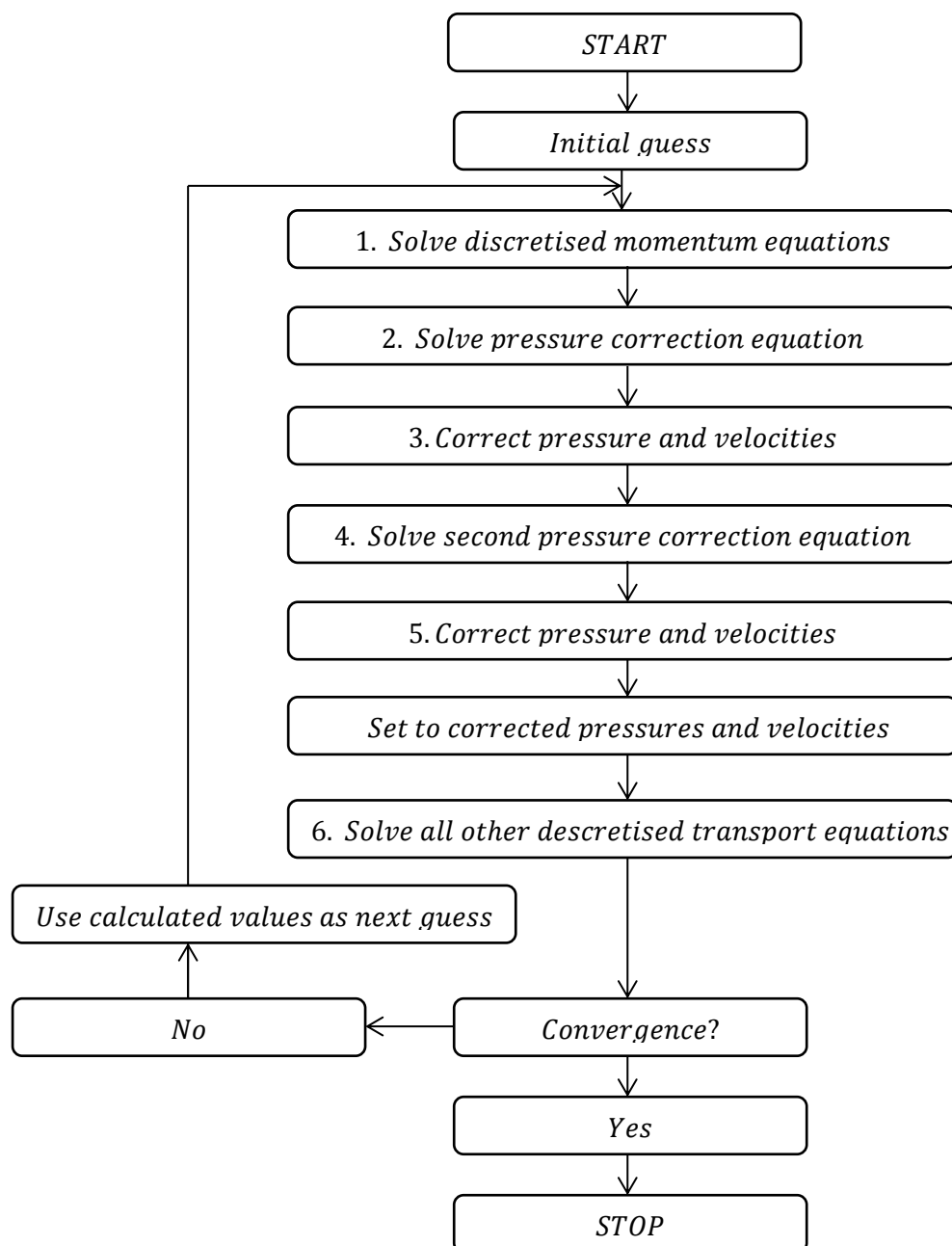
Figure 2.2 - Simplified representation of the PISO algorithm in words (Versteeg and Malalasekera, 2007)

The additional stability of this algorithm as mentioned above was a large factor when choosing a pressure-velocity coupling algorithm for this study.

Turbulence Model

For this study, the most widely validated and used turbulence model, the k-ε turbulence model was used. The modelling of turbulence is a complex task, as it is a highly unsteady phenomenon. The k-ε turbulence model is of the RANS (Reynolds-Averaged Navier-Stokes) type, thereby focusing on the mean flow and its properties. The computational time required for these calculations are lower than most others, therefore they are popular.

The model is defined by two equations, one for k (the turbulent kinetic energy) and one for ε (the dissipation of kinetic energy). They can be simplified in word form as done by Versteeg and Malalasekera (2007) as follows:

$$
\textit{Rate of change of k or ε + Transport rate of k or ε by convection}
$$
$$
= \textit{ Transport of k or ε by diffusion + rate of production of k or ε } -
$$
$$
\textit{Rate of destruction of k or ε}
$$

This equation is written in terms of k and ε separately, resulting in two equations, one for k and one for ε, respectively.

These equations lead to five constants, which are adjustable to suit various flows. In the standard model the parameters have the following values that have been extensively researched for various turbulent flows. The parameters are defined as follows by Versteeg and Malalasekera (2007):

$$C_\mu = 0.09$$

$$\sigma_k = 1.00$$

$$\sigma_\varepsilon = 1.30$$

$$C_{1\varepsilon} = 1.44$$

$$C_{2\varepsilon} = 1.92$$

For this study, the parameters were left to their default values as indicated above.

Validation

The complexity of CFD modelling is one of the reasons that the quality of the results is questioned. The results are highly dependent on user input and selection of algorithms, etc. and therefore there needs to be some way to check that the simulation is in fact representing reality. Generally this is referred to as validation. Validation can be carried out in several ways, the most common of which is the comparison of some important value between simulation and physical model. This requires high quality physical model data, else the comparison is meaningless.

Versteeg and Malalasekera (2007) discuss two methods of input uncertainty comprised of sensitivity or uncertainty analysis. The former being the monitoring of the effects of a single input parameter variation and the latter taking into account the interactions between various parameters changed simultaneously.

This study makes use of physical model validation, as well as a mesh independence analysis to ensure the effects of the mesh element size are minimal.

CFD simulation results can therefore not be taken as a true representation of reality until they have been adequately validated.

2.5   Previous Studies

Several studies that have been carried out with the same or similar focus will be discussed below. They will be listed chronologically in a short paragraph about each work.

Rajendran et al. (1998) modelled a simple pump sump in CFD and validated by means of PIV (Particle Image Velocimetry) measurements in a physical model. They conclude that as CFD is based on steady flows, the prediction of vortices which are highly time dependent, will be a challenge.

Constantinescu and Patel (1998) investigated the use of the k-ε turbulence in modelling pump intakes for electric-power generating plants. They conclude that the numerical model predicted the location, size and strength of vortices sufficiently, although considerable post

processing is required to reach that point. They also mention that the k-ε turbulence model proved to be robust, but it requires validation with a physical mode for this application.

Li et al. (2006) modelled a practical water –pump intake using a three-dimensional CFD model and compared it to a scale physical model. They used an ADV and a pitot-tube for the various velocity measurements in the physical model. They tested for two flow conditions, namely 'no-cross-flow' and 'cross-flow' conditions. They conclude that steady state solutions yield poor results and that the k-ε turbulence model they used may not be approximating the swirl conditions near the bell mouth throat appropriately and recommended that other turbulence models be tested for this.

Wicklein et al. (2006) carried out a CFD simulation on a proposed influent pump station and compared the results to a physical model, after which the CFD model was used for design optimizations and later for possible changes at the time of construction. They reported good results from the CFD model and highlighted its advantage over physical model studies. One major advantage being that results produced are digital and can be kept to investigate changes at time of construction or even later.

Okamura et al. (2007) carried out a benchmark test on several CFD codes and validated using a small scale model wherein they used the PIV and LLS (Laser Light Sheet) methods for determining the velocities and general flow structure respectively. The CFD codes they tested are listed as follows:

- STAR-CD 3.22
- ANSYS CFX 10.0
- STAR-CD 3.26
- Virtual Fluid System 3D
- SCRYU/TETRA V6

They conclude that some of the CFD codes predict the visible vortex location and occurrence accurately enough to be used in industry, although the results of magnitudes near the bell mouth are poor and only agree qualitatively. The prediction of critical submergence is not easily achieved and would require additional post processing.

Tokyay and Constantinescu (no date) used an LES (Large Eddy Simulation) model to predict the flows in a pump sump and validated it by means of PIV measurements in a physical

model. They conclude that with a sufficiently fine mesh, the model can simulate the qualitative as well as the quantitative aspects well in terms of the mean flow.

Shukla and Kshirsagar (2008) carried out a study using a commercially available CFD code to model multiphase flows in a pump sump and compared it to 1:10 scale physical model results. They used photographs and analysis of swirl in the intake pipe by means of a four bladed swirl meter. They concluded that overall the results were satisfactory and mention that the location, size and strength of the vortices appear to be modelled accurately.

Desmukh and Gahlot (2010) validated a CFD simulation of flow through a pump sump. They made use of ANSYS CFX 10.0 and pitot tubes for velocity measurement in the physical model. They conclude that CFD can predict the flow conditions well, although large amounts of post processing is required to obtain them. They also state that CFD will become a valuable design tool for the optimization of pump sump geometry.

2.6   Conclusion

A general overview of theory as well as previous studies related to the research to be carried has been presented. The various limiting factors with regards to pump intake design and modelling have been presented and where applicable, the chosen method indicated.

The general conclusion from the previous studies is that CFD can model the flow characteristics well, but generally the velocity magnitudes, for example, are not estimated accurately. Therefore current research suggests qualitative use of the CFD models is acceptable. However the models require research to enable use for quantitative results.

3. METHODOLOGY

3.1 Introduction

The structures of the flow field in pump intakes are of a complex nature, thus limiting successful analytic solutions in the design phase. The current approach to pump sump design implements the use of rule-of-thumb ratios and empirically developed formulae obtained from generic physical model studies. The use of CFD models to model the intake flow conditions and provide reliable predictions on safe submergence levels is to be investigated as it could be a useful tool and ideally reduce the requirement of physical model studies.

The chapter below details the method that will be used to carry out the above mentioned research. The physical model study should provide results for both quantitative and qualitative analysis. The quantitative data will be in the form of 3-dimensional point velocities obtained with an Acoustic Doppler Velocimeter (ADV). The qualitative results obtained from the physical model will be in the form of video footage and photographs, as well as any noted observations by the author. The CFD model has large amounts of output data which can be chosen to be presented after the solution has been obtained; this allows various output forms to be plotted. The outputs from the CFD model will include the 3-dimensional point velocities as in the physical model averaged over a specified period of time, as well as contour and vector plots of the flow characteristics and various fluxes monitored and recorded during the simulation.

The sections below will discuss the standard research designs used for the physical and CFD modelling in this study (section 3.2) followed by the specific implementation of these research designs in the methodology (sections 3.3 and 3.4) which addresses the research instruments (sections 3.3.1 and 3.4.1), Data handling (sections 3.3.2 and 3.4.2) and the analysis techniques used (sections 3.3.3 and 3.4.3). Furthermore the limitations with respect to the study will be discussed in sections 3.5 and 3.6.

3.2   Research Design

The following section discusses the standard research designs that were used in this study. The research designs will be listed and their relevance to the study will be briefly discussed.

The first standard research design that will be discussed is experiments. The experiment in this study is carried out by means of a scale physical model, operated in a controlled environment. Point velocity measurements, photographs and visual observations are recorded, processed and used for analysis and comparison.

The second standard research design employed is that of simulations. The CFD model is a simulation which can be defined as a simplified representation of the processes that occur in reality, in this case in the physical model. Numerous assumptions and various approximations are made when defining boundary conditions, turbulence models, solver settings and many other details.

The third and final standard research design employed is that of a comparative analysis. The data gathered by the experiments and the simulations will be compared to identify similarities with the aim of verifying that the simulation does in fact represent reality to a sufficient degree to enable it to be used for the replacement of physical model studies in the design phase of pump intakes.

The above three standard research designs complement one another and are all three required in order to carry out the scope of this study. The main goal is the comparison of the results in order to obtain evidence whether or not the CFD model can be used as a replacement for the physical modelling, but the physical model (Experiment) and CFD model (Simulation) are required in order to obtain the data required for the comparative analysis.

Alternatives could be used, if the data from either the physical modelling or the CFD modelling were available from a previous study, or if the study was two separate, simultaneous studies focusing on the same problem but with different research tools, as was done by Hundley (2011), who investigated the use of a single phase CFD model and Kleynhans (2012) who carried out physical model testing, based on the same geometry. However, in this study both aspects were combined into a single study, which increases the work load, but does allow for a more complete understanding of the flow details and thereby allowing greater control over the study.

3.3   Methodology – Physical Model

The above sections of this chapter discuss a general overview of the type of research methods used for the collection, analysis and comparison of data. This section will detail how the methods were implemented for the physical model as well as provide details regarding the research instruments, the data obtained with the research instruments followed by the analysis of that data.

3.3.1   Research Instruments

The research instruments that were used for the physical modelling are as follows:

- Design spreadsheet
- Physical model, a 4000 mm long, 240 mm wide glass channel with a depth of 1000 mm. With a head box, 750 mm x 750 mm, for flow stilling and an instrument trolley with x,y and z axes.
- Lowara FHS4 50-160/11 centrifugal pump
- WEG CFW-08 Frequency Inverter for controlling the pump speed
- Proline Promag 50W Electromagnetic Flow Measuring System
- Nortek Vectrino Velocimeter
- Dell Studio XPS 16 Laptop
- Camera equipment
- Dye injection system

The equipment listed above will now be detailed individually.

Design Spreadsheet

A design spreadsheet was set up to estimate the size of the various parameters required for the physical model. Various dimensionless numbers had checks run to ensure they were within the required limits to enable the model to be run based on Froude similitude. This spreadsheet contained the pump curves, sump sizing, pipe and bell mouth sizing, head losses in the system as well as a costing estimate for the construction of the physical model, which as mentioned below was not constructed due to the availability of the model used by Kleynhans (2012).

Physical Model

Originally, a new hydraulic model was designed and planned to be constructed. However, due to lack of funding and the availability of the model that will be discussed below, it was decided to use the available model with some modifications that were agreed upon.

The physical model available was a 4000 mm long, 240 mm wide and 1000 mm deep glass channel with steel supporting structure. Originally the model was only the channel as dimensioned above, similar in concept to that used by Hoppe (2010), however the flow conditions were unsatisfactory and a head box was added for flow stilling, straightening and dampening of wave action caused by the high velocity inflow.

The physical model was previously used by Kleynhans (2012) for his study of the physical modelling of the critical submergence of raised intakes. Kleynhans (2012:9) mentions that the Trans Caledon Tunnel Authority (TCTA) postponed the planned laboratory testing using the hydraulic model but allowed the Stellenbosch University to make use of the physical model for other research projects, such as his study and now this one.

Figures 3.1 and 3.2 below show the model before any modifications were made, indicating the eccentricity of the inflow pipe into the head box and the flow straightening PVC pipes in a view looking downstream from the head box respectively. Figure 3.3 shows a drawing of the physical model including some of the modifications.

Figure 3.1 - Eccentricity of the inflow pipe into the head box as used by Kleynhans (2012)

Figure 3.2 - Downstream view of the approach channel showing the flow straightening PVC pipes on the physical model before modifications
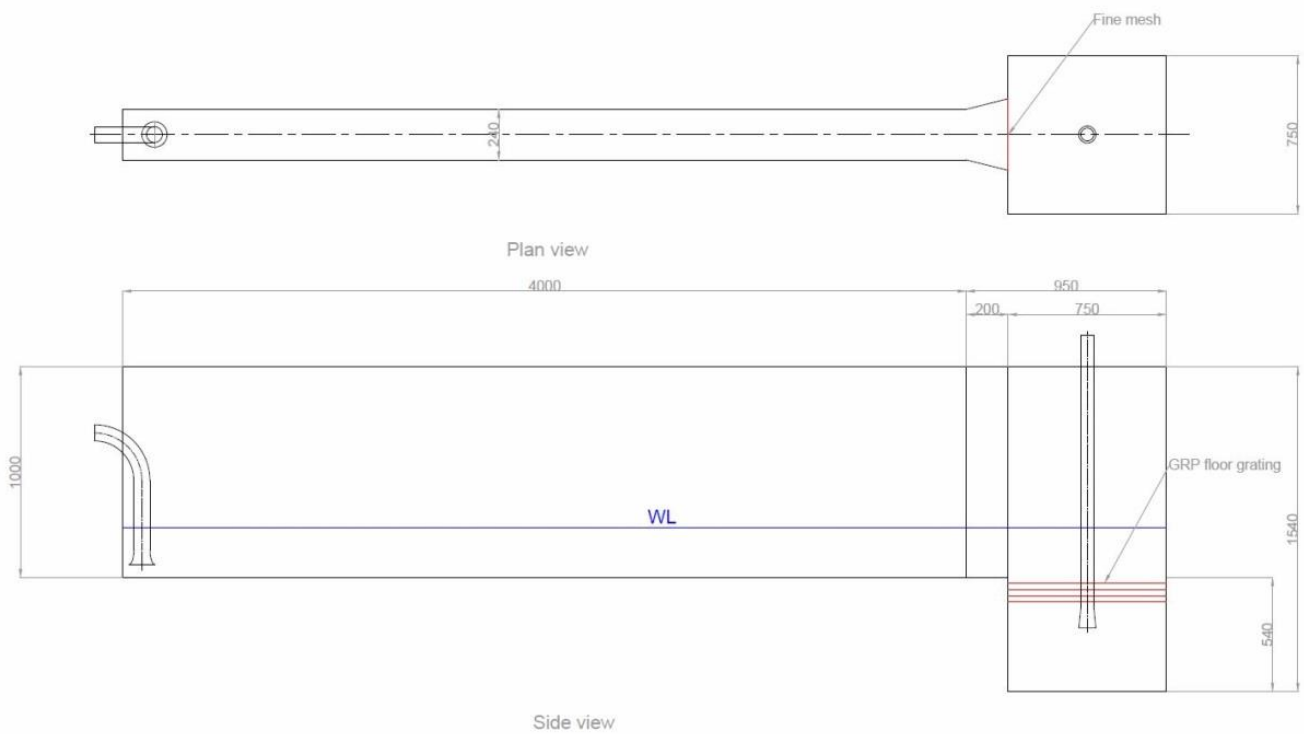
Figure 3.3 - Drawing of the physical model including modifications.

The above images are provided to give the reader a better understanding of the initial state of the model. The flow conditions within the model were not ideal and the author made various changes to the model. The changes made to the physical model will be listed followed by an explanation of each change and the results thereof. The changes made were as follows:

- The pump was removed from the tank frame and PVC piping adjusted.
- The inlet pipe was centred in the head box and an additional means of fixing was added.
- Horizontal mesh system added in head box for flow stilling.

- A fine mesh (1 mm^2 nominal opening) was added to the entrance to the transition section.

- Small wave damper was added in exit from transition section into channel.

- Addition of a top mounted rail system with a trolley which has adjustability in x, y and z axes.

- Rounding of the edges in the head box at the entrance to the transition section.

- Removal of the PVC pipe flow straighteners which are shown in Figure 3.2 above.

The pump was moved to a rubber mat on the floor and therefore required a rather long suction hose attaching the bell mouth and vertical suction pipe to the inlet of the pump. A 50mm diameter reinforced rubber hose was initially tested, but it was too small a diameter for the high flow rate required, thereby throttling the pump. This was changed to a 75 mm diameter reinforced rubber hose, which improved the maximum achievable flow rate significantly. All short 90 degree bends in the system that were accessible were replaced for long 90 degree bends which too had a significant effect on the maximum achievable flow rate.

The inlet pipe into the head box was originally eccentric and had no support along the drop length into the head box. This caused asymmetrical flow patterns in the sump as well as excessive vibration of the inlet pipe which resulted in wave generation. The original inlet pipe had a diffuser, although this diffuser was not ideal, it contributed to the improvements. It was requested that the inlet pipe be centred, protrude through the grating, be sealed around this protrusion and be attached to some support to add stiffness and ensure flow induced vibration was kept to a minimum. This modification increased the stilling capabilities and the reduction of wave generation in the head box ultimately leading to favourable flow conditions downstream.

The addition of a mesh system in the head box, parallel to the head box floor, was implemented in order to aid in flow stilling and straightening before it enters the approach channel to the bell mouth. This was done by the use of GRP floor grating (1220 mm x 2440 mm x 25 mm with a nominal spacing of 38 mm and 68% open area), cut to an appropriate size and stacked in four layers, each which could be moved independently of one other to alter the ratio of open area. The layers were offset by 19 mm in the x and y axes, with layers 1 and 3 and layers 2 and 4 having the same location in the xy plane respectively. The GRP

floor grating was mounted on a simple four legged base that stood on the head box floor. Pieces of mild steel angle were corrosion protected and placed around the borders to ensure no gaps were left around the grating. This modification made a large improvement in the uniformity of the flow approaching the bell mouth and was thus a positive improvement and can be seen in Figures 3.4 and 3.5 below (mesh – green, mild steel angle – red).

A fine mesh was installed in the outlet of the head box to the transition section, which creates a pressure drop resulting in the removal of smaller turbulences in the flow. The mesh is available in various materials and sizes, but local availability was a problem. However, a PVC coated fibreglass mesh, used on doors and windows to block insects from entering buildings was discovered. This mesh is beneficial as it doesn't corrode, handles the submerged conditions well, and is easy to clean of any fouling. The mesh had a nominal opening of approximately 1 mm, which was the required size. This too helped improve the flow conditions by the removal of the smaller pockets of turbulence. The mesh can be seen in Figures 3.4 and 3.5 below, with the fine mesh (grey).
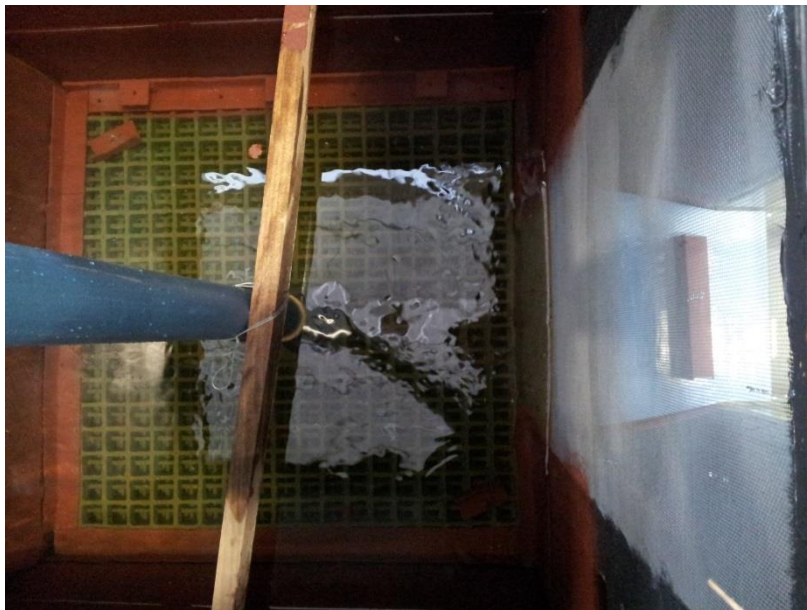
Figure 3.4 - Horizontal mesh and fine mesh added to the head box to improve the flow conditions

A small floating wave damper was added to reduce short wavelength wave action. The wave damper fits in the transition section between the head box and the flume, using the flow to wedge itself in and create a sturdier platform for wave dampening. The wave damper had a

small 'beach' on the upstream side to aid with dissipation of waves originating from the head box and a tapered end on the lower surface to reduce flow break off at the downstream end.

One of the bigger modifications to the flume was the addition of a top mounted rail system and trolley to allow for the attachment of the measuring equipment as well as allowing the trolley to move along the three primary axes, using rulers glued to the frame work as a means of locating the trolley.

The transition from the head box to the flume was rather crude and had 'sharp' edges which are unsatisfactory for maintaining uniform flow conditions as it causes the flow to 'break off' the wall and form additional turbulences. A simple modification was proposed to solve this problem that being the addition of PVC pipes cut to shape to add a rounded transition from the head box to the flume. This was done for the side walls, using a 110 mm diameter PVC pipe, and for the lower side using a 50 mm diameter PVC pipe. Figure 3.5 below shows the PVC pipes in the process of being glued in place, still held in place by the masking tape.
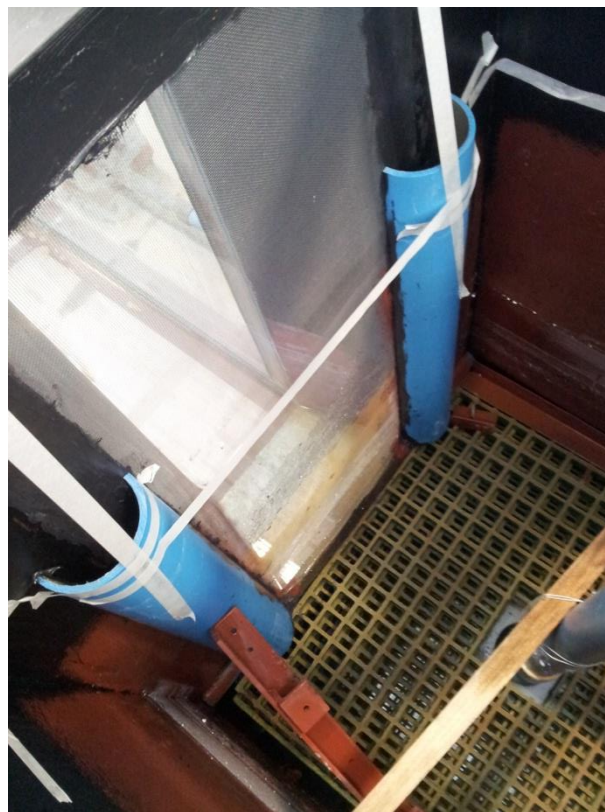
Figure 3.5 – Rounding added to the edges of the head box to reduce flow separation as it enters the transition section

The PVC pipe flow straighteners that can be seen in Figure 3.2 were removed as it was observed that they were causing unwanted turbulences downstream.

A ruler was also added to gauge the depth of the flow.

The removal of the pump from the tank frame reduced vibrations and aided in capturing cleaner data. The above mentioned changes, relating to flow improvement, drastically improved the flow conditions in the flume, resulting in a smooth steady approach flow, which is satisfactory for the task at hand of comparing physical and numerical models. The non-flow related changes aided in the monitoring of water levels as well as the increased ease of equipment handling and locating due to the installed trolley and rail system.

The bell mouth shape is an important part of a suction pipe, reducing the losses and thereby increasing the efficiency of the system where, as in this case, horizontal flow in a rectangular channel must transition to pipe flow in a vertical pipe. There is very limited literature on bell mouth design and implementation for use in pump sumps, or even for general use of a bell mouth in water. The only research literature found by the author was that for the use of a bell mouth on the suction inlet of an internal combustion engine.

The PD CEN/TR 13930:2009 has reference ratios for the dimensioning of a bell mouth for the use in pump sumps; however they are rather crude and are merely a guideline with no details of any research into the shape of the bell. (This can be expected from a design standards document)

Considering the abovementioned research regarding the design of the bell mouth, a standard bell mouth with an elliptic profile was chosen. The diameter ratio between the bell mouth inlet diameter and the suction pipe diameter was chosen to be 1,6 which falls within the recommended range of 1,4 to 1,8.

Various construction techniques were investigated, but the final product was constructed by forming a heated clear PVC pipe over a wooden mould that was formed on a lathe. This technique worked well although the mould should include a long piece of the pipe at its original diameter to prevent any misalignment with the suction pipe and bell mouth. The bell mouth profile was measured and found to be mostly similar to the designed elliptic profile as can be seen in Figure 3.6 below.
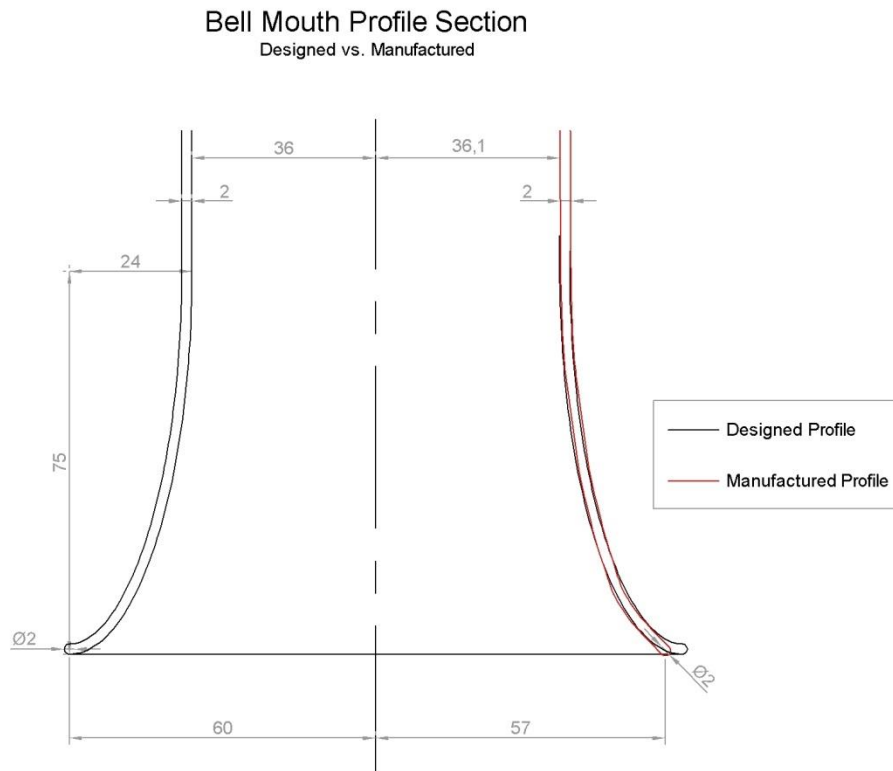
Figure 3.6 - Designed bell mouth profile section vs. manufactured bell mouth profile section

Pump

The pump used was a Lowara FHS4 50-160/11 centrifugal pump. The pump has a 1.1 kW 4-pole three phase AC motor which runs at approximately 1450 rpm at 50 Hz at an efficiency of 81.4 %. The pump has a maximum flow rate of 11.7 l/s with a corresponding head of 5.1 m.

The maximum flow rate attainable with the piping system on the physical model was approximately 8.8 l/s, which is sufficiently high to allow for a high, average and low flow rate tests to be run for the intake system. There are several reasons for the lowered maximum flow rate, one being the use of a 50 mm PVC pipe section which is required to insert the flow meter in the system. Another reason is the use of several 90 degree bends to allow a non-intrusive piping system that allows the tank to be easily separated from the piping system.

Figure 3.7 below shows the pump operating characteristics and highlights the three flow rates used for the model testing, with the following operating points: 2,4 l/s (purple diamonds), 4,2 l/s (green squares) and 8,6 l/s (red dots).

The lowest flow rate, 2.4 l/s, was achieved by running the Variable Speed Drive (VSD) at approximately 23 Hz and then adjusting a ball valve on the outlet pipe of the pump. It can be seen that this flow rate is not in the preferred operating range for this pump. The highest flow rate, 8.6 l/s, is run at the optimum operating point on the pump curves.
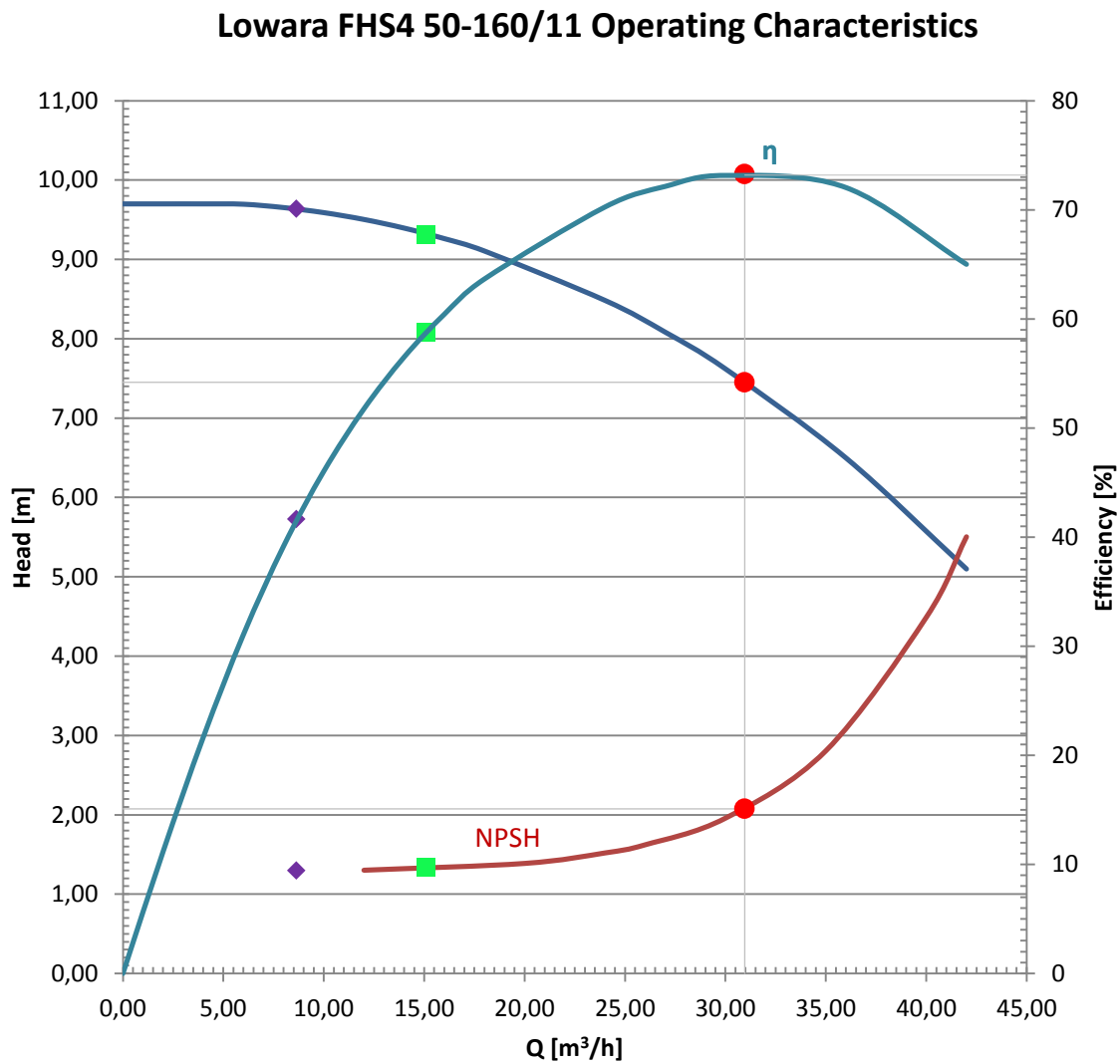
Figure 3.7 - Lowara FHS4 50-160/11 operating characteristics with indication of the three flow rates used (2.4 l/s – purple, 4.2 l/s – green and 8.6 l/s – red)

Variable Speed Drive (VSD)

A WEG CFW-08 Frequency Inverter, further referred to as the VSD, was used for adjusting the input frequency to the pump motor, thereby changing the pump speed resulting in an adjusted flow rate. The VSD had an output frequency range of 20 Hz to 52.50 Hz.

Flow Meter

A Proline Promag 50W Electromagnetic Flow Measuring System was installed inline in the pipe system. This allowed for close visual monitoring of the flow rate; however no data logging was possible due to lack of equipment. The flow meter operates on Faradays law of magnetic induction.

Acoustic Doppler Velocimeter (ADV)

The ADV used for the velocity measurements in this study was a Nortek Vectrino Velocimeter, also referred to as the ADV in this thesis. The ADV makes use of the Doppler Effect to measure the 3 dimensional velocities in a sample volume by transmitting short acoustic pulses from a centre transducer and the Doppler shift introduced from the reflections of particles in the flow are then received by four receiver probes. The ADV uses an acoustic frequency of 10 MHz and can sample data at a frequency of up to 25 Hz. The sample volume is 6 mm in diameter and has a user selectable height of 3 to 15 mm, at a nominal distance of 50 mm from the probe.

The ADV comes with software for instrument set-up and data recording as well as a function for file conversion to allow easier manipulation of the files with non-OEM software packages.

The ADV can be seen attached to the vertical axis of the equipment trolley, as it was used for the velocity measurements, in Figure 3.8 below. The ADV was attached to the vertical axis, an aluminium square tube section, by means of two large diameter hose clamps. It was aligned by means of a printed sticker, containing a centre line as well as various parallel lines to enable accurate reproduction of the attachment position, which was attached to the flat face of the ADV. The ADV was checked with a Samsung Galaxy S4 (SGS4) running the Clinometer application to establish whether or not the instrument was vertical, which the device indicated within $\pm$ 0.2 °. The SGS4 running the Clinometer application was tested

using a Lucas AngleStar DP60 Digital Protractor which indicated accuracy within the first decimal place.

Figure 3.8 - Nortek Vectrino attached to the vertical axis of the equipment trolley, measuring flow velocity

Laptop

A Dell Studio XPS 16 – 1640 laptop was used for the data recording. The ADV connected to the laptop via a USB to serial adapter and was then available to the Vectrino software via a COM port.

Camera

The primary camera used for video recording and photography was a Canon EOS 550D SLR camera. The advantage of the full manual control, larger imaging sensor and higher quality optics made capturing the various flow characteristics easier.

Additionally, two smartphones were used for photography and video recording, namely a Samsung Galaxy S2 and a Samsung Galaxy S4.

Dye Injection System

The use of dye injection in the fluid can enhance certain flow characteristics aiding in identifying them. Therefore it would be necessary to have a method of injecting dye into the model. A simple syringe pump, made up of a frame with two rails, a spindle and a stepper motor was created, as can be seen in Figure 3.9 below. The stepper motor controller, EasyDriver V4, was controlled by an Arduino MEGA 1280 microcontroller. The circuitry was designed to allow speed control via a potentiometer and forward and reverse directions of the motor, via two push buttons, to compress and extend the syringe plunger. Two indicator LEDs indicated forward (green) and reverse (red) directions.

The syringe was connected to a self-built needle via silicon hose. The needle was made from two sections of brass tubing, one larger diameter for the vertical section and a smaller diameter one for the section containing the 90 degree bend, soldered at the joint and smoothed off and sealed with epoxy containing micro balloons. A medical needle was epoxied to the end of the small brass tube to ensure a fine dye trace.
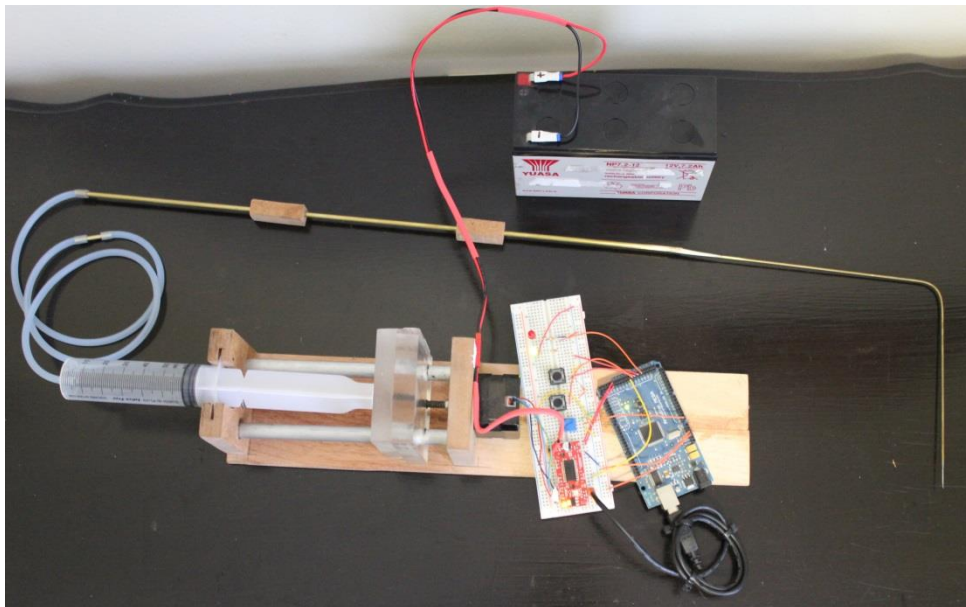
Figure 3.9 - Dye injection system as detailed above

The dye injection was used to identify subsurface vortices as well as dye core surface vortices. Due to the highly turbulent nature of the flow, defined streamline visualization was not possible.

3.3.2   Data

In section 3.3.1 above the various research instruments used for the physical modelling were introduced and their intended use or purpose stated. This section will focus on the various tests and calibrations run to ensure that adequate data was recorded as well as detailing the type or applicability of that data.

The various flow rates and water levels used for the tests are now discussed before the various aspects relating to the data to be recorded and analysed is presented.

Due to time constraints, three water levels and three flow rates were run, resulting in 9 tests. Only 8 tests were run, due to the constant steady air entraining vortices that resulted due to the highest flow rate at the lowest water level (8.6 l/s at 150 mm). The CFD model running in the implicit state also had difficulty in modelling the aforementioned scenario accurately.

The three chosen water levels are:

- 235 mm
- 190 mm
- 150 mm

The first water level, 235 mm, was chosen on the basis of the rule-of-thumb recommendation of the safe submergence of twice the inlet diameter. The lowest water level, 150 mm, was chosen by adjusting the water level to the point just before the middle flow rate, 4.2 l/s, resulted in air entraining vortices. The middle water level, 190 mm was chosen as a good value in between the two, but it too showed signs of sucking in the occasional air bubble or floating debris at the highest flow rate of 8.6 l/s. The three flow rates chosen will now be discussed.

The model study will be run with three different flow rates. The three selected flow rates for the model are 8.6 l/s, 4.2 l/s and 2.4 l/s. Figure 3.10 below indicates the various bell mouth inlet velocities for prototypes of varying scale for each of the three modelled flow rates, and it can be seen that the chosen flow rates relate to a large velocity range for the various prototype scales which includes velocities below, of the average and above the recommended values by Prosser (1977), PD CEN/TR 13930:2009 and ANSI/HI 9.8-1998.

Bell mouth inlet velocity vs. Prototype scale ratio
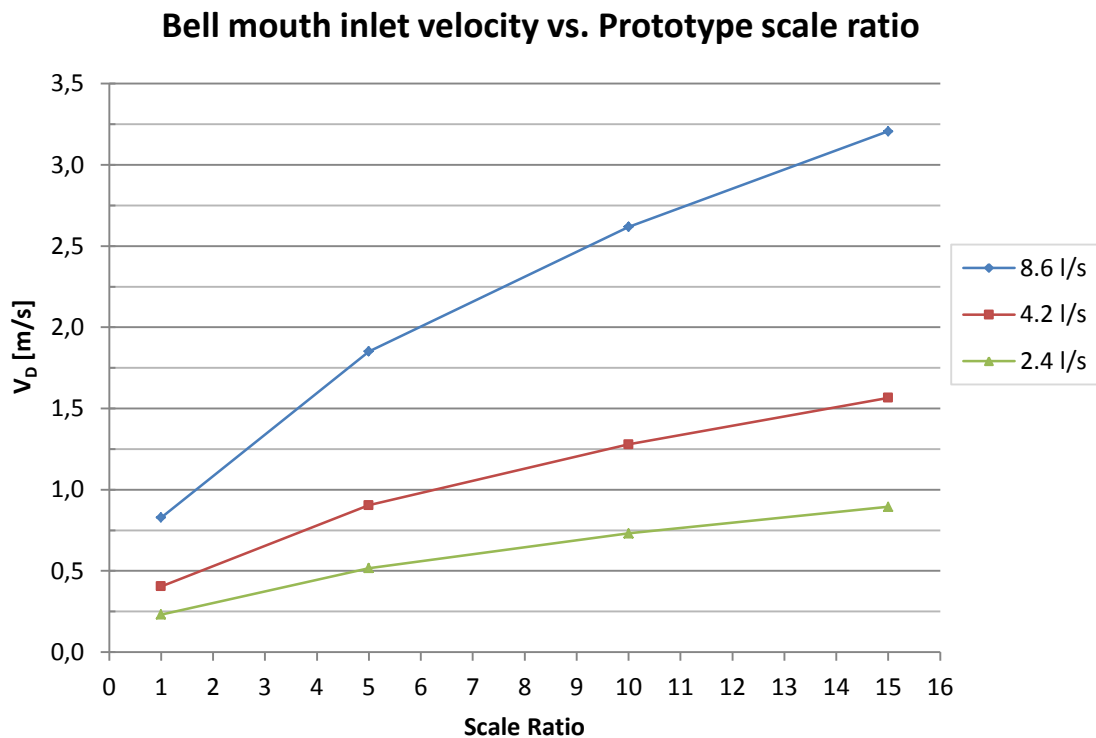
Figure 3.10 - Bell mouth inlet velocities vs. prototype scale ratio for various flow rates tested

The abovementioned flow rates proved a wide scope for application of the results when up scaling to prototype size. These were chosen as they provide modelling below, within and above the recommended ranges of 0.9 to 1.5 m/s. The author thought it would be beneficial to under and overshoot the recommended velocity ranges to check the capability of the CFD modelling for those extreme flows as well.

Physical Model Data

This section will discuss the data obtained from the physical model, its applicability and use as well as any tests or calibrations run to ensure that the data is of acceptable quality. The following types of data were obtained from the physical model:

- Flow rate
- 3-Dimensional point velocities
- Images and videos

Flow Rate

The flow rate was measured using the above mentioned Proline Promag 50W Electromagnetic Flow Measuring System. As mentioned above, no data recording from this instrument was possible, therefore periodic visual readings of the results were required. The flow rate was monitored on several occasions before the other data was obtained and then periodically while the data capture was in progress. The monitored flow rates were recorded by hand and later checked to ensure it was within an acceptable tolerance. The deviations from the required flow rate were all within a 1% tolerance, which is acceptable.

3-Dimensional Point Velocities

The point velocities were measured using a Nortek Vectrino Velocimeter, which as described above makes use of the Doppler Effect to measure particle velocities in the flow. The ADV measures the point velocities at a distance of 50 mm away from the probe reducing the interference caused to the natural flow characteristics. The addition of the top mounted rail system and the removal of the pump from the tank frame were all carried out in an attempt to reduce the vibration that could affect the ADV.

The ADV is very sensitive to noise in the measured fluid, therefore adequate seeding is required in the fluid to reduce the noise and enable usable readings. The seeding materials provided by the manufacturer of the instrument are very expensive, therefore cheaper alternatives were investigated.

Due to the improved operation of the ADV in natural streams, fine sand was chosen as one of the seeding materials to test. The OEMs seeding material is generally glass beads, strictly controlled for size to ensure neutral buoyancy. The other material chosen was glass micro balloons; these are generally used in fibre glass work to thicken epoxies to use as filler. Although these are not strictly controlled to ensure neutral buoyancy, after a short while, those that are heavier or lighter tend to float or sink out and only the more adequate ones remain in suspension. An added advantage of the micro balloons that float on the surface is the increased visibility of surface swirl and other vortex action.

Velocity measurements were taken in a bucket with still water with each respective seed material as well as clean water. Figure 3.11 below shows the ADV measuring the "zero velocity" flow in the bucket.

Figure 3.11 - Test setup for determining the best seed material, in still water

The fine sand showed considerable improvement over the clean water readings; however there were still too many spikes in the recorded data. The micro balloons had the highest average Signal-to-Noise Ratio (SNR) of all the tests (with the lowest being 17,7 above the minimum of 15 as recommended by Lohrmann, Cabrera and Kraus (1994)) as well as the best average correlation (all above 95%) for the still water tests in the bucket. It was therefore chosen as the preferred seed material and it was used for the flow tests in the sump. Three test points were measured in the sump, at 137 mm from the sump floor along the centre line of the sump at 2900 mm, 2000 mm and 225 mm, from the back wall, respectively. The water level was set at 235 mm and the flow rate was 8.77 l/s. Figure 3.12 shows the velocity comparison in the x-direction (Normal to flow direction) of the clean water and the micro balloon seeding at point 2 (x =0 mm, y = 2000 mm and z = 137 mm), as this is the lateral axis in the sump, it has much lower flow velocities and is therefore more prone to noise.
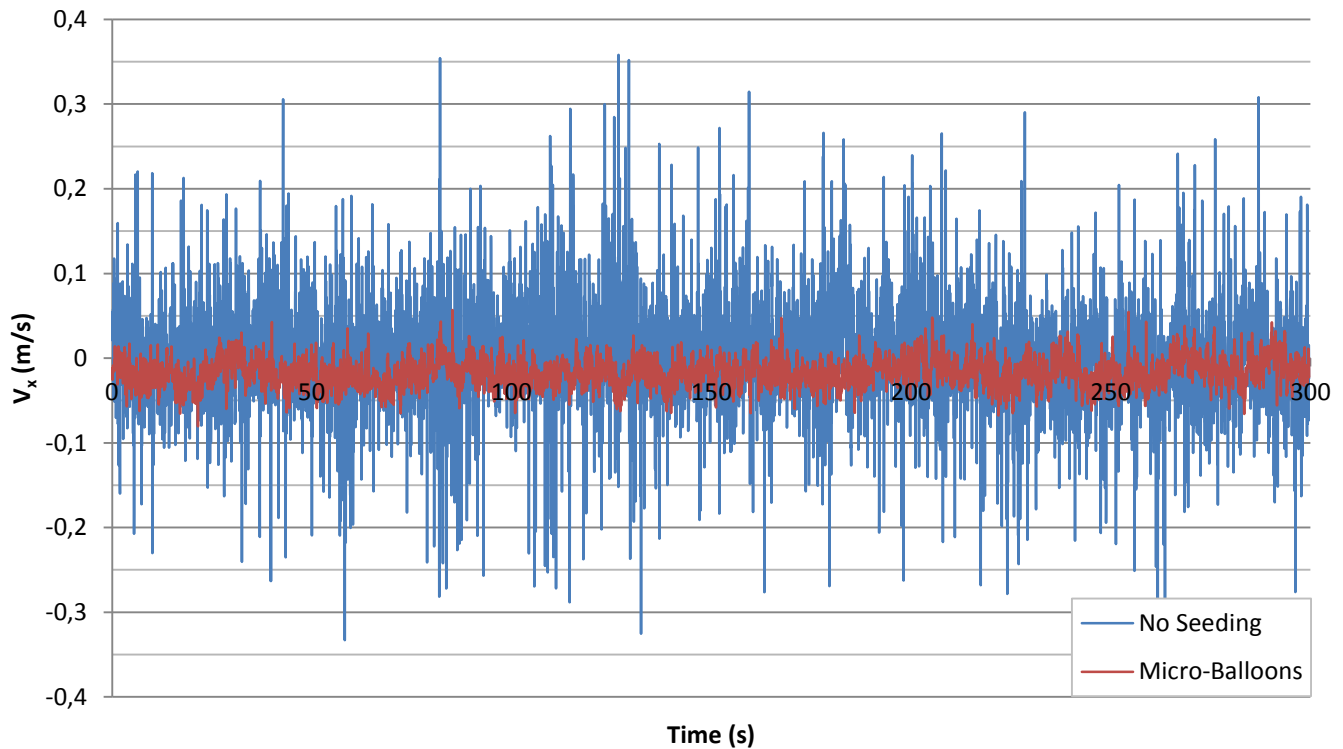
Figure 3.12 - Velocity in the lateral direction without seeding (blue) and with micro balloons (red)

Visual inspection of Figure 3.12 above leads to the conclusion that the clean water readings result in unacceptably large noise spikes which severely distort the final average velocities. The seeded flow indicates spikes on a much smaller scale and a general trend can be seen, most likely due to turbulences in the flow passing through the sample volume of the instrument.

The micro balloons were chosen as the preferred seed material, being both effective and relatively cheap. The velocity readings where micro balloons were used showed improvement compared to the other materials and the average SNR and correlation values were well above the recommended values for lab tests of 15 and 70% respectively.

The sample count of the velocity measurements made by the ADV is an important factor in the quality of the results of average point velocity in a turbulent flow. Therefore a test was carried out to determine the minimum acceptable count to accurately represent the average point velocity.

An overhead crane was operated in the lab while the first test was carried out. Due to the VSD supplying a relative frequency to the pump, this could have resulted in reduced flow rates. As the flow rate is only monitored and not recorded, due to location of the flow meter

and lack of available recording equipment, this could not be verified after the testing was complete. Furthermore discussions will relate to the second test in which more samples were recorded in the sample count analysis and when there was no heavy machinery in use at the time of testing.

The sample count sensitivity was analysed from a count of 25 up to a count of 10 000 with varying resolution. The number of counts for each test was as follows 25, 50, and 100 then in increments of 100 till 1000 then increments of 1000 till 7000 and 10 000 samples. The ADV was set up to measure at 25 Hz, thereby allowing the time of measurement, in seconds, to be easily calculated by dividing the sample count by 25. The flow rate and temperature of the water was for practical consideration, steady. The position of the measurement point was in the centreline of the sump at a height of 60 mm from the sump floor and 615 mm from the back wall. Figure 3.13 shows the average velocity magnitudes calculated from each test plotted against sample count and in Figure 3.14 the average velocity components can be seen plotted against sample count.
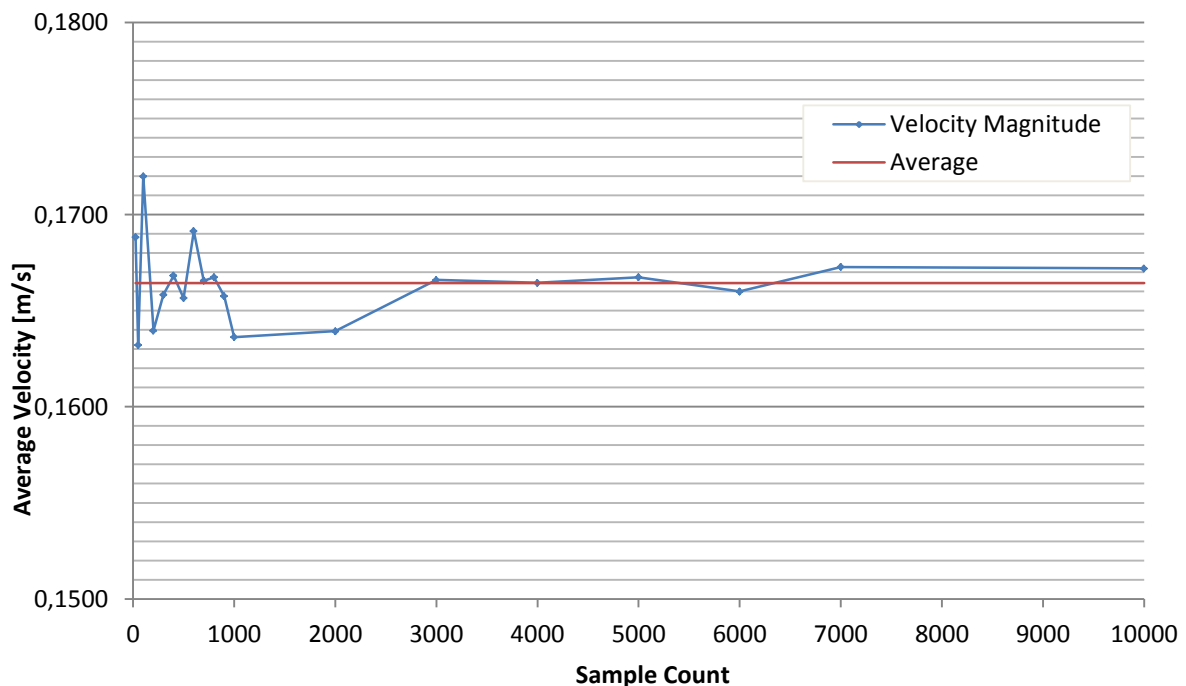
Figure 3.13 - Average velocity magnitude vs. sample count

The average indicated in Figure 3.13 is the arithmetic average of the mean velocity magnitudes from each test at the various sample count numbers which are biased due to the short measurement period.
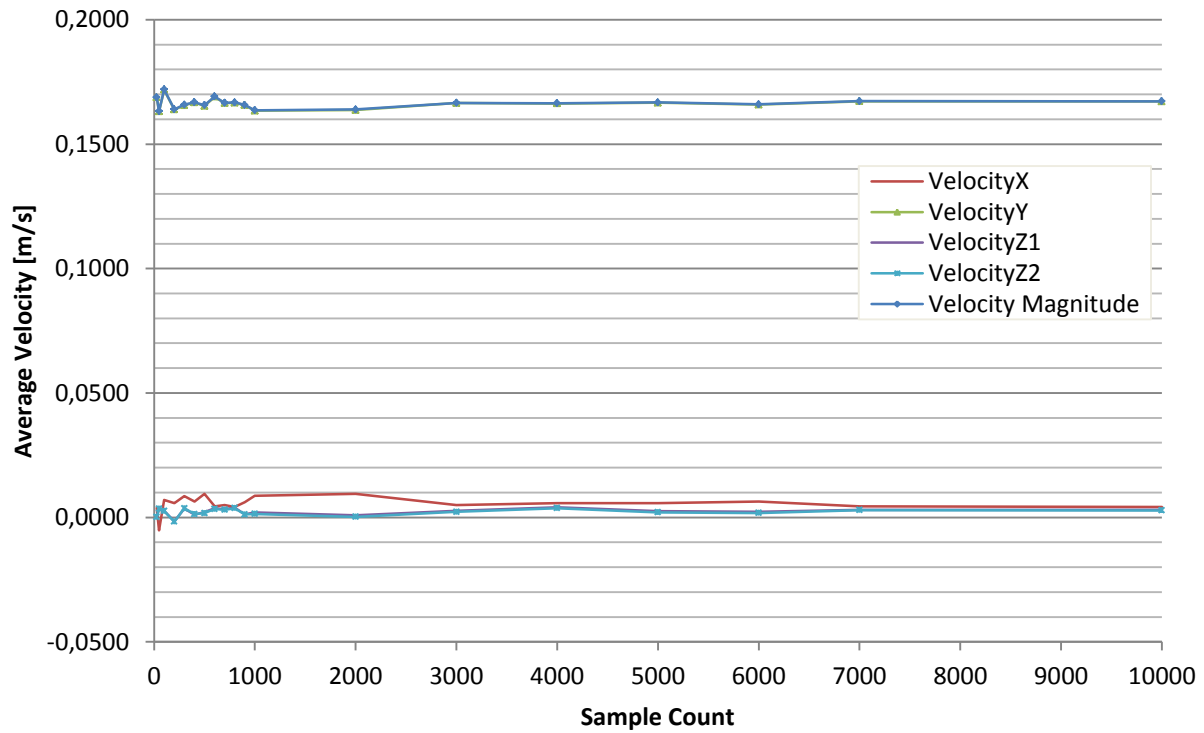
Figure 3.14 - Average Velocity Components vs. Sample Count

Turbulences in the flow can cause either high or low biased results depending on the state of the flow at the time of measurement. Sufficiently accurate averages are achieved with sample counts of 3000 or higher.

The velocity components for each test are indicated in Figure 3.14, and it can be seen that the Y-direction is the primary direction of the flow with the X-, Z1- and Z2-directions velocities being less than 0,01 m/s (roughly 6% of the main flow stream velocity).

The chosen sample count for the main test series was chosen as 3000 samples per point, which corresponds to 2 minutes or 120 seconds of flow time. This value was chosen for practical reasons, as each main test consists of 51 points, to enable the tests to be carried out within one day to ensure that the fluid properties and flow rate remain sufficiently constant. Figure 3.15 below shows the points that will be measured.

The above tests were carried out to ensure that the velocity data recorded was usable, although it would still require certain processes to remove spikes from it. That, however, will be discussed in section 3.3.3 below.

The ADV picks up on a lot of noise in the fluid, and as has been mentioned above, the flow seeding was investigated in order to reduce this noise. The ADV also gives a velocity reading in 'zero-flow', which is dependent on the nominal velocity range and sample volume settings. This was measured with the seeded flow in the sump for the two velocity and sample volume settings used. The velocity magnitudes for the two tests can be seen in Table 1 below.

Table 1 - zero-flow velocity readings from ADV with micro-balloon seeding

Nominal Velocity Range [m/s]	Sample Volume [mm]	Velocity Magnitude [m/s]
±0.3	7.0	0.0135
±0.1	2.5	0.0066

The above zero-flow velocity readings were not accounted for in the data analysis, but are mentioned here to inform future researchers about this occurrence. The zero-flow velocities can be substantial when measuring low velocity flows, or in the low velocity cross-flow direction in a fairly steady flow.

The ADV settings were tested with the tests above and the optimum ones used resulting in acceptable data for use as the main data in the quantitative analysis between the physical and CFD models. As previously mentioned the data does go through some manipulation before use, and this will be discussed in the analysis section below.

51 points were measured using the ADV. Figure 3.15 below shows the location of these points. The points are named, for example, as follows @165-D2W1 which refers to a point at 165 mm from the back wall, 60 mm from the sump floor and at 75 mm from the centre line. The naming convention used for the points is as follows:

- @165 - indicates the distance in mm from the back wall
- D2 - indicates the height in mm from the sump floor
- W1 - indicates the distance in mm from the centre line

There are three depth locations, three width locations and 6 stations along the length of the sump; they can be seen in Figure 3.15 below.
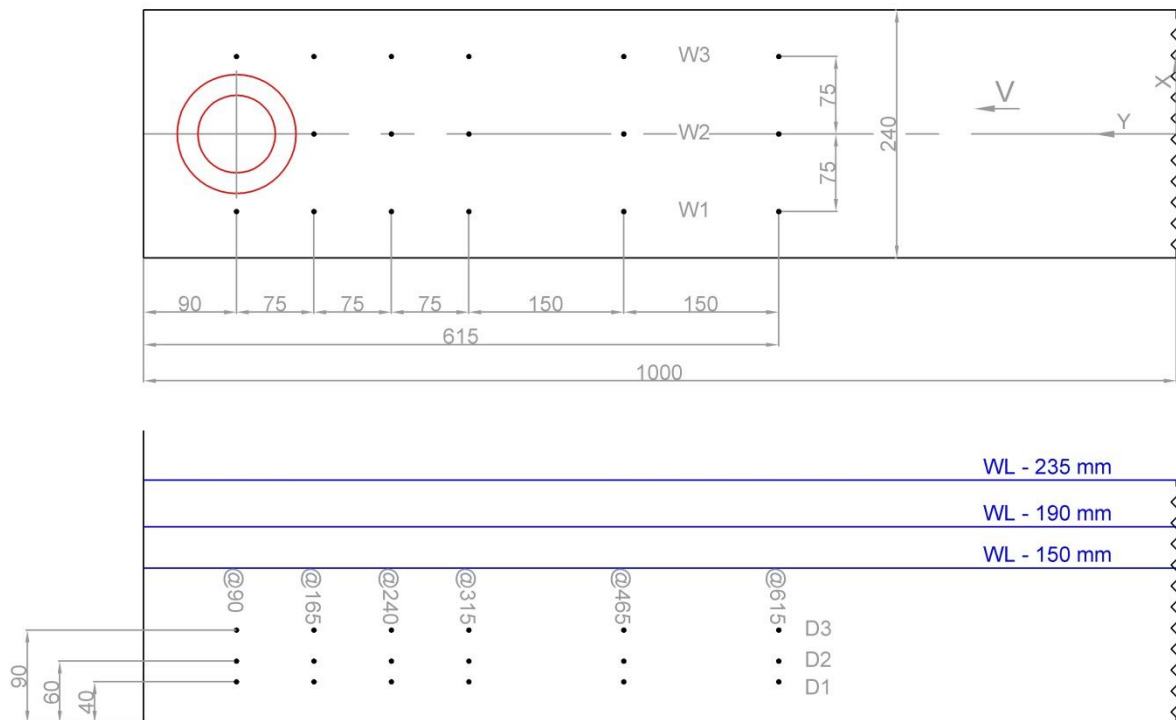
Figure 3.15 - Measuring points used for the comparison of the CFD and physical models

Photography and Video Recording

The photographs and videos recorded are to be used for qualitative analysis only. They highlight flow patterns, vortex location (of the surface and submerged type), vortex size and vortex type as well as any dye traces.

Full manual control was used on the camera to ensure the best defined images were captured. Black back screens and black covers were placed over the tank and the camera which was taking the photographs and videos in order to reduce reflection and unwanted light.

3.3.3   Analysis

The research instruments, the data they gather and various checks done to verify that it is sufficiently accurate were mentioned in the previous sections of this chapter. Now the focus moves to the analysis of the data. Techniques used to despike the ADV data will be described and the method of comparing the physical and numerical results discussed.

ADV Data

The ADV data is inherently noisy, and the outliers, further referred to as spikes, in the data need to be removed in order to obtain a reasonable sample for statistical purposes. There are numerous methods for dealing with these spikes, as discussed by Goring and Nikora (2002). It was decided that a simple method be used, defining acceptable data as:

$$\mu_s - 3\sigma_s < x_i < \mu_s + 3\sigma_s$$

With μ_s is the sample mean and σ_s the standard deviation of the sample. Assuming the data follows a normal distribution, the above formula includes 99.7 % of all real (non-outlier) data points. It was accepted that 0.3 % of the real data may be removed. Once the spikes were detected, they were replaced by using the sample mean. Though this still contains the bias from the data including the spikes, it was accepted as it is a significant improvement over the raw data.

The algorithm was implemented in Microsoft Excel, and therefore using simple spreadsheet functions, it had to be executed in a stepwise manner. First all spikes in the velocity component along the positive y-axis were identified and the entire row of data, each velocity component, replaced with the means calculated from the raw sample, followed by the same process for the negative y-axis. The same was then done for the positive and negative x-axes. A single iteration of the abovementioned steps significantly improved the data and it was therefore decided not to run additional iterations. The algorithm for a single axis can be seen in Figure 3.16 below. As this is for a single axis, it was carried out twice, once for the y-axis (longitudinal axis) and then for the x-axis (lateral axis).
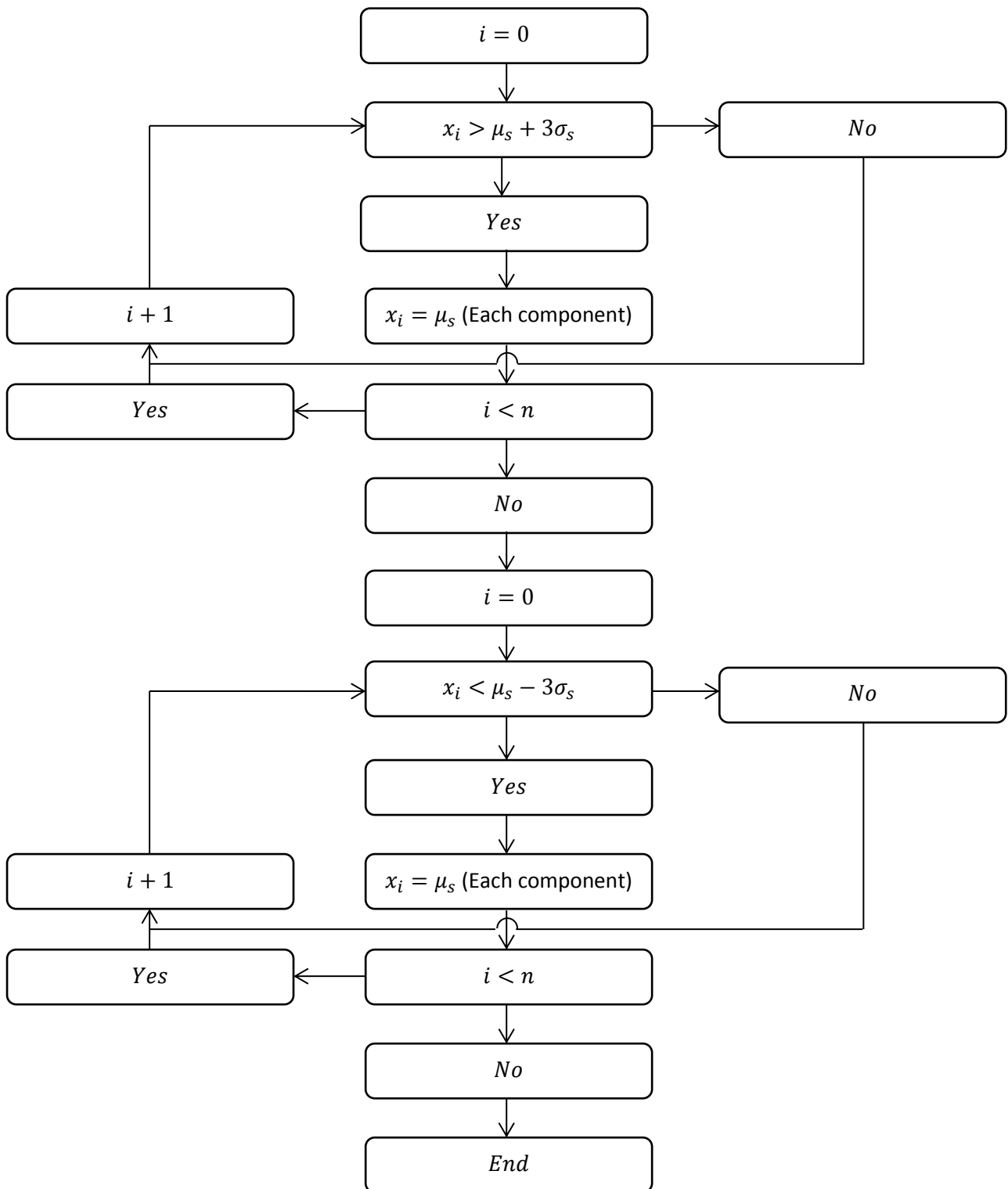
Figure 3.16 - Despiking algorithm used to remove outliers from the dataset on a single axis

The velocity magnitude was calculated using two methods, one based on the mean values of each component and the other based on the mean of the magnitudes calculated for each data

point. The raw data showed large differences between these two methods, however the despiking technique decreased this difference significantly.

The despiking technique proved simple yet effective and Figure 3.17 below is an example of the technique applied to a data sample for the velocity magnitude in the lateral direction of the sump which contained a large amount of noise. A significant improvement is evident from visual inspection of the graphs.
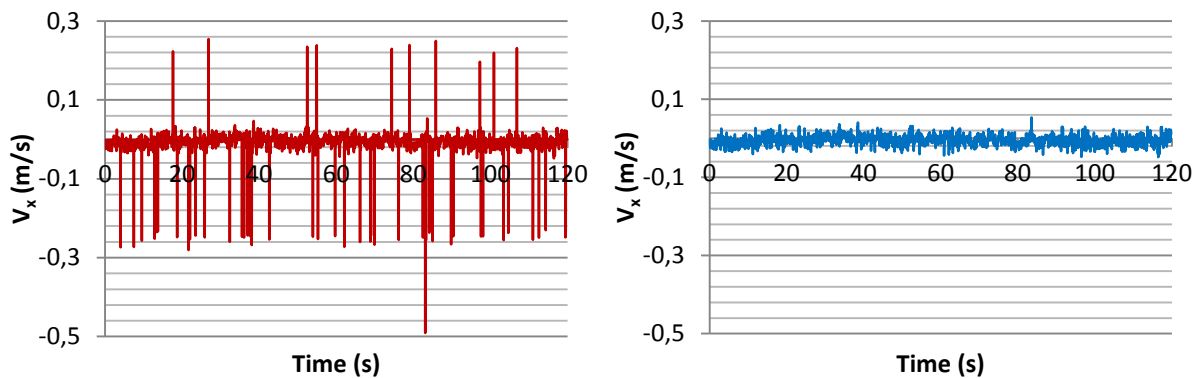
Figure 3.17 – Despiking algorithm applied to velocity magnitude in the lateral direction - raw data (red/left) and despiked data (blue/right)

A spreadsheet was set up for each data point, with various tabs displaying the raw data, each of the four phases of despiking (+y, -y, +x and −x axes), graphs indicating each velocity component (x, y, z_1 and z_2) and despiked graphs for the x and y-components, graphs indicating the SNR for each velocity component as well as graphs indicating the correlation for each velocity component. A spreadsheet containing the calculated velocity magnitude for each of the 51 data points in a test was then set-up and linked to the 51 data point spreadsheets linking both the calculated velocity magnitudes as described above.

The data was then linked to a spreadsheet containing the instantaneous and averaged velocity data from the CFD simulation and the graphs of the velocity magnitudes, along the 9 lines as defined in Table 2 (Section 3.4.2) from the various models were plotted against each other. This was then used as the primary quantitative analysis resource.

Photograph and Video Analysis

The photographs and video recordings were analysed visually and compared to the contour and vector plots obtained from the CFD simulation as well as any relevant visual observations made by the author during testing.

3.4   Methodology – CFD

Sections 3.1 to 3.2 above discuss a general overview of the type of research methods used for the collection, analysis and comparison of data obtained from the physical model. The ensuing section will detail how the methods were implemented for the CFD model as well as provide details regarding the research instruments, the data obtained with the research instruments followed by the analysis of that data.

3.4.1   Research Instruments

The research instruments that were used for the CFD modelling are as follows:

- Dell Optiplex 980 for running Simulations
- ANSYS 14.0
- Spreadsheets for input calculation

The equipment used for the CFD modelling is listed above and details will now be given individually.

Simulation Computer

The computer used for the computation of the CFD model was a Dell Optiplex 980 Tower system running Windows 7 Professional. The specifications are as follows:

- Intel i7-870 Quad Core CPU @ 2.93 GHz
- 16 GB RAM

- 1 TB HDD
- ATI Radeon HD 4550 graphics card

The computer was primarily operated by means of remote login using the integrated Windows Remote Desktop function.

Simulation Software

An academic version of ANSYS 14.0 software suite was used for the CFD modelling. The modules Design Modeller, Meshing and Fluent were used for the geometry creation, mesh generation and solving respectively.

Input Calculation

A spreadsheet was set up to calculate inlet velocity (upstream boundary condition) and outlet pressure (downstream boundary condition) input parameters for the CFD model in order to achieve the correct water levels and flow rates. The spreadsheet required the following input:

- Flow rate
- Water level
- Distance from water surface to suction pipe boundary
- The loss coefficients for the bell mouth and the pipe

The spreadsheet then calculates the various velocities and by applying the Bernoulli equation, calculates the required suction pressure.

A second spreadsheet was set up in order to verify the suction pressure based on the water levels obtained from CFD simulation. This spreadsheet simply uses linear interpolation to approximate the simulated water level, assuming the water surface is indicated by a volume fraction of 0.5. The input to this spreadsheet was in the format of an output file from ANSYS Fluent, being two vertical rakes plotted with 99 points at two locations down the centre line of the sump with the volume fraction at each point plotted against z-axis value.

3.4.2 Set-up and Data

This section will discuss the data obtained from the CFD model, its applicability and use as well as any tests runs to ensure that the data is of acceptable quality. The following types of data were obtained from the CFD model:

- Water level checks
- Point velocities
- Contour and Vector plots

Before more details regarding the various types of data is given below, tests and checks carried out on the model will be discussed.

Various mesh types and sizes were generated and tested to obtain a small mesh which yielded acceptable results. Unstructured meshes were tested, which yield higher element counts for the same maximum and minimum element size compared to the cut cell method as well a less defined water surface.

Geometry Set-up

The geometry set-up for the CFD model was carefully considered, to enable the inlet flow to be at the correct water level, while maintaining a simple mesh creation process and solver set-up. It was decided that the easiest method to satisfy the above mentioned conditions was by the use of two main volumes within the model, the volume primarily occupied with water and the other occupied with air. The model was created as such and the bell mouth and suction pipe wall thickness was removed from the combination of the water and air volumes which can be seen in Figure 3.18 below. This allowed for a simple yet complete model of physical set-up as well as the easy modelling of the inflow, providing a constant water level for the approach flow. The CFD model was modelled on the physical model with the full sump width of 240 mm, and had a section of the length at 1000 mm in order to reduce computational time. The water volume was dimensioned to suit the depth of the water and the air volume had a thickness 60 mm.
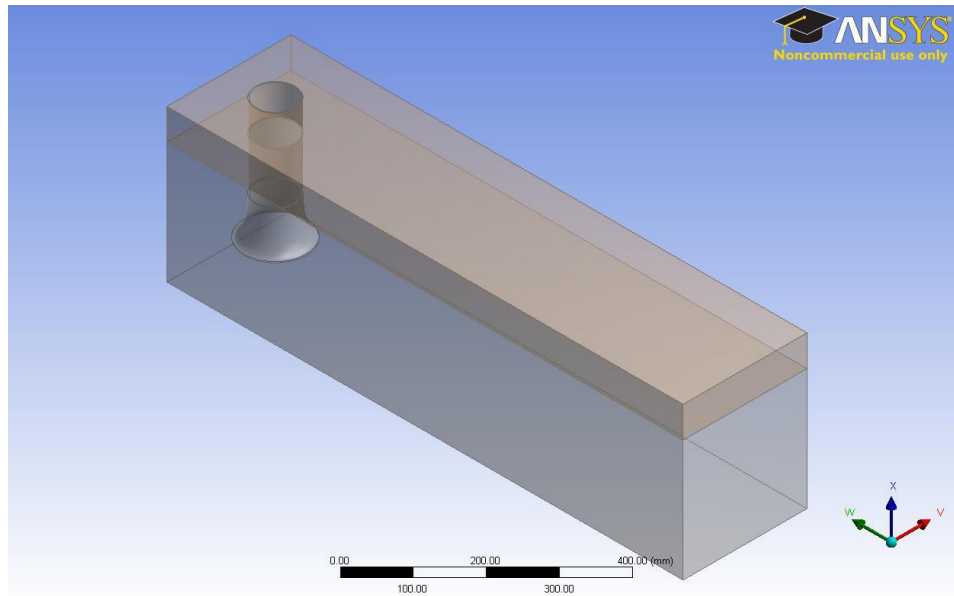
Figure 3.18 - CFD model Geometry

In-Fluent Mesh Refinement

A low element count unstructured mesh was generated and set-up to solve for the highest flow rate at the highest water level. This simulation was run for several thousand iterations after which the mesh refinement capability of ANSYS Fluent was used to refine the mesh in strategic locations. These locations included areas of high velocity, areas of high velocity gradient, areas of high Reynolds number, and areas of high vorticity and the maximum size of cells. The refinement method worked well in terms of generating a solution in a short period of time, however, it was discovered that there were large errors in results due to inadequate mesh elements. Highly skewed elements were found which yielded velocities that were too high by a factor of 10^4. The method was attempted again and yielded very similar, unsatisfactory results. The method of using the refinement within ANSYS Fluent was discarded and it was decided to use the cut cell meshing scheme which will now be described.

Cut Cell Mesh

Originally a cut cell mesh (which can be seen in Figure 3.28) was to be used for the simulations. The cut cell meshes originally generated didn't adhere to the 'rules' of a mesh for the purpose of CFD simulations. They had unacceptably high maximum skewness and

were unsatisfactory. After revisiting the cut cell mesh generation, improved critical parameter settings were chosen, leading to a satisfactory mesh. Once water level adaptation was carried out, each water level required a new mesh, it was discovered that the parameters chosen for the mesh generation were highly satisfactory and did not require any changes for the various meshes that were generated.

With the critical parameters known, meshes with various cell counts were created. An attempt was made to stay below one million cells in the mesh in order to reduce computational time. Three meshes were generated with a 235 mm water level, with the following element counts for a fine, medium and coarse mesh respectively, 460 000, 860 000 and 960 000 cells. The mesh refinement didn't follow the usual half/double element size or cell count.

These three meshes were run at the high flow rate and high water level of 8.6 l/s and 235 mm respectively. The three models were then compared quantitatively by means of velocity comparisons along 9 lines running in the flow direction of the tank and qualitatively by visual analysis of animations of velocity vectors on planes parallel to the sump floor at various heights, namely 0.06 m, 0.1 m, 0.2 m and 0.235 m, for comparison of vortex size and location.

Comparison of the 3 Meshes

A comparison of the results of the three mesh sizes will be given, considering the quantitative and qualitative comparisons. Firstly, the quantitative comparison of the velocities in the sump will be discussed.

Quantitative Comparison

The quantitative comparison is done by means of the comparison of velocities along nine lines that run parallel to the general direction of flow in the sump, which is for this particular model in the y-direction(along the length of the sump). These nine lines were chosen to include all the points of velocity measurements that were taken by the ADV in the physical model. The lines are defined in Table 2 below. Figure 4.1shows these lines graphically.

Table 2 - Lines used for point velocity comparisons

Line	x [m]	y_0 [m]	y_1 [m]	Z [m]
1	-0.075	0.385	0.91	0.04
2	-0.075	0.385	0.91	0.06
3	-0.075	0.385	0.91	0.09
4	0	0.385	0.835	0.04
5	0	0.385	0.835	0.06
6	0	0.385	0.835	0.09
7	0.075	0.385	0.91	0.04
8	0.075	0.385	0.91	0.06
9	0.075	0.385	0.91	0.09

The velocity plots of the 3 models along six of the lines (lines 1 - 6) as defined above will be shown and a conclusion as to which model will be used for the further analysis of the sump. These six lines are representative of the tendencies of the velocities along the abovementioned lines in the sump. The bell mouth centre line corresponds to 0.9 m in the plots.
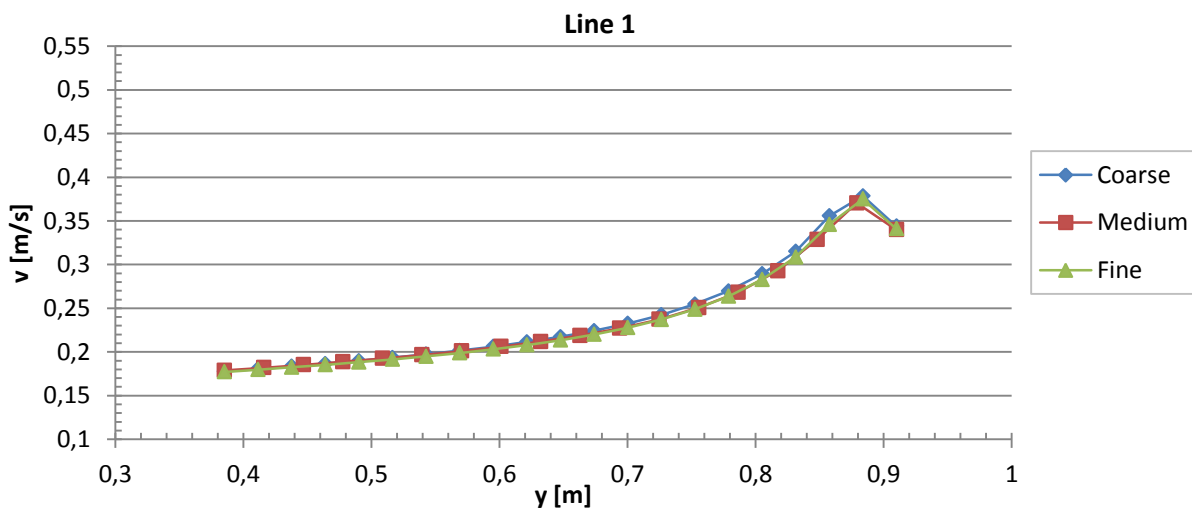
Figure 3.19 - Point velocities along line 1 as defined in Table 2
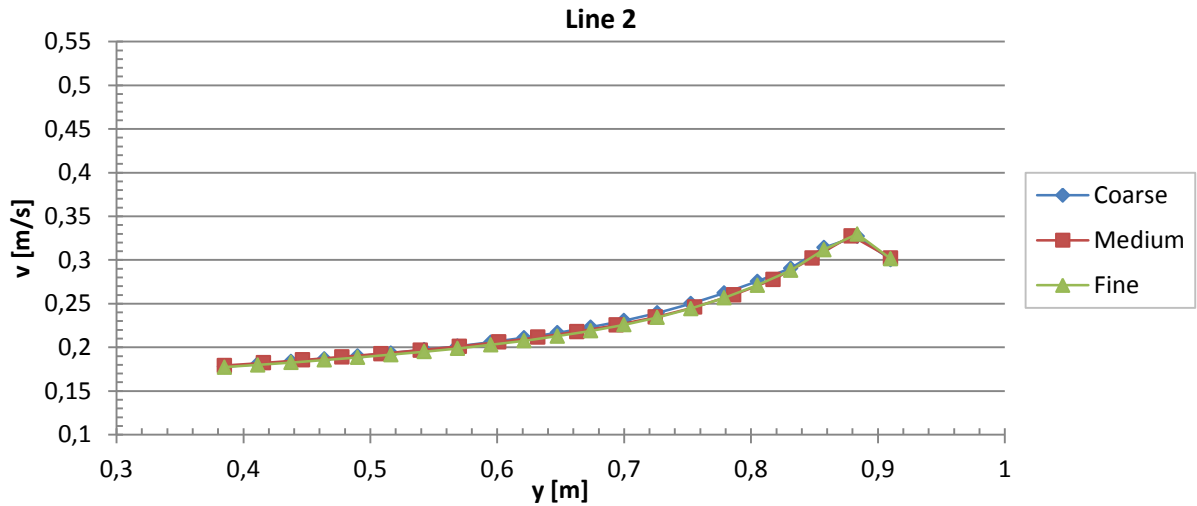
Line 2

Figure 3.20 - Point velocities along line 2 as defined in Table 2
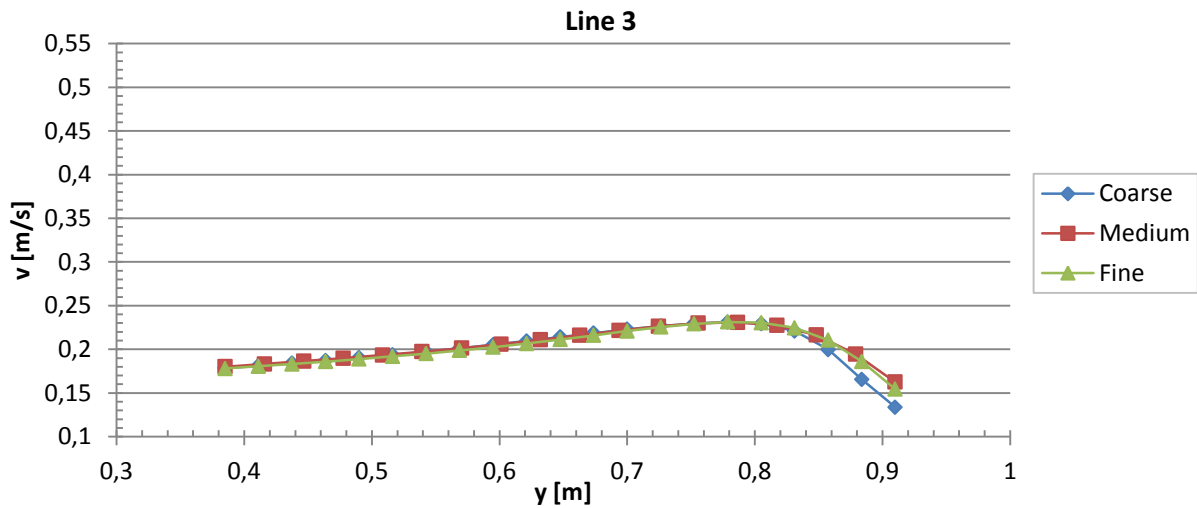
Line 3

Figure 3.21 - Point velocities along line 3 as defined in Table 2
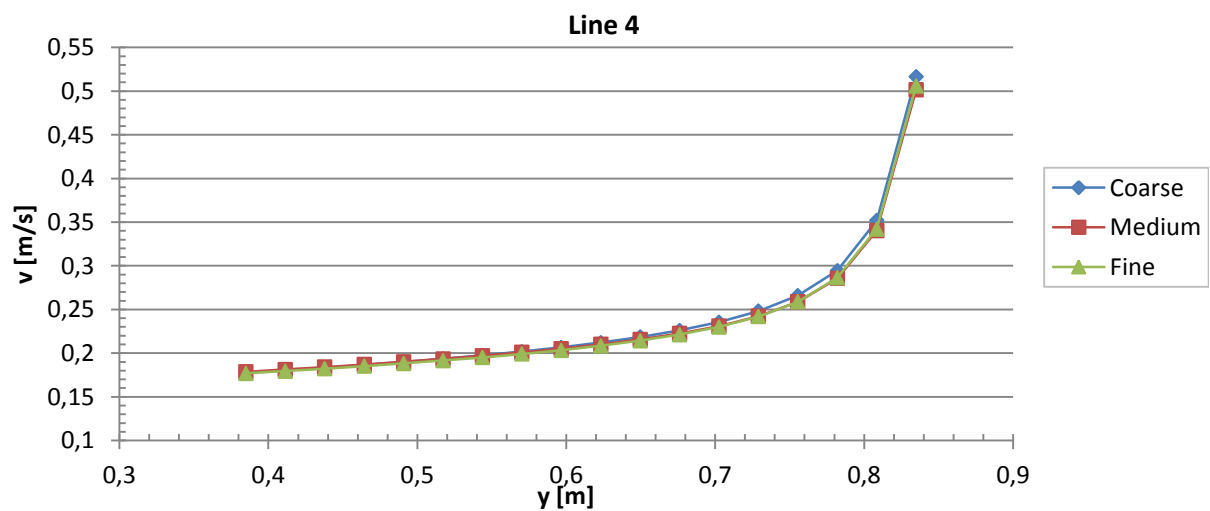
Line 4

Figure 3.22 - Point velocities along line 4 as defined in Table 2
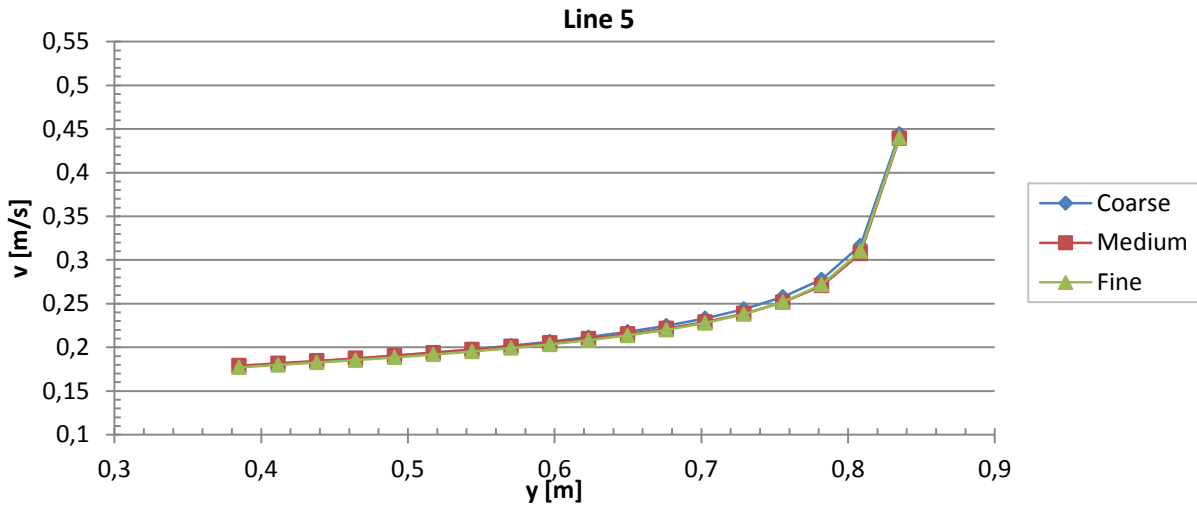
Line 5
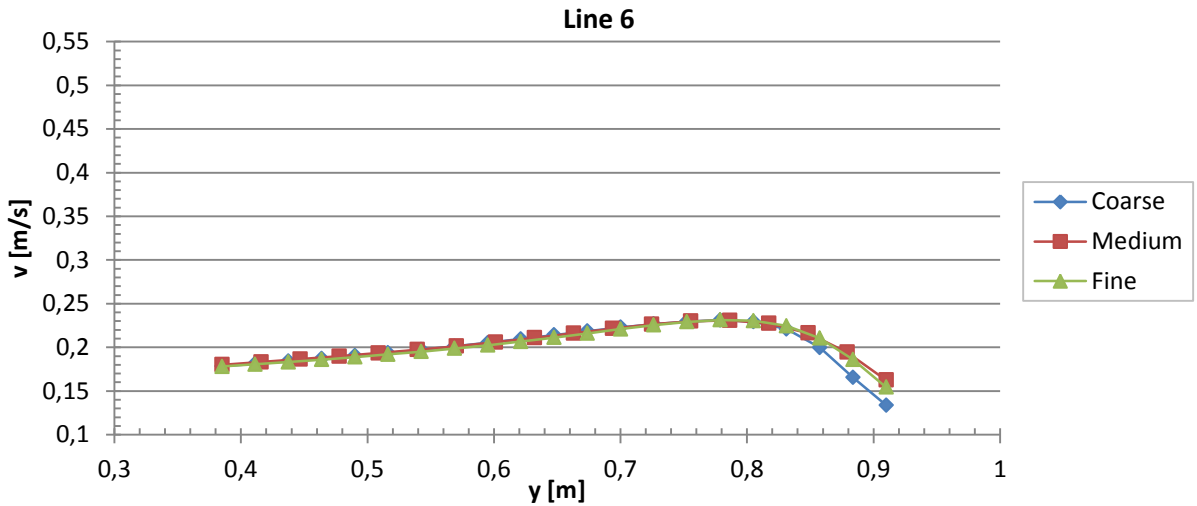
Line 6

Figure 3.24 - Point velocities along line 6 as defined in Table 2

Inspection of Figures 3.19 to 3.24 above, which show the velocity distributions along lines 1 - 6 in the sump, indicate that the coarse mesh is a good overall approximation of the medium and fine meshes, especially taking into consideration the significantly reduced computational time required to achieve numerical model convergence (Approximately half the time of the fine mesh). The coarse mesh was therefore chosen as the preferred mesh for further simulations due to the reduced storage required as well as the reduced computational time required for convergence.

Qualitative Comparisons

The qualitative comparison is carried out by means of a visual inspection of the velocity vector plots on various planes that are parallel to the sump floor. Not all planes plotted will be indicated, therefore only the plane with strongest indication of a vortex will be shown. These plots are then compared for vortex location, rotation and estimated size.
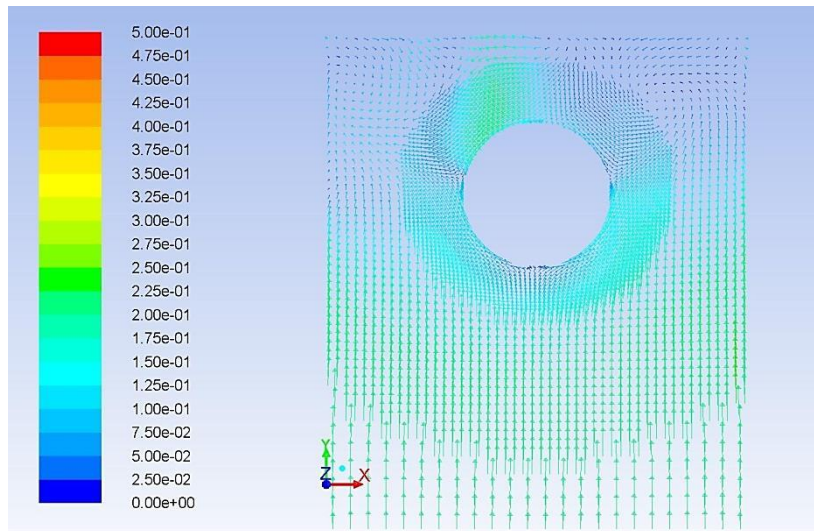
Figure 3.25 - Coarse mesh, velocity vectors coloured by magnitude, z = 0.1 m [m/s]
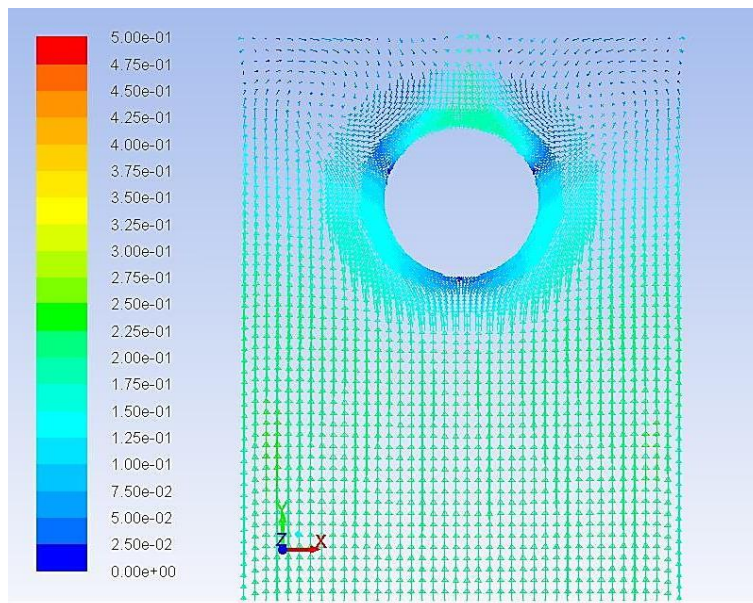
Figure 3.26 - Medium Mesh, velocity vectors coloured by magnitude, z = 0.1 m [m/s]
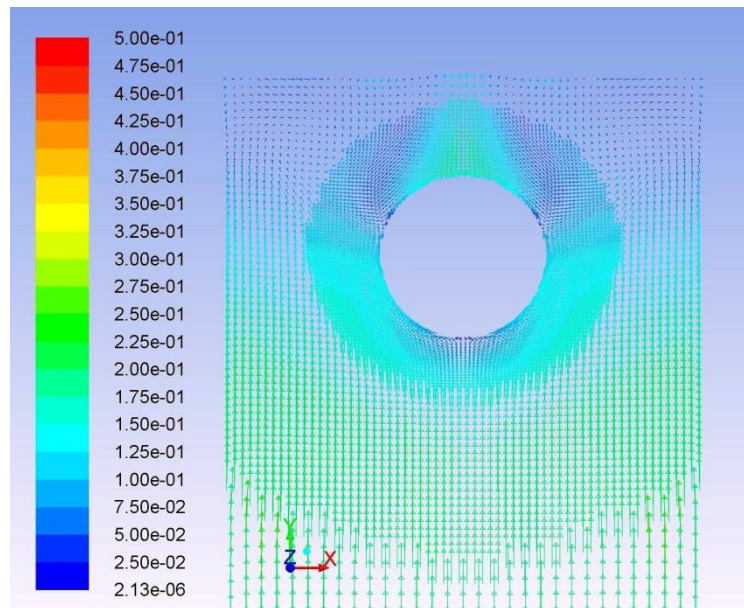
Figure 3.27 - Fine Mesh, velocity vectors coloured by magnitude, z = 0.1 m [m/s]

Inspection of the Figures 3.25 to 3.27 above indicates a steady vortex formation on the right hand side of the bell mouth. The coarse mesh has a vortex on the left hand side of the bell mouth, but more in the corner of the sump, whereas the medium and fine meshes indicate a more symmetrical vortex formation. This could be due to the stage of the transient simulation, as vortices are generally unsteady and move around continuously. Based on the previous quantitative analysis and the above qualitative analysis, it was decided to use the coarse mesh for further simulations as it appears to model the flow in the sump with adequate precision and indicates good comparison to the finer meshes. It had a much lower computational time requirement, which was a large factor when choosing a mesh.

A cross-section of the mesh, for the model with a 235 mm water level, down the centre line can be seen in Figure 3.28 below. This image as well as various other images of the 3 meshes can be seen in full size in Appendix B.
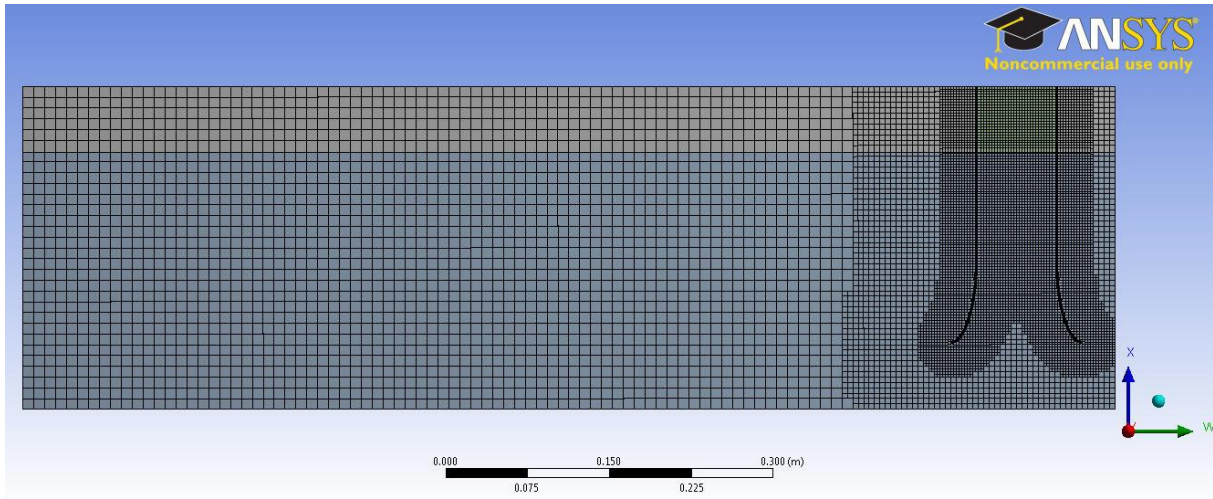
Figure 3.28 - Longitudinal section of the mesh for the model with a 235 mm water level

The details of the chosen mesh can be seen in Table 3 below. The number of nodes, element count as well as the maximum skewness and minimum orthogonal quality are indicated. The quality check values of maximum skewness and minimum orthogonal quality are both within the acceptable limits of < 0.98 and > 0.2 respectively.

Table 3 - Mesh statistics for the various cut-cell meshes used for the simulation

Water Level [mm]	150	190	235
Nodes	351 727	417 191	493 501
Elements	325 381	387 466	460 061
Maximum Skewness	0.949	0.943	0.955
Minimum Orthogonal Quality	0.445	0.444	0.317

Boundary Conditions

The geometry design and mesh generation have been discussed above and now the focus will be on the boundary conditions. The boundary conditions of the inlet, air vent and the outlet will be briefly described with the main parameters indicated in Tables 4 to 7. The indicated values for the boundary conditions are for the case of a 235 mm water level and a flow rate of 8.6 l/s.

The inlet was of rectangular section and spanned the full width of the channel with the height being that of the water level for that respective test. It was specified as a velocity inlet and the critical parameters were defined as in Table 4 below. The turbulence intensity was specified as a relatively low value due to the uniform appearance of the flow in the physical model at the location where the CFD model starts, however this is one of the parameters to be discussed in the Chapter 8.

Table 4 - Velocity inlet specification (Water level: 235 mm, Flow rate: 8.6 l/s)

Velocity Inlet		
Momentum		
Velocity Specification Method	Magnitude, Normal to Boundary	
Reference Frame	Absolute	
Velocity Magnitude (constant)	0.1525	m/s
Supersonic/Initial Gauge Pressure (constant)	0	Pa
Turbulence		
Specification Method	Intensity and Hydraulic Diameter	
Turbulent Intensity	10	%
Hydraulic Diameter	0.16	m

The model study focused on the flow within the sump only and not on the flow characteristics further up the suction pipe, therefore the suction pipe was only modelled up to 60 mm above the water level. The outlet was defined as a pressure outlet on the inner diameter of the suction pipe. The details for the specification of the outlet values are shown in Table 5 below. The outlet pressure was calculated by means of a spreadsheet as discussed in section 3.4.1 above.

Table 5 - Pressure outlet specification (Water level: 235 mm, Flow rate: 8.6 l/s)

Pressure Outlet		
Momentum		
Gauge Pressure	-3468	Pa
Backflow Direction Specification Method	Normal to Boundary	
Turbulence		
Specification Method	Intensity and Hydraulic Diameter	
Backflow Turbulent Intensity	10	%
Backflow Hydraulic Diameter	0.072	m

The boundary condition for the air vent, being the horizontal plane 60 mm above the water level, was specified as the outlet vent type. This type of boundary condition indicated the best results for this boundary while maintaining a stable solution process. The air vent is a boundary open to the atmosphere, and was specified as indicated in Table 6 below.

Table 6 - Outlet vent specification (Water level: 235 mm, Flow rate: 8.6 l/s)

Outlet Vent		
Momentum		
Gauge Pressure	0	Pa
Backflow Direction Specification Method	Normal to Boundary	
Turbulence		
Specification Method	Intensity and Hydraulic Diameter	
Backflow Turbulent Intensity	1	%
Backflow Hydraulic Diameter	0.2	m

Solver set-up

The solution methods used for the simulations in ANSYS Fluent are summarized in Table 7 below. The PISO algorithm was used due to its ability to maintain stability with a large time step, thereby allowing shorter simulations to obtain the required flow time. The second order upwind settings were used to obtain a higher degree of accuracy within the results.

Table 7 - Summary of solution methods used in Fluent

Pressure Velocity Coupling	
Scheme	PISO
Skewness Correction	1
Neighbour Correction	1
Skewness-Neighbour Coupling	Yes
Spatial Discretization	
Gradient	Least Square Cell Based
Pressure	Body Force Weighted
Momentum	Second Order Upwind
Volume Fraction	Second Order Upwind
Turbulent Kinetic Energy	Second Order Upwind
Turbulent Dissipation Rate	Second Order Upwind
Transient Formulation	Second Order Implicit

Simulation plan

The simulation was run as a steady state second order simulation for 2500 iterations to stabilize the mass flow rate monitors and residuals and reach acceptable convergence, followed by the initial transient state as discussed above for 1000 time steps, with 20 iterations per time step, to re-stabilize the mass flow rate monitors and obtain acceptable convergence for a final solution, which it was decided would be a mass flow difference of less than 1.5 % of the mass flow rate on the inlet.

Water Level Checks

The water levels indicated by the simulation were checked on a spreadsheet to ensure that the values are within an acceptable tolerance. As mentioned above, a spreadsheet using linear interpolation of volume fraction values along a 99 point rake was used to determine the simulated water levels. This data allowed the verification that the numerical model is in an adequate state for comparison to the physical model.

Point Velocities

The velocity magnitudes at 51 points in the model were extracted to be used for the comparison to the physical model results.

The CFD model was run in the implicit transient state, therefore the flow was 'steadier' than it would have been if run in the explicit state, therefore the instantaneous and average velocities did not differ significantly. The average velocity magnitudes were obtained by activating the Data Sampling for Time Statistics option in ANSYS Fluent and running the model to obtain 25 s flow time.

Contour and Vector Plots

Contour and vector plots on various planes were used for qualitative comparison with the photographs and observations from the physical model. These plots provide insight into vortex location, size, direction of rotation and water level, among other things. Interesting flow characteristics where two main flow streams meet near the bell mouth can be visualized using vector plots along a vertical plane

3.4.3   Analysis

Velocity Data Analysis

Two types of velocity data was obtained from the CFD model. Namely time averaged point velocity magnitudes and instantaneous point velocity magnitudes. These were then imported into a spreadsheet where they were plotted against the processed data from the physical model. The differences in the instantaneous and averaged data were small; therefore the main comparison graphs in this thesis contain only the time averaged and physical model velocity data.

Contour and Vector Plot Analysis

The contour and vector plots obtained from the CFD simulation were plotted on planes identified by observation of the physical model and were analysed visually and compared to the photographs and videos obtained from the physical model.

3.5   Limitations – Physical Model

This section will discuss the limitations relating to the physical model. The limitations relating to the physical model will be discussed with focus on equipment limitations as well as limitations of manufacturing model components.

The limitations for the physical model range from tasks the available instrumentation was unable to perform, instrumentation that was not available, manufacturing constraints as well as financial restraints.

The limitations relating to the ADV will be discussed first, in list form followed by a brief discussion. The ADV is unable to:

- Measure behind the bell mouth
- Measure below the bell mouth entrance level when the probe is near the bell mouth
- Measure within 45 mm of the side walls
- Measure in close proximity to the glass sump floor due to excessive noise caused by the reflections
- Generate velocity profiles. Only single point velocities can be measured
- Measure nearer to the water surface than approximately 58 mm

Elimination of the limitations would yield a study that includes velocity profiles in the sump as well as behind the bell mouth would yield more data for comparison in critical areas. Originally it was proposed that the velocity profile on the physical model be measured and used as input for the CFD model. The ADVs limitation of 45 mm wall clearance resulted in measurement of areas of near constant velocity only. Analysis of the CFD model indicated that this change in velocity starts to be evident at a distance of 40 mm from the side wall and nearer.

The ADV did not allow for the two lowest points alongside the bell mouth to be measured, as the probe contacted the bell mouth and was unable to measure deeper than the 60 mm bell mouth height.

The lack of a data logger to be used with the flow meter meant no verification could be done after testing to ensure that the flow rate was acceptably constant. This could have been used to check and compare the flow rates of data entries with unusually high or low velocities compared to the averages. It would have been an extra measure to filter the ADV data with.

The use of a Laser Doppler Anemometry (LDA), Laser Doppler Velocimetry (LDV) or Particle Image Velocimetry (PIV) system would have allowed the generation of higher resolution data, which would allow vector plots along certain planes. The PIV system would even allow contour plots, much like those which are obtained from the CFD simulation. This would allow a more precise comparison.

The manufacturing constraints mentioned above are in reference to the manufacture of the bell mouth. Originally, more than one bell mouth was to be tested to investigate the effects of varying the shape. Since manufacturing the standard bell mouth was an issue, it was decided to focus on it alone and not construct other shapes. The manufacturing of the additional bell mouth would have had to be outsourced and the financial implications eliminated it as an option.

3.6   Limitations – CFD model

The limitations for the CFD model include limited computer power, limited number of software licences, limited time and limitations with the CFD methods themselves.

The power of the computer used for a numerical simulation is never enough. There is always something that could have been added to the model or refined to improve results. The available computer for the simulation was described in section 3.3.1 above, and although it is capable of running the simulations, additional power could have been used to speed up the process.

As touched on above, the power of the computer system used for the CFD simulation plays a large role in the quality of the results obtained. The requirement to reduce mesh size and run lower order functions in order to complete the simulations by a deadline all play a role in the final quality of the results. Therefore a computer system with more power is always wanted.

The simulations were run in parallel for this study, two simulations on a single computer.

As noted above, additional software licences and computer systems, to be able to run many simulations in parallel would be beneficial as it would drastically reduce the simulation phase of the study. In the application of the methods discussed in the design phase, it would reduce the design time required.

Another limitation that goes hand in hand with the above is the constraint of time. The CFD simulation had to be modified to reduce time requirements to enable this study to be concluded with in the required time. Therefore available time is also an important limitation for the CFD model.

Additionally the limitations within the CFD methods themselves are to be noted. The approximations and assumptions made for boundary conditions, turbulence modelling in the flow, boundary layers and the surface inter-action are all areas of complex physical processes which are essentially approximated within the CFD codes. The CFD modelling is a simulation, so the approximations are expected, but certain aspects have room for improvement before being able to predict the physics correctly.

4. PHYSICAL MODEL RESULTS

4.1   Introduction

The above sections indicated what has been done in previous research and the details of the methods and equipment used in this study. The results from the application of the techniques mentioned for the physical model in Chapter 3 will be discussed in this section with a brief overview of the type of results obtained. The major results section will be Chapter 6, in which the physical and CFD models are compared which is the main focus of this study.

The various points that are covered in this section include:

- Point Velocities
- Photographs
- Video Clips
- Visual Observations

The above mentioned points constitute the data obtained from the physical model and will now be discussed under their relevant headings below.

4.2   Point Velocities

The point velocities in the physical model were measured with the Nortek Vectrino ADV and processed using the despiking algorithm described in Chapter 3. The velocities were then plotted against position on the y axes, which is the longitudinal axis in the sump. These plots are named according to the longitudinal lines that they are plotted along. The defining dimensions of these lines were given in Table 2 in Chapter 3, but are displayed here for ease of use by the reader. Figure 4.1 below indicates the locations of these lines.
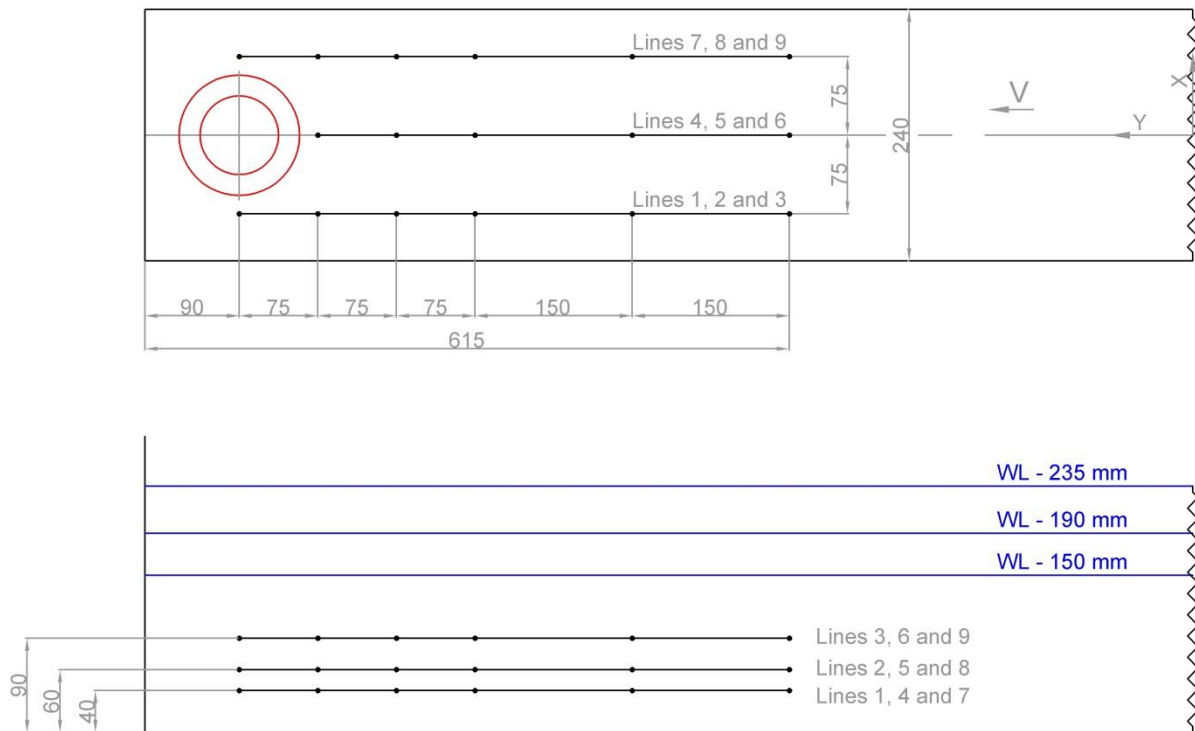
Figure 4.1 - Definition of lines along which point velocities are plotted

Figure 4.2 below is an example of the plotting of only the physical model results, for the case with 190 mm water level and a flow rate of 8.6 l/s. Analysis of thereof indicates the general uniformity of the velocity for this particular case. The plots for lines 4 and 5 in Figure 4.2 are the only ones indicating a significant velocity magnitude change. These two lines are in the centre of tank just upstream of the bell mouth at depths of 40 mm and 60 mm respectively as can be seen in Figure 4.1 above.

Chapter 3 discussed the despiking method for the velocity data from the ADV, which included the comparison of two calculations for the velocity magnitude from each point's data. These two methods, defined in this study as VMAC (Velocity magnitude calculated from the averages of each component) and VMAM (Velocity magnitude averaged from point magnitudes) calculate the velocity magnitude by means of calculating the velocity magnitude from the averaged velocity components (VMAC) and by taking the average of the velocity magnitude for each measurement in the dataset (VMAM) respectively. The percentage difference between these two values was used as a measure of the quality of the data, with a smaller difference relating to higher quality data.
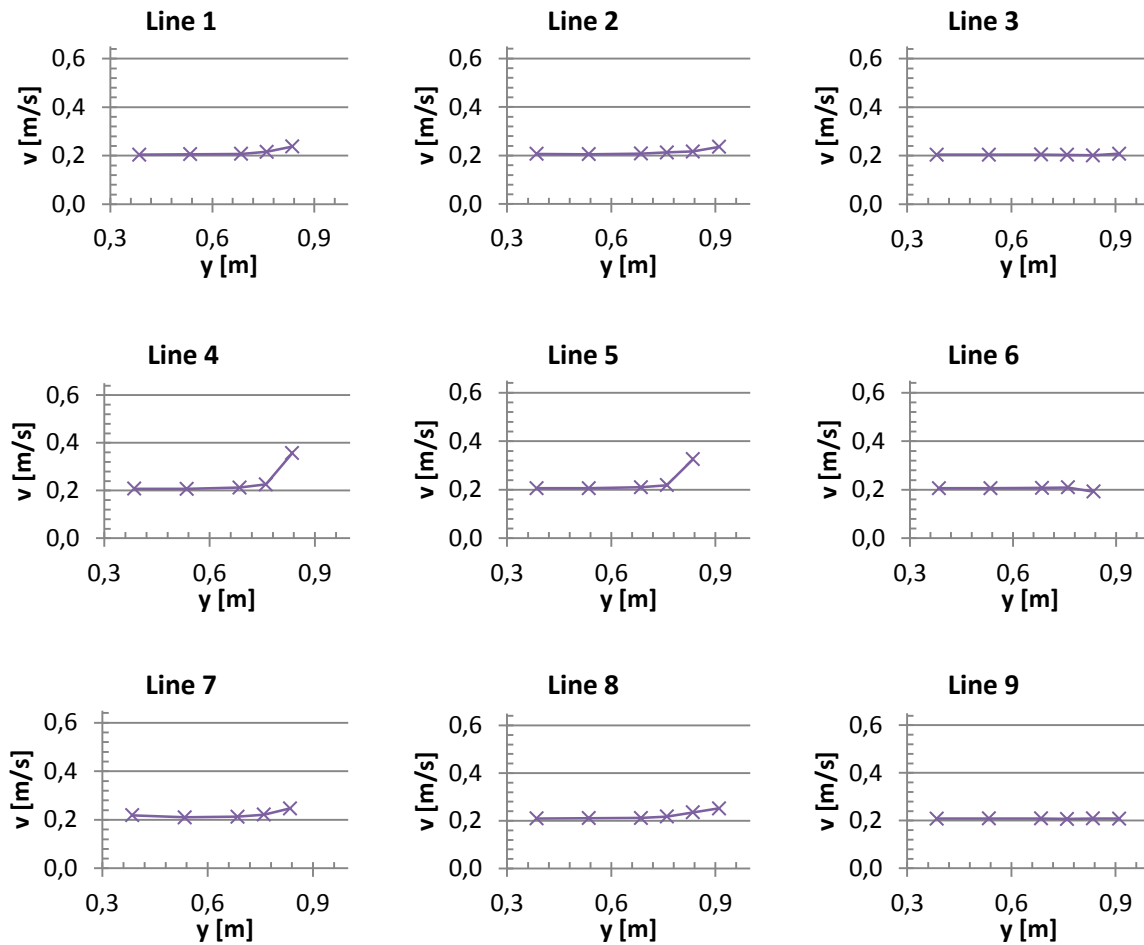
Figure 4.2 - Processed velocity data from physical model (Water Level: 190 mm, Flow Rate: 8.6 l/s)

The difference was calculated per point measured, and then the average over all 51 points was taken to calculate an overall indicator of the data quality for a test scenario. The definition of the percentage difference calculated per point is as follows:

$$\% \, Difference = \left| \frac{VMAM - VMAC}{VMAC} \times 100 \right|$$

The values presented in Table 8 below are simply the sample mean of the calculated differences. The test scenario indicated in red (Water Level: 235 mm, Flow Rate: 2.4 l/s) is as such due to the value exceeding the authors proposed 3% limit for the difference. Analysis of the point data within that dataset yields approximately 10 points that break this 3% limit narrowly and a single point that has a large difference of approximately 58%. This was due to large noise in that specific point data which the single iteration of despiking couldn't remove.

However additional iterations would improve the quality. As it was a single data point that contributed to exceeding the limit, the data was still used for analysis.

Table 8 - Percentage difference between the two methods of calculating velocity magnitude for various test scenarios

% Difference between VMAC and VMAM			
Q [l/s]	Water Level [mm]		
	235	190	150
8.6	0.6	0.6	-
4.2	0.6	0.6	0.6
2.4	**3.4**	0.9	0.8

Majority of the scenarios present acceptable differences of less than 1 %.

The point velocity data obtained from the physical model was discussed above with reference to a measure of quality which is displayed in Table 8. The main use of the point velocity data obtained is the comparison to the same data obtained from the CFD model, which will be compared in Chapter 6.

4.3   Photographs

Various photographs of the flow phenomenon in the physical model in various test scenarios will be presented and discussed. Where applicable, a dark red ring or outline indicates the area of interest of the photograph and the discussion will focus on that particular aspect. This will be used in instances where the area of interest is particularly difficult to identify.

The images are also provided on the DVD attached to this thesis.

The Perspex back plate had a few black markings that could not be removed. They increase the difficulty of identifying the phenomenon to be pointed out. Ideally they should not be present in the images.

The images will now be presented one per page including a brief discussion.

Figure 4.3 - Submerged dye-core vortex attached to wall (Water Level: 150 mm, Flow Rate: 4.2 l/s)

Figure 4.3 above shows a submerged dye-core vortex (type 3) attached to the side wall of the sump entering the intake. It was highlighted using the dye injection system described in Chapter 3. Submerged vortices can lead to pressure fluctuations on the impeller blade which as mentioned in Chapter 2 is detrimental to operational ability.

Additionally, but not highlighted, this image contains a surface vortex (type 5) entraining air bubbles.

Figure 4.4 - Dye-core surface vortex entering the bell mouth (Water Level: 150 mm, Flow Rate: 2.4 l/s)

Figure 4.4 above shows a dye core vortex (type 3) from the surface to the intake. These types of vortices entrain a high degree of swirl which as mentioned above can be detrimental to operational ability. A high degree of swirl was evident while taking this photograph.
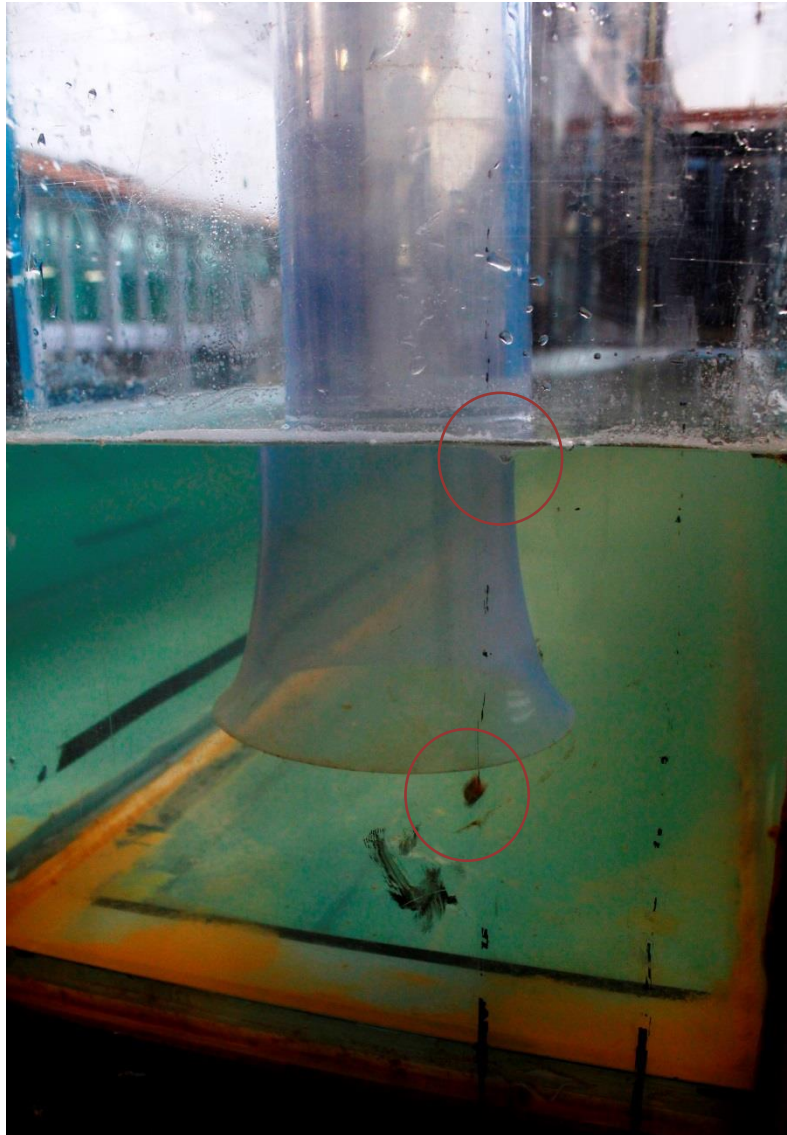
Figure 4.5 - Surface dimple of vortex and floating debris being pulled into the intake
(Water Level: 150 mm, Flow Rate: 3 l/s)

Figure 4.5 above shows a surface dimple along with a small piece of floating debris, a chip of wood, being pulled into the intake by the vortex (type 4). Depending on the size of the debris being sucked in, serious damage can be caused to the impeller and other sensitive parts. Assuming the flow rate is kept constant this type of vortex appears shortly before the vortex type that draws in air bubbles.

Figure 4.6 - Full air core vortex entraining air (Water Level: 150 mm, Flow Rate: 6 l/s)

Figure 4.6 above shows a full air core vortex (type 6) entering the intake and entraining air. This type of vortex can cause pump vibration and cavitation on impeller blades leading to an overall reduction in efficiency as well as reduced maintenance cycles and resulting increased operational costs. It has been shown that with sufficient air entrainment, certain pump types can have a drastic drop in output resulting in service delivery failure.

Figure 4.7 - Dual full air core vortices entraining large amounts of air (Water Level: 125 mm, Flow Rate: 6 l/s)

Figure 4.7 above shows the effects of extremely low water levels coupled with a high flow rate, in this particular case 125 mm with a flow rate of 6 l/s. This occurrence is coupled with loud noises, vibration of irregular frequency and reduced flow rate. It proved to have a large impact on the pump, and therefore was not run in this state for a long period of time.

The scenario with a 150 mm water level and an 8.6 l/s flow rate resulted in a scenario similar to Figure 4.7 and this is one of the reasons that it was not run, the other reason being the unstable and unrealistic water level generated by the CFD model in the implicit state.

In this particular case it was observed that the vortex on the right in the photograph was steadier than the one on the left, which would phase out and re-develop often.
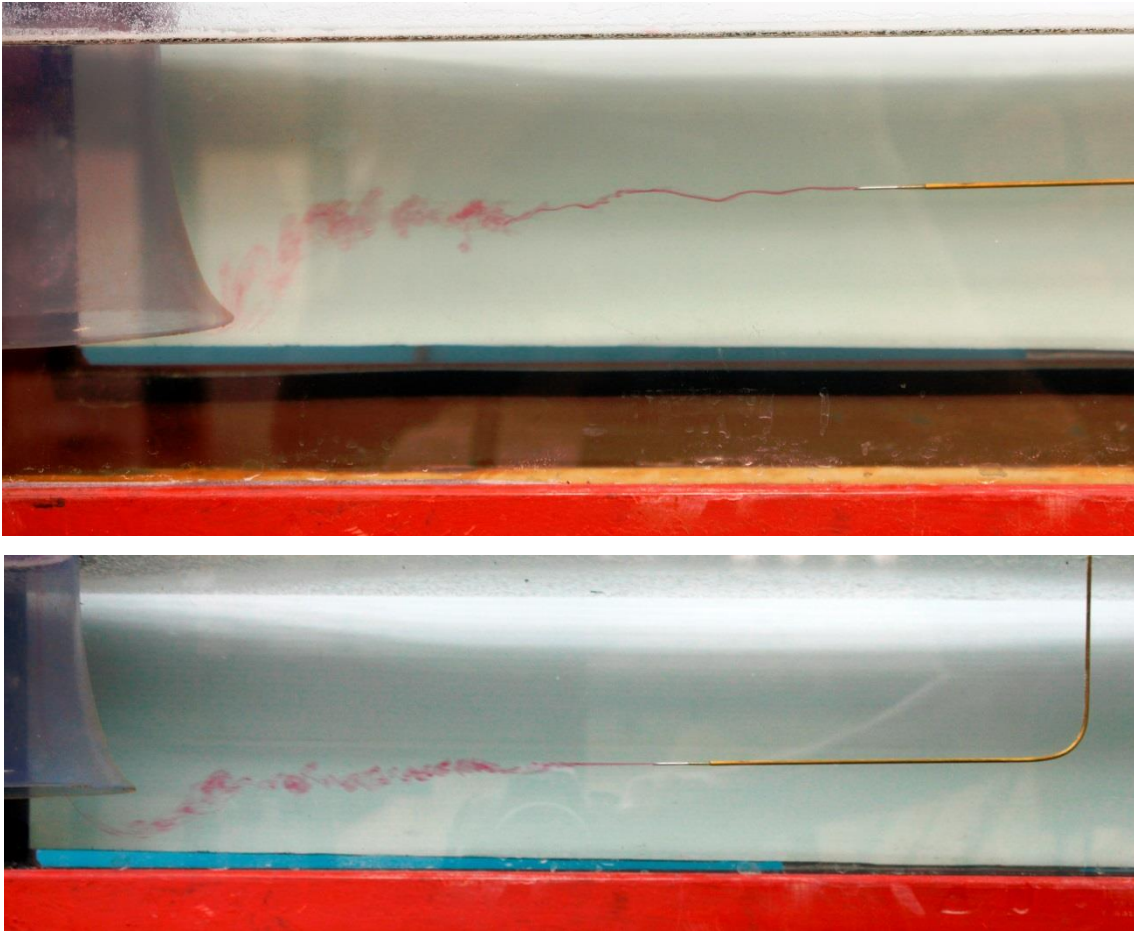
Figure 4.8 - Dye injection indicating flow lines in sump

Figure 4.8 above shows the dye traces used to visualize the flow lines along the centreline of the sump. In the upper image the needle is at 90 mm above the sump floor and in the lower image it is at 60 mm. The general flow tendencies can be seen with the turn down of the flow as it approaches the bell mouth made visible. The level of turbulence in the flow is indicated by the dissipation of the dye trace very soon after the release from the needle.
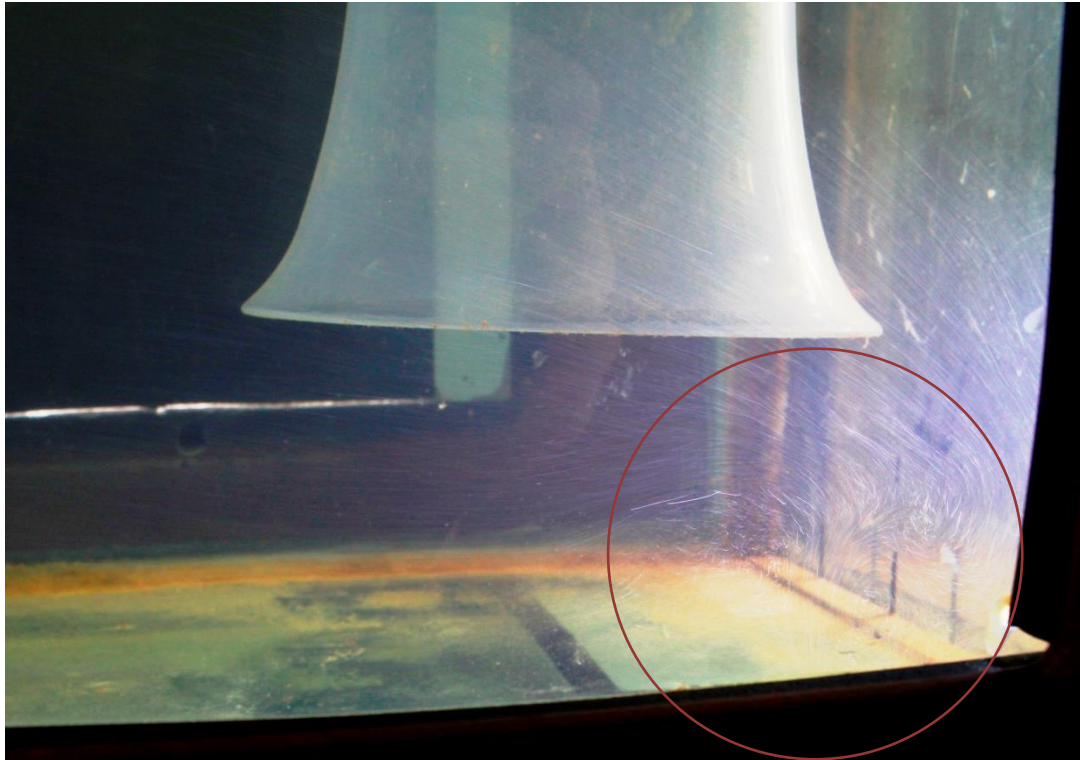
Figure 4.9 - Side wall attached vortices and other irregularities in the flow (Water Level: 190 mm, Flow Rate: 8.6 l/s)

Figure 4.9 above shows the particle traces of the irregular flow and side wall attached vortices. The image was taken by covering the sump in a black sheet and placing a black board on the side window opposite the photographer. A high power LED torch was modified to only release a narrow plane of light, which was used to illuminate the micro balloon particles in the water that were used for seeding the flow for the ADV. Using a long exposure setting, the camera was able to capture the tracer lines as can be seen in the image.

The area in the red circle is generally unsteady but indications of swirl which travelled to the intake were observed. A video was recorded with a similar perspective, which highlights the unsteady nature of the flow in this area. It can be seen on the attached DVD.
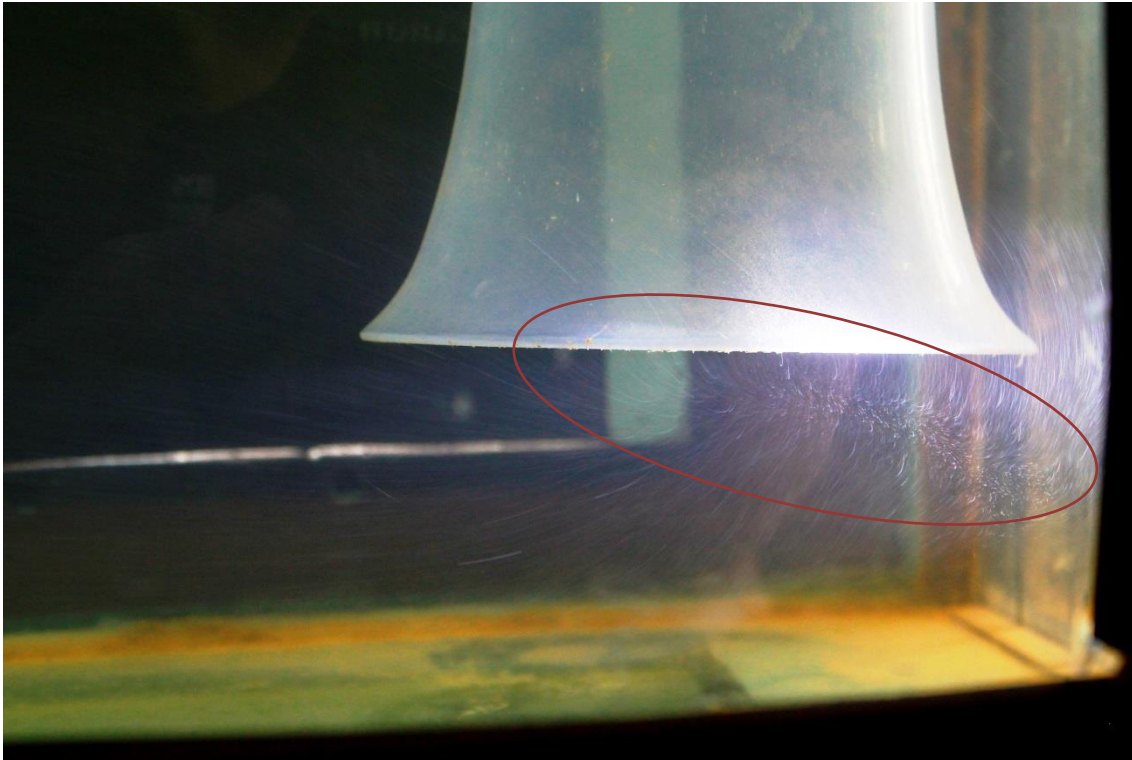
Figure 4.10 - Upper and lower flow streams joining as they enter the bell mouth (Water Level: 190 mm, Flow Rate: 8.6 l/s)

Figure 4.10 above shows the particle traces of two joining flows in a plane parallel to the side wall at the tip of the bell mouth. A lower flow stream turning up into the bell mouth meets an upper flow stream turning down into the bell mouth causing a turbulent region where they meet and outwards towards the side wall. This occurrence is near the region where the side wall attached vortices formed as can be seen in Figure 4.9.

The same photography technique was used as described for Figure 4.9 and as mentioned above, a video of a similar perspective can be seen on the included DVD.
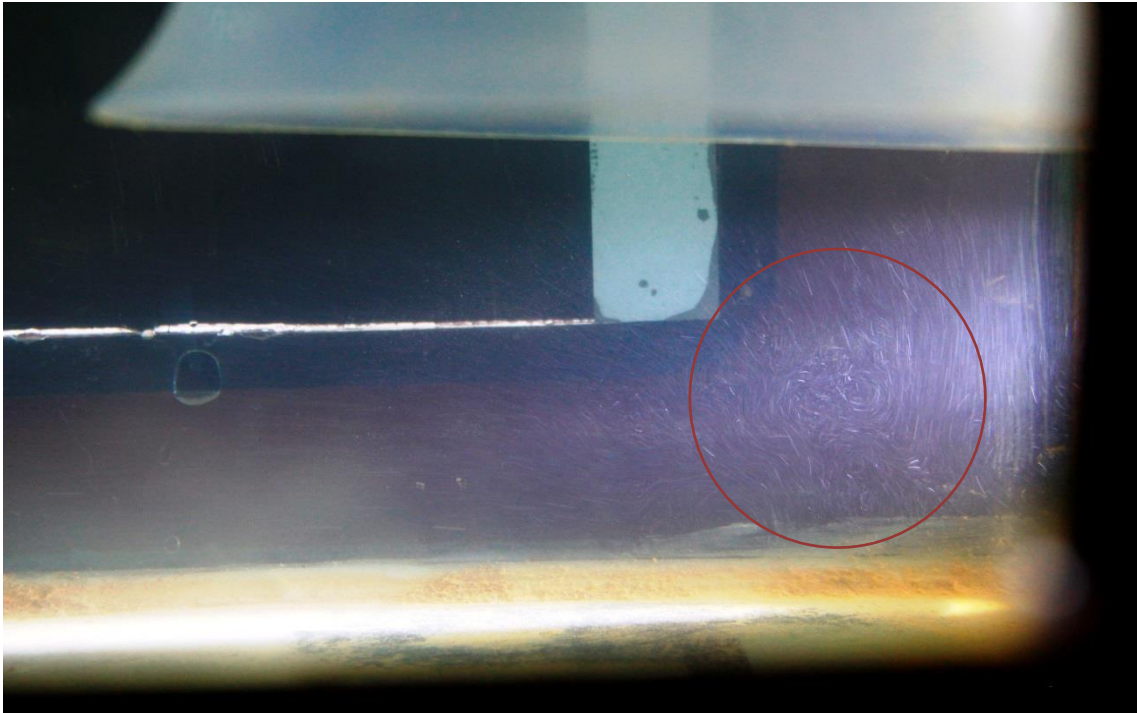
Figure 4.11 - Side wall attached vortex (Water Level: 190 mm, Flow Rate: 8.6 l/s)

Figure 4.11 gives an indication of a side wall attached vortex, similar to the one shown with a dye core in Figure 4.3. The view as in this photograph was used to position the needle for injecting the dye to be able to photograph the dye core.

The same photography technique was used as described for Figure 4.9 and as mentioned above, a video of a similar perspective can be seen on the included DVD.

4.4   Video Recordings

The video recordings of the model include views similar to Figures 4.9 to 4.11. They detail the flow characteristics well and are self-explanatory. The same phenomenon as described for those figures above are visible, but with the added degree of motion, enable easier understanding of the complex flow characteristics around the bell mouth region.

Other views recorded include views from behind the bell mouth of vortex formation and patterns for various flow rates and water levels. These videos give an indication of when air entrainment occurs for certain flow rates.

The videos are available on the attached DVD.

4.5   Observations

General observations made by the author while testing will be discussed here. These are not used for comparison to CFD, but cover some interesting aspects.

The seed material used in the flow to improve the ADV data was micro-balloons, used in industry for GRP work. Some of these remained joined together and this resulted in them floating. It was observed that the air entrainment was reduced when a large amount of this floating seed material was allowed to be around the bell mouth region of the sump. It is an interesting aspect, as it effectively reduced the level of critical submergence.

When running an initial calibration test of the physical model, which contained large albeit non air entraining vortex action, the author made use of a small wooden beam, 10 mm x 30 mm, and held it up against the side of the bell mouth and this simply resulted in a shift of the vortex towards the outside, as though instead of a vortex breaking away from the suction pipe, it was now breaking away from the piece of wood. When the obstruction was placed with a 10 mm to 20 mm gap from the side of the bell mouth, the vortex action was reduced to occasional surface swirl.

4.6   Conclusions

The physical model results were discussed above and a brief summary of the conclusions reached with respect to the physical model results will be given. The order of the conclusions will be the same order in which the results were discussed.

The point velocities from the model were recorded, cleaned and averaged to obtain the velocity magnitudes for each of the 49 points after which they were plotted along longitudinal lines. The only test scenario that produced air entrainment, was that with a 150 mm water level and a flow rate of 4.2 l/s, in the form of occasional air bubble entrainment. The point velocities are the only form of data obtained for quantitative analysis and the reliability of this data could not be verified due to the ADV being the only available equipment suitable for the task at hand.

The photographs were used for qualitative analysis, as a tool to visualize the flow characteristics as well as a means to identify key areas that were to be considered in the CFD model. They provide an easy method for understanding the complexities of the flow field.

The video clips were used to assist the photographs by providing a dynamic view of a scene thereby providing an easier understanding of the flow field. The use of illuminating the micro balloons in the flow to provide flow tracers made the visualization of the flow patterns simple and complete.

The general observations regarding the reduction of the air entrainment when a large 'carpet' of fine floating debris was surrounding the bell mouth and the placement of an obstruction to the flow which reduced the vortex action were provided for interest.

A discussion of the CFD model results will be presented followed by comparing it to the physical model results under the same flow conditions.

5. COMPUTATIONAL FLUID DYNAMICS MODEL RESULTS

5.1   Introduction

Sections 1 to 3 indicated what has been done in previous research and the details of the methods and equipment used in this study. The results from the application of the techniques mentioned for the CFD model in Chapter 3 will be discussed in this section with a brief overview of the type of results obtained. The CFD model was run in the transient implicit multiphase state solved with the PISO algorithm and was solved in ANSYS Fluent 14.0. The main results will be discussed in Chapter 6, in which the physical and CFD models are compared which is the main focus of this study.

The various points that are covered in this section include:

- Point Velocities
- Contour Plots
- Vector Plots
- Pathlines
- Animations
- Monitors

The above mentioned points constitute the data obtained from the CFD model and will now be discussed under their relevant headings below.

5.2   Point Velocities

The point velocities obtained from the CFD model will be briefly discussed, with an example of a test scenario's results shown. The velocity data from the CFD model was averaged over a period of 25 seconds of flow time using the method described in Chapter 3.

Figure 5.1 below is an example of the plotting of only the CFD model results, for the case with 190 mm water level and a flow rate of 8.6 l/s, the same as that shown for the physical model results in Chapter 4. The CFD results present a more pronounced behaviour of the tendencies. The tendencies are generally similar to those of the physical model, with the

sharp drop-off on the plots for lines 1 and 7 not being included in the physical model results as that point was not accessible using the ADV. More relating to the comparison will be discussed in Chapter 6.
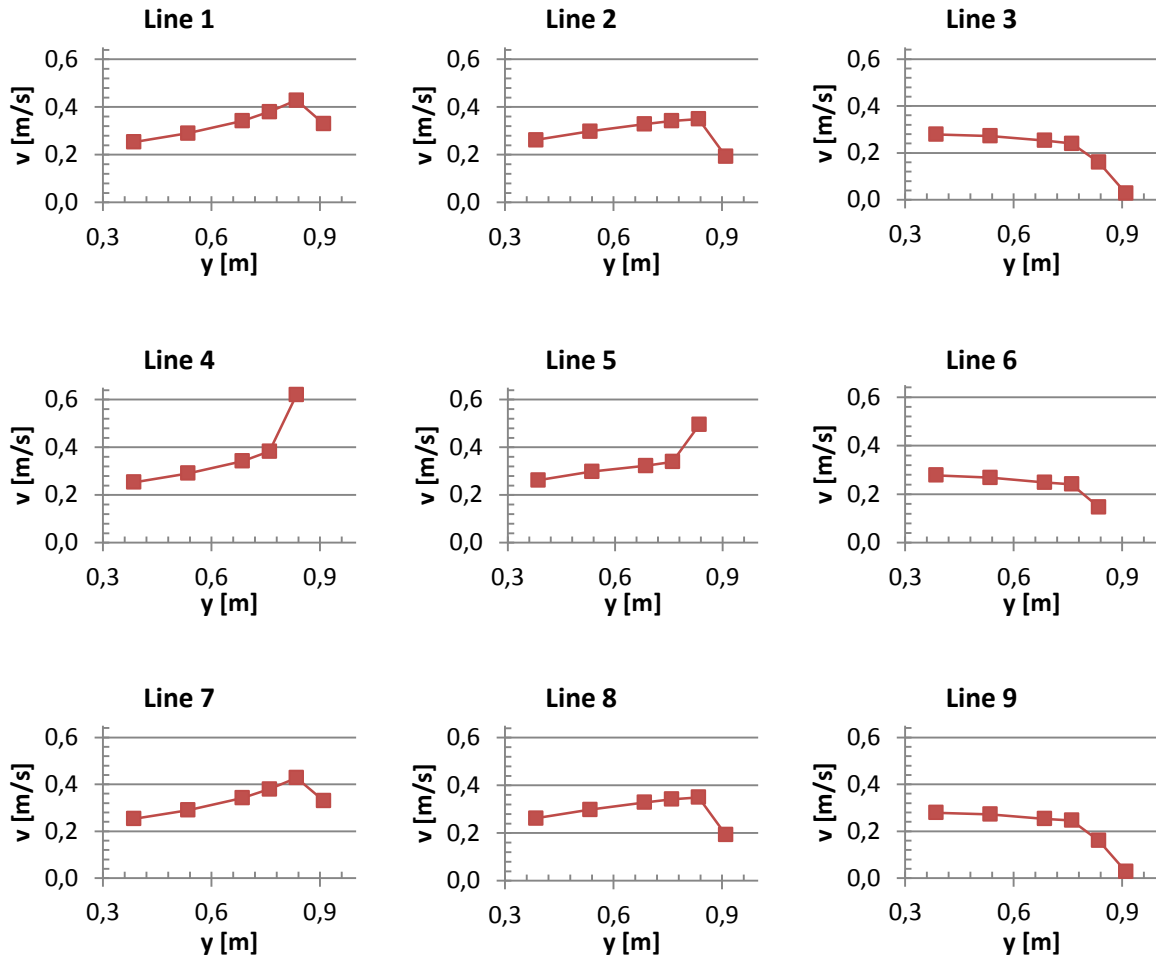
Figure 5.1 - Averaged velocity data from CFD model (Water Level: 190 mm, Flow Rate: 8.6 l/s)

5.3   Contour Plots

Four contour plots from the CFD simulations are shown below, used as a quality check or to highlight interesting phenomenon. The model details, namely water level and flow rate are provided in the captions of the figures.
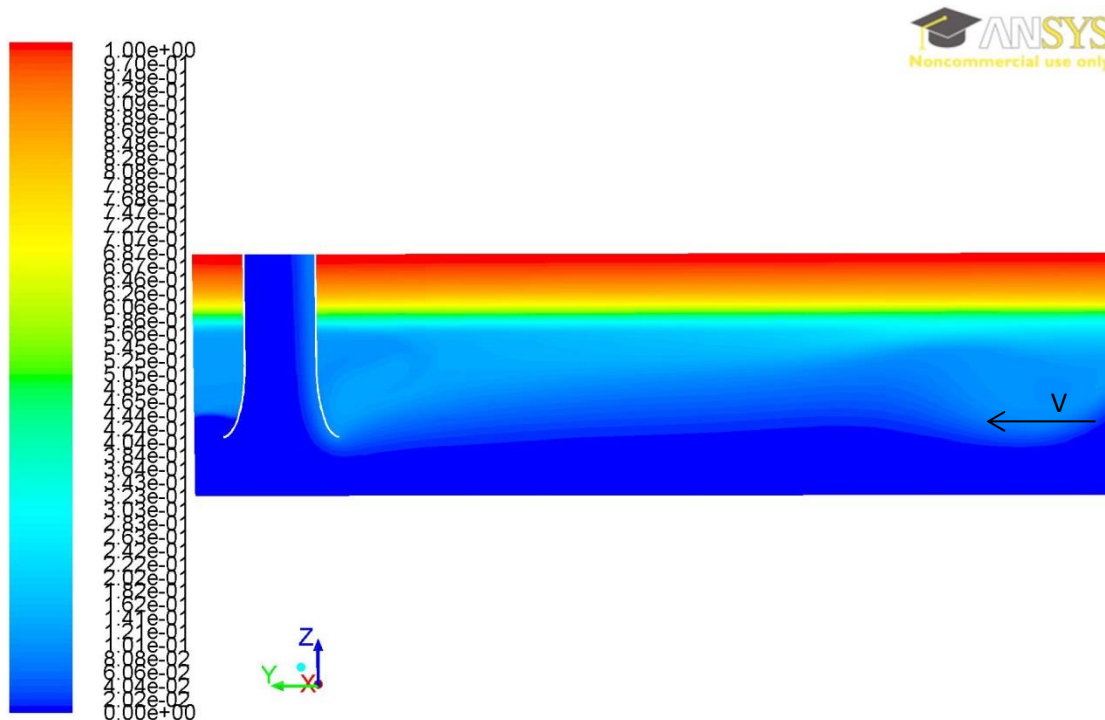
**Figure 5.2 - Contour plot of volume fraction of air indicating the water surface at a value of 0.5
(Water Level: 190 mm, Flow Rate: 4.2 l/s)**

Figure 5.2 is provided to indicate the accurately defined and stable water level for the entire length of the CFD model. The water level is defined by a volume fraction of 0.5, which indicates cells in the model that contain 50% air and 50% water and is indicated by the bright green colour in the image. The model geometry design was carefully considered to enable realistic modelling of the water level. The variation in volume fraction below the water surface is attributed to air entrainment at the inlet boundary, due to turbulence on the lower end of the vertical boundary condition on the air volume, which was modelled as a wall.
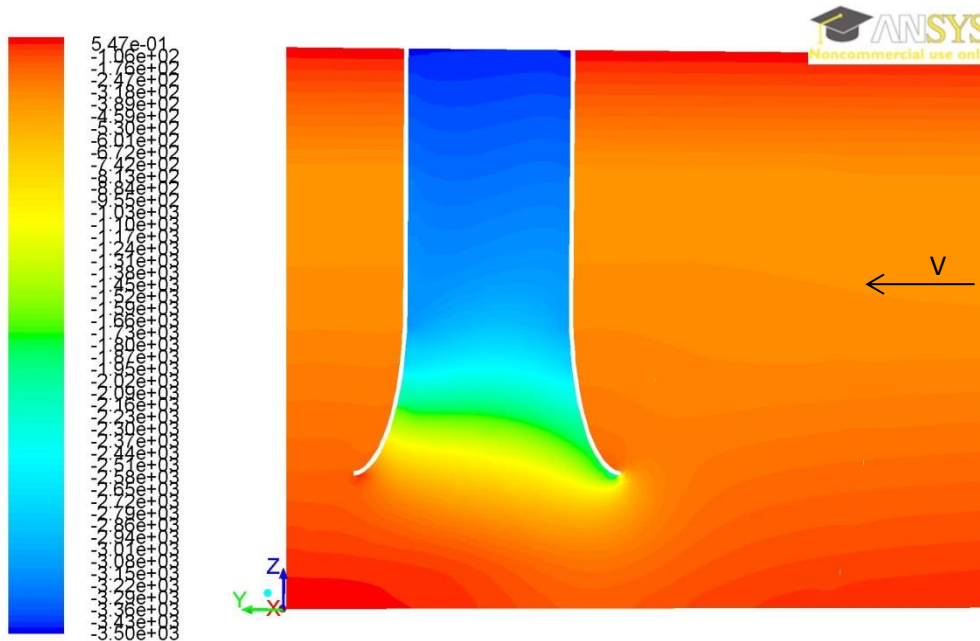
Contours of Mean Static Pressure (mixture) (pascal) (Time=1.3750e+02)   Nov 27, 2013
                                        ANSYS FLUENT 14.0 (3d, dp, pbns, vof, ske, transient)

**Figure 5.3 - Contours of mean static pressure in the bell mouth
(Water Level: 190 mm, Flow Rate: 8.6 l/s, Operating Pressure: 0 Pa)**
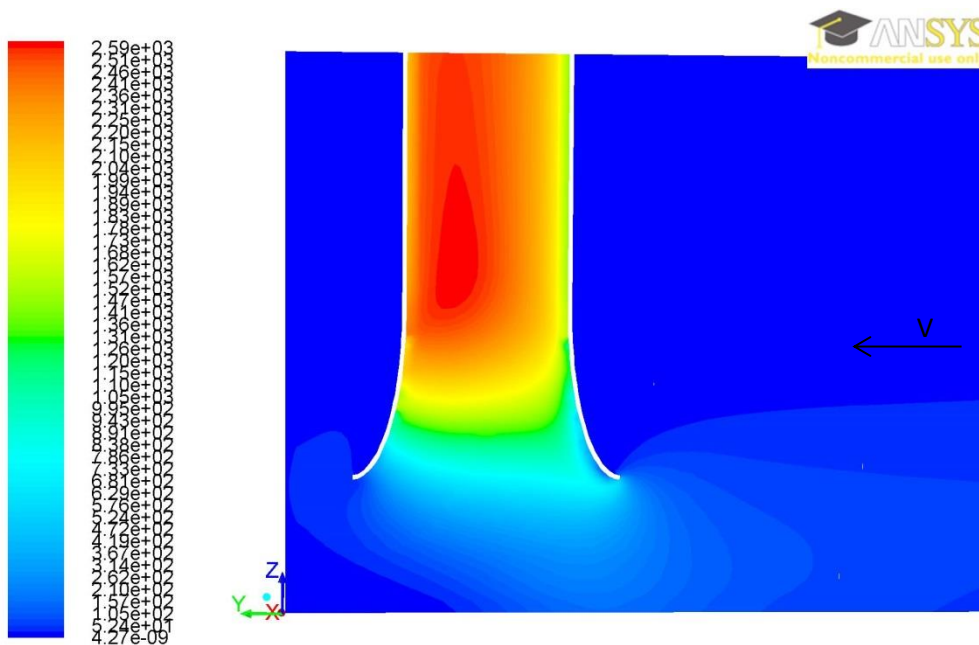
Contours of Dynamic Pressure (mixture) (pascal) (Time=1.3750e+02)   Nov 27, 2013
                                        ANSYS FLUENT 14.0 (3d, dp, pbns, vof, ske, transient)

**Figure 5.4 - Contours of instantaneous dynamic pressure in the bell mouth
(Water Level: 190 mm, Flow Rate: 8.6 l/s)**
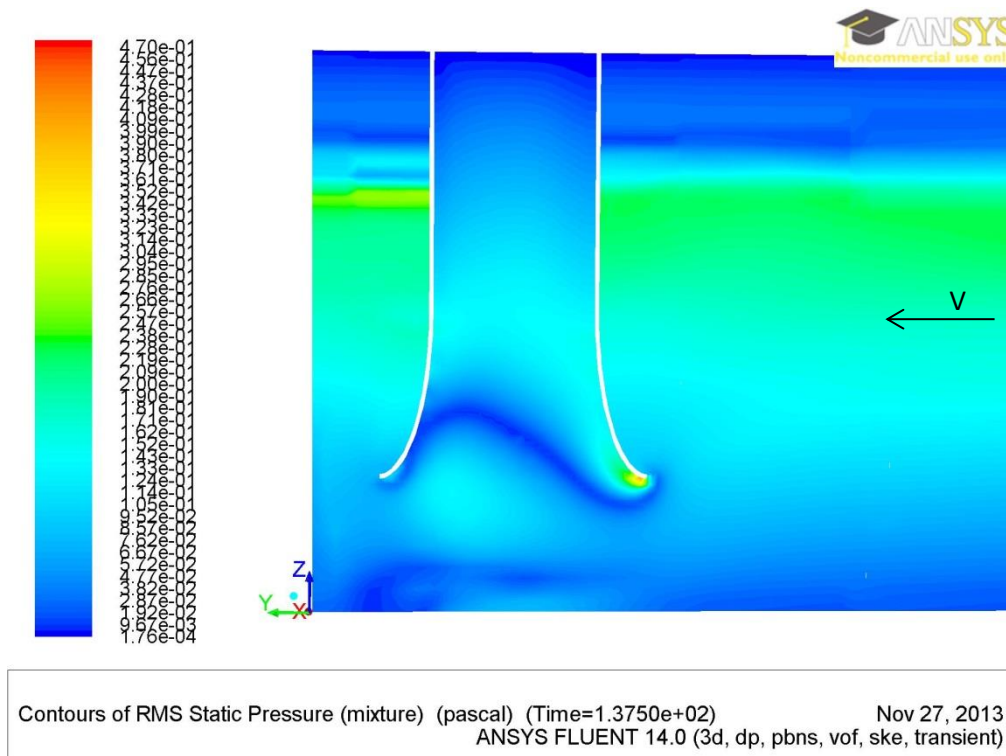
**Figure 5.5 - Contours of Root-Mean-Square static pressure in the bell mouth
(Water Level: 190 mm, Flow Rate: 8.6 l/s)**

Before discussion of the above contour plots of pressure in the bell mouth, the definition of the three types of pressures shown will be given.

ANSYS Fluent defines the static pressure as a gauge pressure relative to the operating pressure prescribed for the simulation, set as 0 Pa in this study. The mean is simply the arithmetic mean over the flow time for the simulation, in this case 25 seconds. The RMS static pressure is simply the root-mean-square of the static pressure over the flow period simulated. The dynamic pressure is defined as $\frac{1}{2}\rho v^2$. The operating pressure is 0 Pa.

Figures 5.3 to 5.5 indicate an asymmetric pressure distribution in the entrance to the bell mouth. This pressure distribution deviates significantly from the generally preferred single bend curve. This could lead to increased entrance loss coefficients and be a factor in the generation of unsteady flow surrounding the bell mouth. Therefore it will be included in the later discussion regarding recommendations for future research. The water level is not clearly visible in these contour plots due to the gradual variation in pressure at the interface.

Figure 5.4 highlights the reduced pressure along the entire length of the inner front face of the suction pipe, which would influence the velocity distribution entering the pump, which can lead to pump vibrations, reduced efficiency of the pump, and cavitation erosion on the impeller blades, increased maintenance frequency and reduced life cycle of the pump.

5.4   Vector Plots

Four vector plots from the CFD simulations are shown below, and are to be used as a means of qualitative analysis with the physical model. The model details, namely water level and flow rate are provided in the captions of the figures.
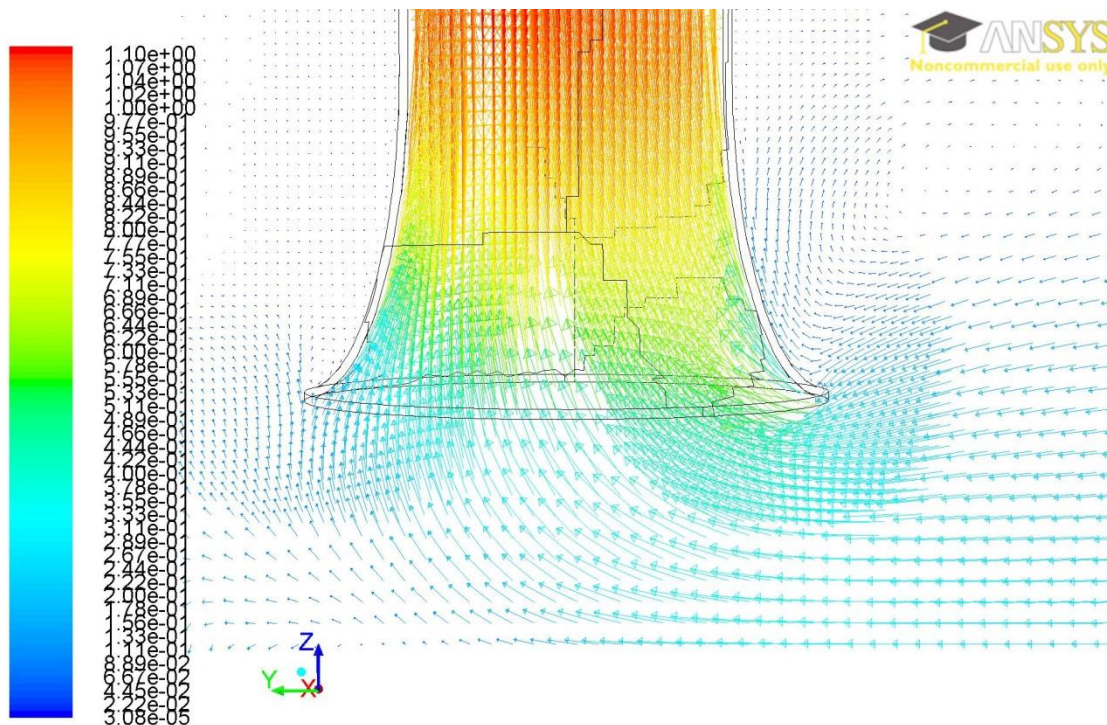
Velocity Vectors Colored By Velocity Magnitude (mixture) (m/s) (Time=5.0000e+01)   Nov 27, 2013
ANSYS FLUENT 14.0 (3d, dp, pbns, vof, ske, transient)

**Figure 5.6 - Velocity vectors coloured by velocity magnitude at the entrance to the bell mouth
(Water Level: 190 mm, Flow Rate: 4.2 l/s)**

Figure 5.6 indicates the symmetry of the inflow into the bell mouth entrance as well as a high velocity angle as the flow needs to turn around to enter the bell mouth on the upstream side. (Right hand side in the figure)

Velocity Vectors Colored By Velocity Magnitude (mixture) (m/s) (Time=1.3750e+02)   Nov 27, 2013
ANSYS FLUENT 14.0 (3d, dp, pbns, vof, ske, transient)
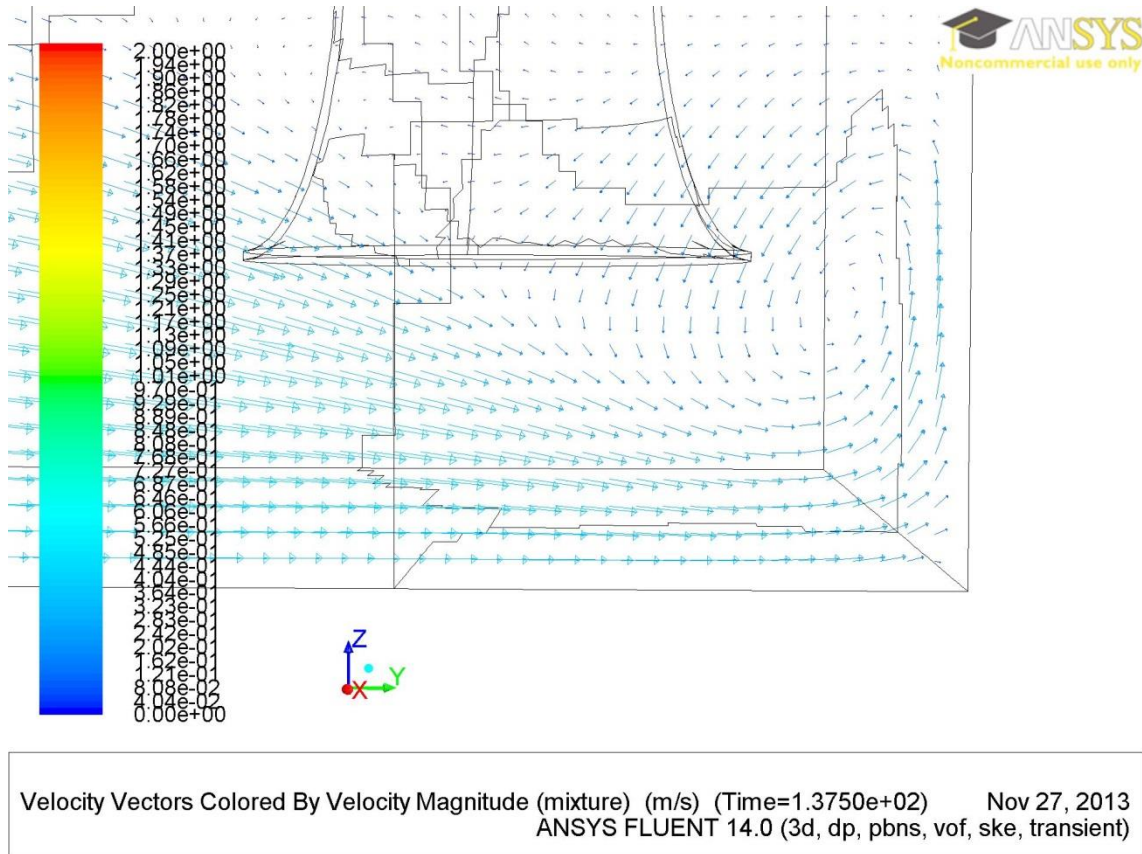
Figure 5.7 - Velocity vectors coloured by velocity magnitude plotted on a plane offset by 20 mm from the side wall (Water Level: 190 mm, Flow Rate: 8.6 l/s)

Figure 5.7 indicates rotational flow in the near wall region indicating the presence of vortex action in a similar location as observed in the physical model. The image contains instantaneous velocity magnitudes only, and therefore the location of the vortex centre is likely to move around, which should be kept in mind when a comparison is made in Chapter 6.

Velocity Vectors Colored By Velocity Magnitude (mixture) (m/s) (Time=1.3750e+02)   Nov 27, 2013
ANSYS FLUENT 14.0 (3d, dp, pbns, vof, ske, transient)
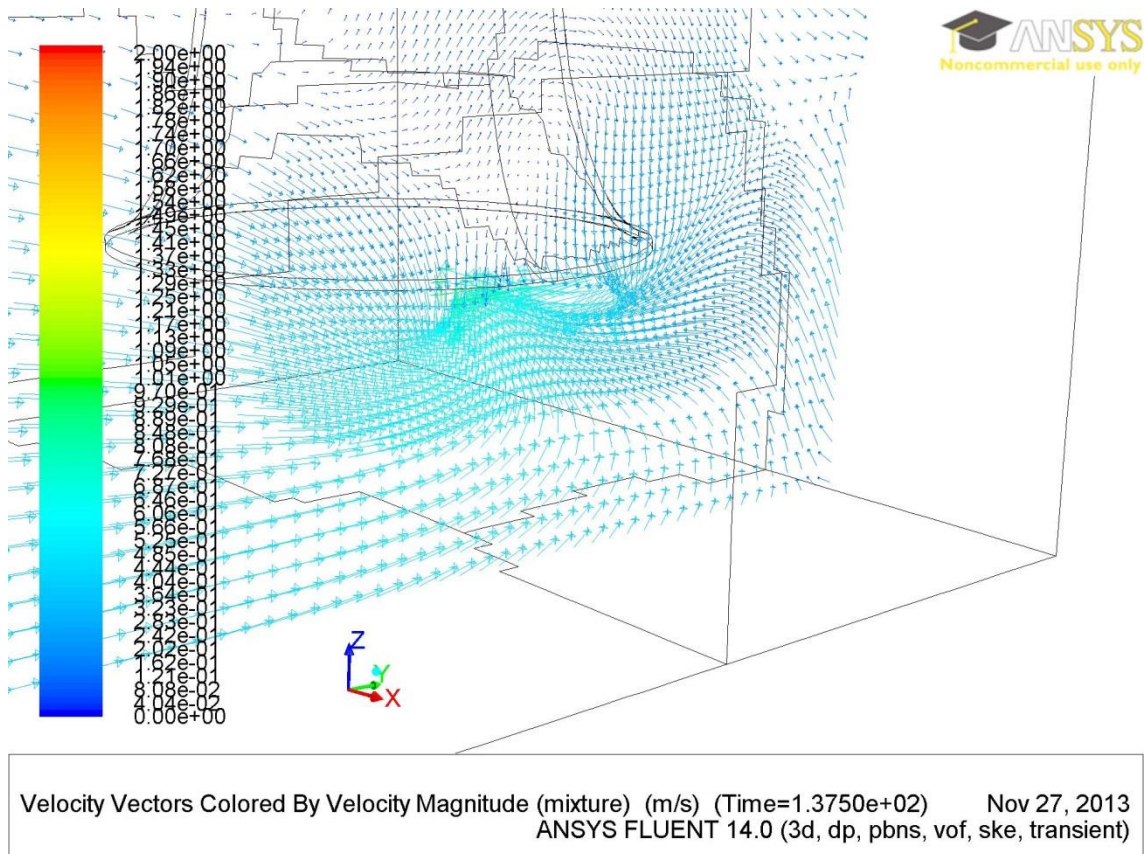
Figure 5.8 - Velocity vectors coloured by velocity magnitude plotted on a plane offset by 60 mm from the side wall (Water Level: 190 mm, Flow Rate: 8.6 l/s)

Figure 5.8 shows the meeting of two main flow streams, one from above and one from below, causing unsteady flow behaviour in the surrounding regions. This is similar to the observations in the physical model and will be dealt with further in Chapter 6.
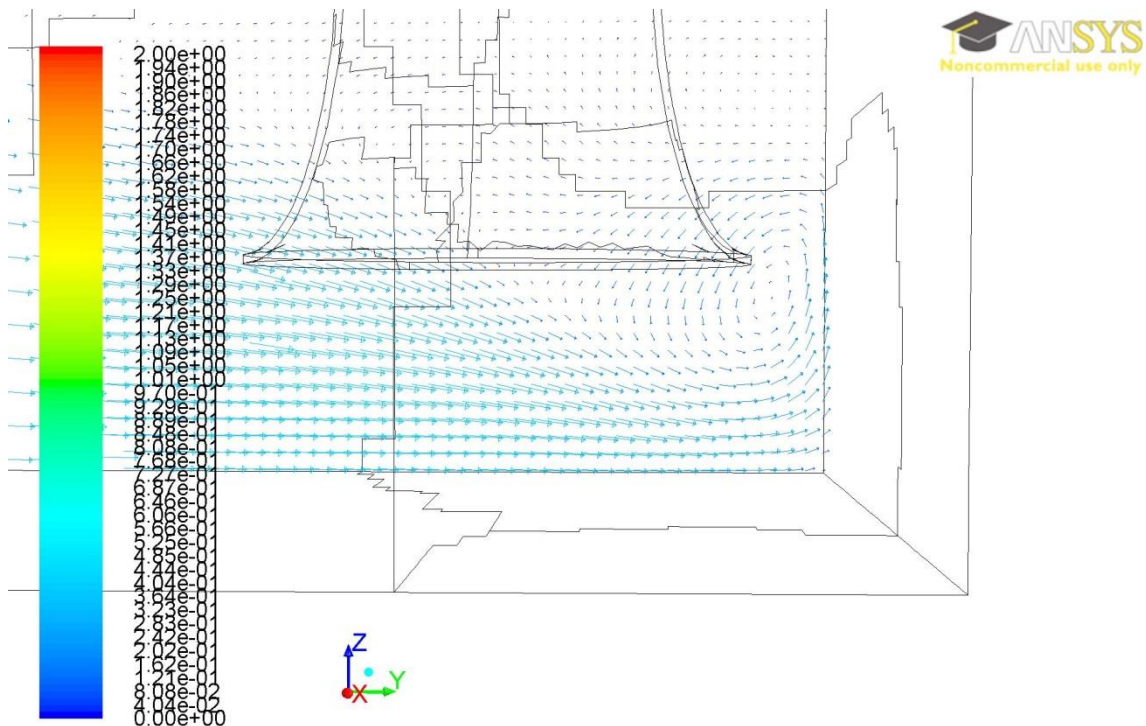
Velocity Vectors Colored By Velocity Magnitude (mixture) (m/s) (Time=1.3750e+02)   Nov 27, 2013
ANSYS FLUENT 14.0 (3d, dp, pbns, vof, ske, transient)

Figure 5.9 - Velocity vectors coloured by velocity magnitude plotted on a plane offset by 20 mm from the side wall (Water Level: 190 mm, Flow Rate: 8.6 l/s)

Figure 5.9, similar to Figure 5.7, indicates rotational flow in the near wall region indicating the presence of vortex action in a similar location as observed in the physical model. The image contains instantaneous velocity magnitudes only, and therefore the location of the vortex centre is likely to move around, which should be kept in mind when a comparison is made in Chapter 6.

5.5   Pathlines

Two images of pathlines generated by the CFD model will be shown to highlight the turbulent flow characteristics in the sump. The model details, namely water level and flow rate are provided in the captions of the figures.
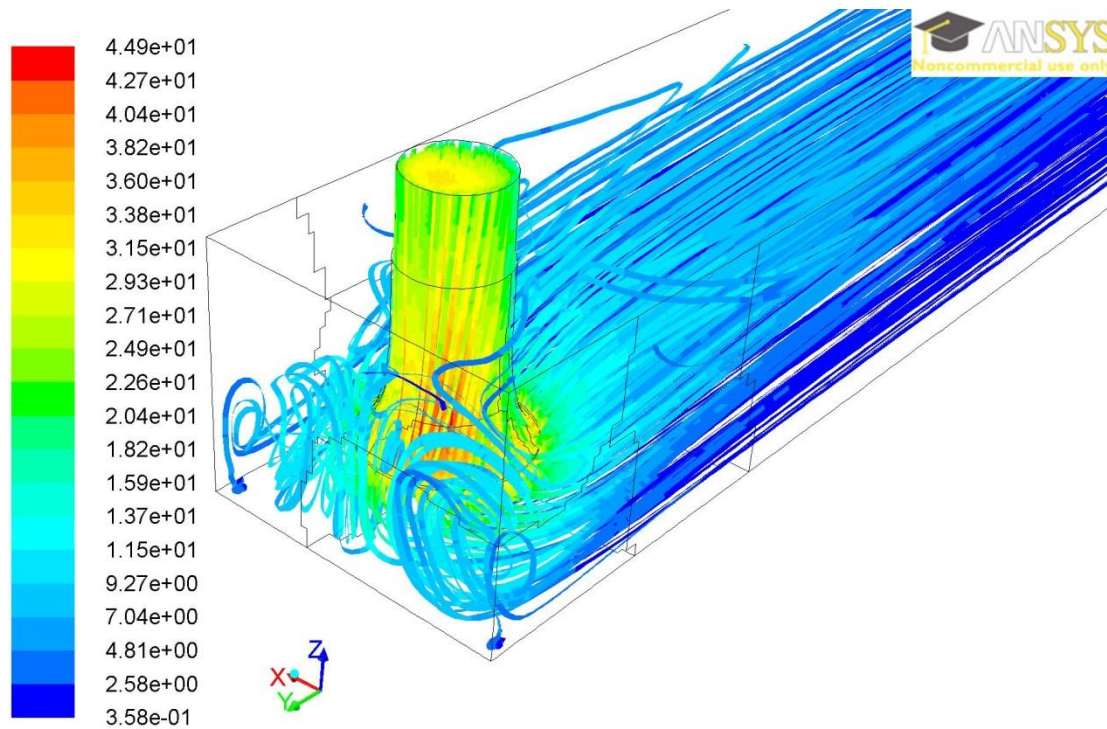
Figure 5.10 - Pathlines coloured by turbulent intensity indicating flow patterns
(Water Level: 190 mm, Flow Rate: 8.6 l/s)

Figure 5.10 provides a good overview of the turbulent flow characteristics in the sump surrounding the bell mouth. Two submerged vortices are visible, attached to the floor in each of the back corners of the sump. The complexity within the flow is highlighted with this figure, and the reasons why analytical techniques are unsuccessful can be understood. This image is an instantaneous capture, with the pathlines constantly moving and changing if it were to be viewed as an animation.
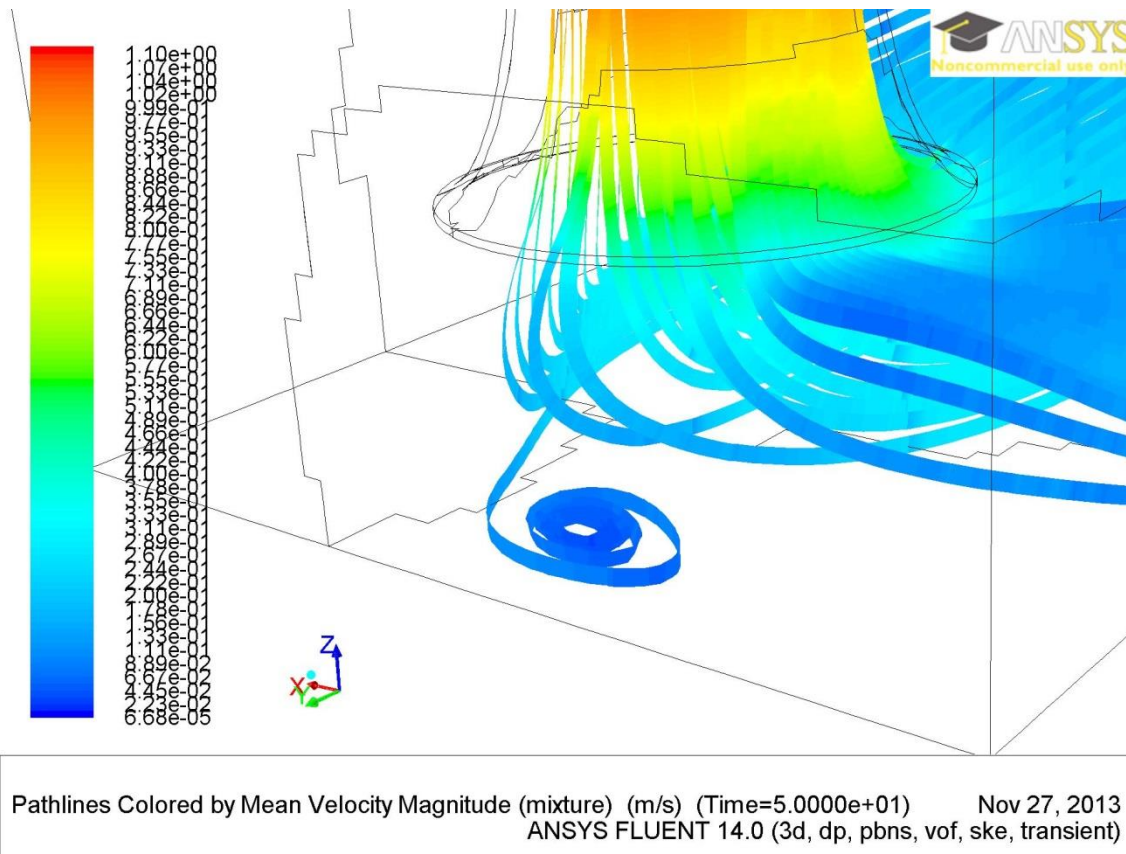
Figure 5.11 - Pathlines coloured by mean velocity magnitude indicating rotation below bell mouth
(Water Level: 190 mm, Flow Rate: 4.2 l/s)

Figure 5.11 shows a submerged vortex on the floor below the bell mouth entrance which had a high frequency of occurrence during observations in the physical model under all flow conditions tested.

5.6   Animations

Animations of vectors on the water surface and various parallel planes were monitored on the initial simulations to determine the suitability of the model. These indicated that although running in the transient state, the implicit multiphase model runs very stable and the general flow characteristics are near constant with only slight velocity variations observed on the aforementioned planes.

5.7   Monitors

Flow monitors were set up to monitor the mass flow difference of the CFD model in order to validate that the model has reached an acceptable state of convergence. The acceptable level of convergence was defined as the state when the mass flow difference is acceptably steady and below 1% of the overall mass flow on the inlet. This was reached for all models.

Mass Flow Rate Difference
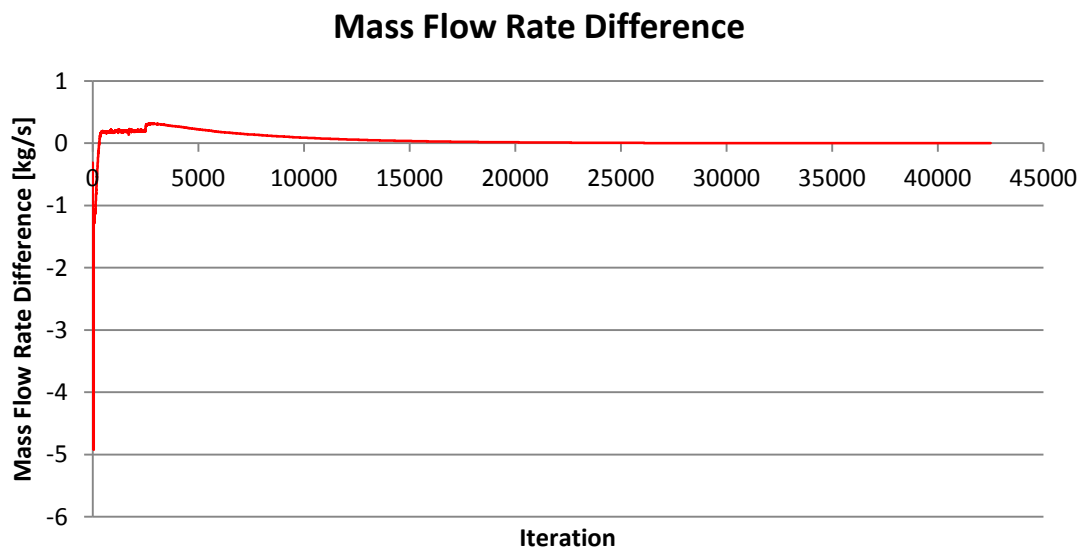
Figure 5.12 - Mass flow rate difference between the inlet, outlet and air vent on the CFD model
(Water Level: 190 mm, Flow Rate: 4.2 l/s)

Figure 5.12 indicates the history of mass flow difference over a period of 42 500 iterations. At 14 200 iterations acceptable convergence, as defined above as 1% of total mass flow rate on the inlet, was reached. The mass flow rate difference after the 40 000th iteration was in the order of 3.05 g/s, which is well within the 1% convergence criteria. After the initial steady state run, of 2500 iterations, where the mass flow difference showed large fluctuations, it begins to follow a smooth asymptotic approach to the ideal value of 0 kg/s.

Additionally, a monitor was set up to monitor the volume flow rate of air crossing the outlet boundary. Mathematically, this monitor is the integral with respect to the area of the product of the volume fraction of air (VOF_{air}) and the velocity magnitude and is defined as follows:

$$Q_{air} = \int VOF_{air} \times |V|\, dA$$

A dimensional analysis on the formula for Q_{air} indicates that the unit of measure is m^3/s, which is in agreement with its definition as a volume flow rate.

Figure 5.13 shows the air flow rate for the test scenario of 150 mm water level and a 4.2 l/s flow rate, which was observed on the physical model to be on the verge of critical submergence.
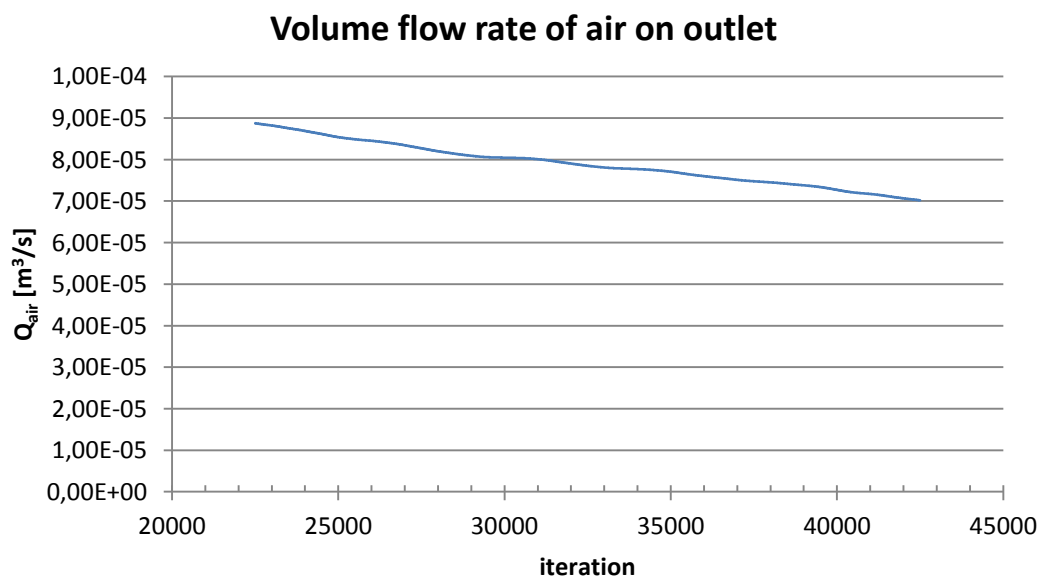
Figure 5.13 - Volume flow rate of air monitored on outlet (Water Level: 150 mm, Flow Rate: 4.2 l/s)

As can be seen in Figure 5.13, the volume flow rate is rather low, and indicates no sign of convergence, which is not expected for this type of data from an unsteady simulation. Even in the physical model, the air entrainment fluctuates greatly with time. The reliability of this monitor in this test series is uncertain, as it has not provided the expected results. It indicates a higher percentage of air entrainment at lower flows which in the physical model indicated no air entrainment. This monitor yields very small values and the percentage of air with respect to the overall volume flow rate will be detailed in a Table 9.

Table 9 - Percentage volume flow of air as monitored on the outlet of the CFD model, average flow over 25 seconds and maximum flow in italics in brackets

Q [l/s]	Water Level [mm]		
	235	190	150
8.6	0.80 (*0.86*)	0.94 (*0.94*)	-
4.2	1.15 (*1.23*)	1.50 (*1.59*)	1.88 (*2.11*)
2.4	0.98 (*1.04*)	1.51 (*1.53*)	1.94 (*1.99*)

The high air entrainment volumes at high water levels can be attributed to the possible air entrainment at the inlet boundary of the model as was mentioned for Figure 5.2.

The lack of a cyclic plot of the air flow monitor indicates that the model was not run for a long enough period of time to monitor this data. Although due to the unsteady nature of the phenomenon that causes the air entrainment, whether or not a repeated pattern will occur is unknown. Also, due to the lack of equipment availability, the air volume flow cannot be verified by the physical model.

5.8   Conclusions

The various results obtained from the CFD model were discussed above and a brief conclusion will be presented here.

The point velocities were obtained as time averaged over a period of 25 seconds of flow time. They were compared to the instantaneous velocities and indicated small differences, generally in the order of 10 %, which indicates the reduced level of the unsteady flow characteristics of the implicit multiphase model. The time-averaged velocities were then plotted for comparison to the physical model results.

The contour plots were used to evaluate the state of the water level, and to identify interesting characteristics. They showed that the water level was in the expected region and was accurately maintained in a level state. The identification of an interesting pressure distribution in the bell mouth was a result of visual inspection of these plots. However it will not be treated further in this study and is left for future research.

The vector plots were used to identify key flow characteristics such as the submerged vortices attached to the side wall as well as the intersecting flow streams at the entrance to the bell mouth. They indicated these characteristics well.

The pathline images obtained from the CFD simulation show the complexity of the flow field as well as identify some of the submerged vortices, which are indicated by the termination of the pathline against the wall or floor.

The animations were used to identify the unsteadiness related to time with regards to the magnitude and direction of velocity vectors in the high activity vortex regions as well as the consistency of the water level.

The various flow monitors were used to determine when the model has reached acceptable convergence as well as the determination of the amount of air entrainment over the flow time simulated. The data from the air entrainment monitor indicates that the model should have been run longer, in order to verify if any cyclic patterns are present. This monitor can be important if the model is used in the determination of the level of critical submergence as after a certain volume of air is ingested, delivery interruptions or installation damage can occur as mentioned in Chapter 2.

The discussion of the various results obtained from the physical and CFD models has been presented individually and the comparison of the two will follow.

6. COMPARISON OF PHYSICAL AND COMPUTATIONAL FLUID DYNAMICS MODEL RESULTS

6.1 Introduction

Chapters 4 and 5 provided an indication of the type of results obtained from each of the models. The core focus of this study is the comparison of the physical and CFD models in an investigation as to the applicability of CFD as a design tool in pump intake design. The various comparisons that are to be made in this section include:

- Point Velocities
- Photographs vs. Vector Plots

6.2 Point Velocities

The comparison of the magnitudes of 51 point velocities was the primary means of quantitative analysis due to equipment limitations. Two of the points could not be measured on the physical model due to the point being in close proximity to the bell mouth and the probe on the ADV was obstructed, however these two points are still shown in the plots of the CFD results. A total of 8 tests scenarios were run for comparison, one of which will be indicated below and all can be seen in summary form in Appendix D.

The test scenario of 150 mm water level and a 4.2 l/s flow rate will be shown in Figures 6.1 to 6.9 below. This scenario was chosen as the main representation due to the water level being near the level of critical submergence for this flow rate, which in relation to prototype scale ratios of 5, 10 and 15 results in low ($V_D \approx 0.9$ m/s), medium ($V_D \approx 1.3$ m/s) and high ($V_D \approx 1.5$ m/s) bell mouth inlet velocities. Additionally, it has a low overall average deviation, which will be described later.

The figures below indicate the point velocities along lines as defined in Table 2 and Figure 4.1, which defines the points in terms of co-ordinates and graphically, respectively.
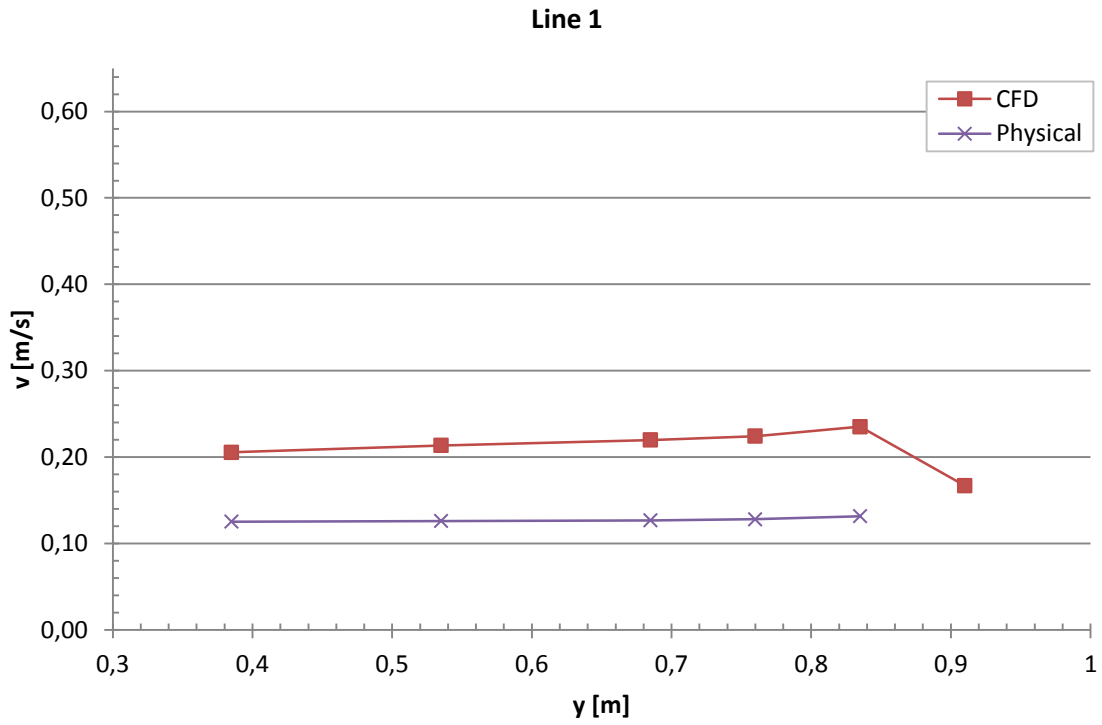
Line 1

Figure 6.1 - Comparison of velocity magnitudes along line 1 (Water Level: 150 mm, Flow Rate: 4.2 l/s)
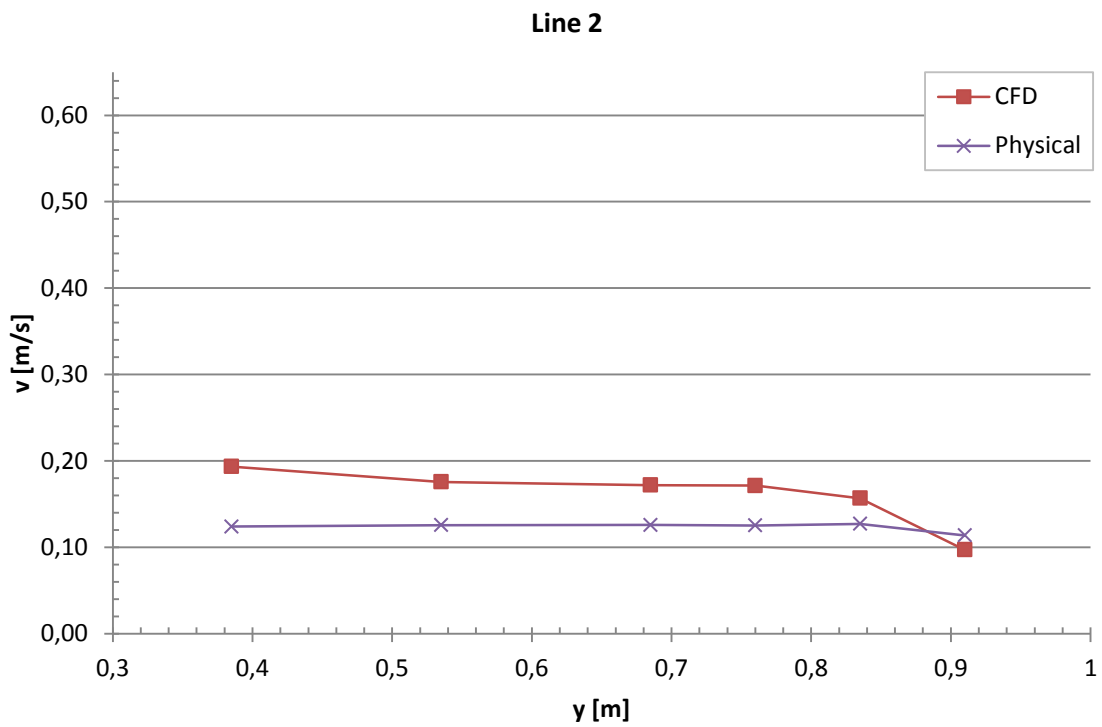
Line 2

Figure 6.2 - Comparison of velocity magnitudes along line 2 (Water Level: 150 mm, Flow Rate: 4.2 l/s)
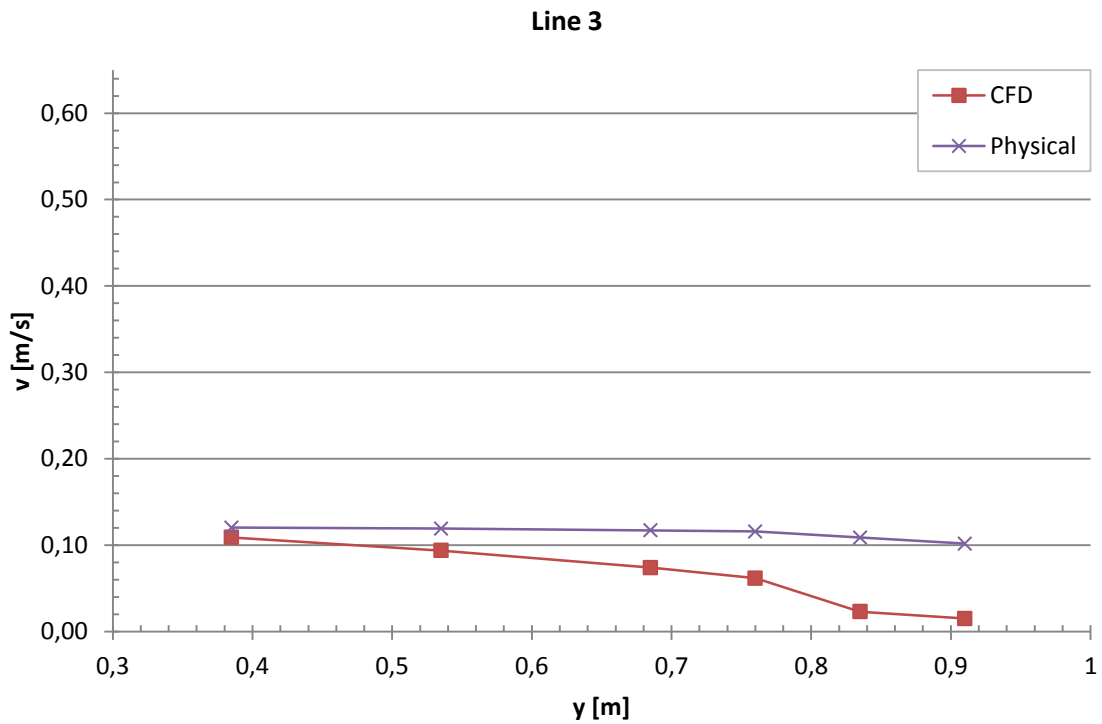
Line 3

Figure 6.3 - Comparison of velocity magnitudes along line 3 (Water Level: 150 mm, Flow Rate: 4.2 l/s)
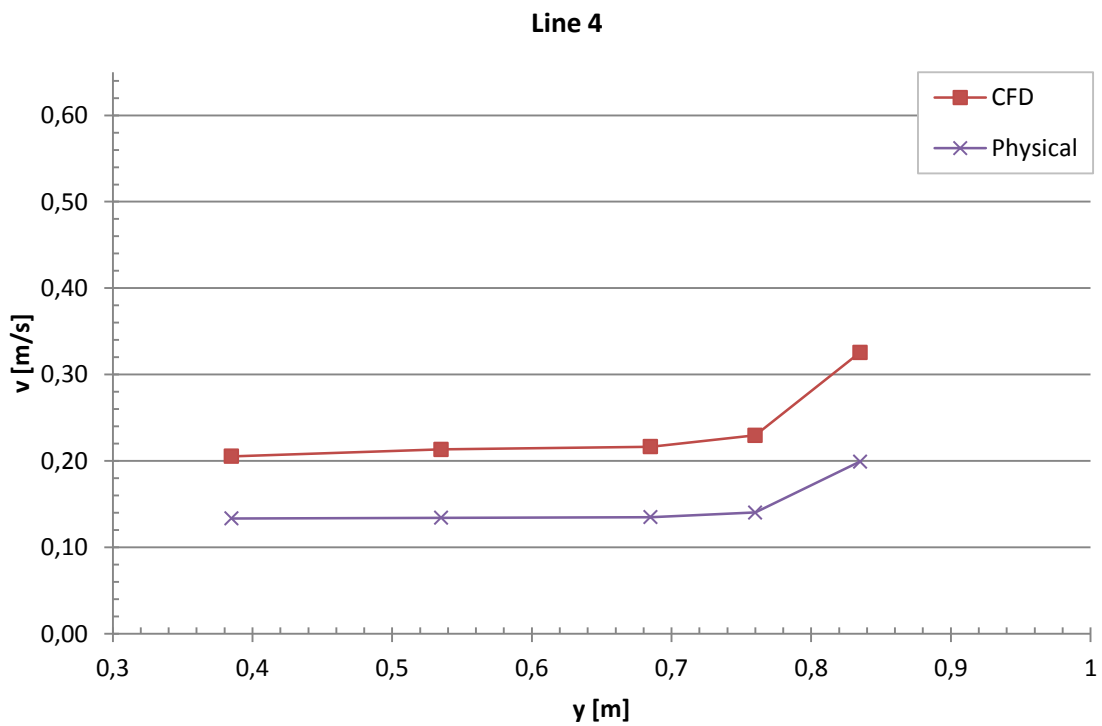
Line 4

Figure 6.4 - Comparison of velocity magnitudes along line 4 (Water Level: 150 mm, Flow Rate: 4.2 l/s)
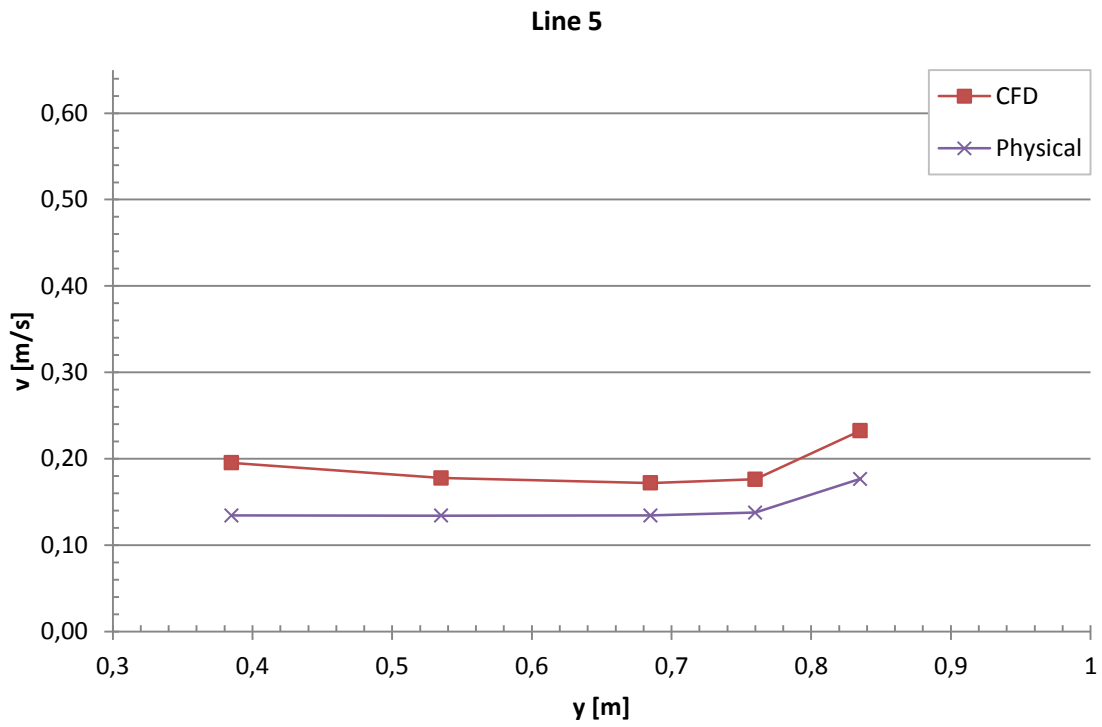
Line 5

Figure 6.5 - Comparison of velocity magnitudes along line 5 (Water Level: 150 mm, Flow Rate: 4.2 l/s)
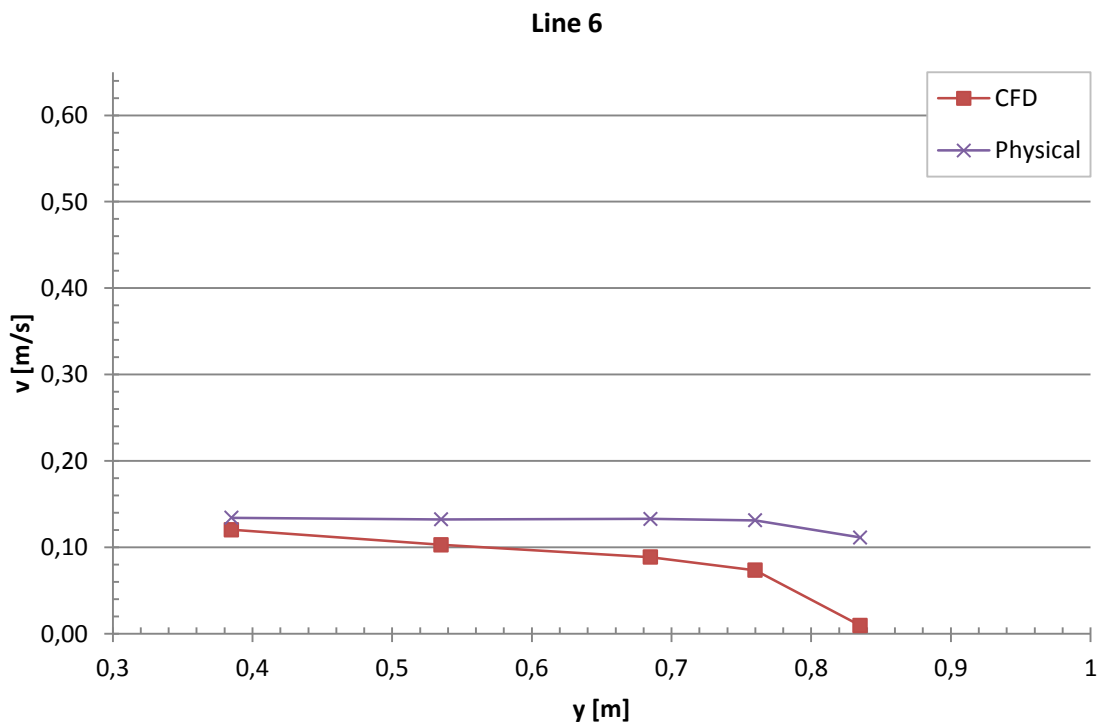
Line 6

Figure 6.6 - Comparison of velocity magnitudes along line 6 (Water Level: 150 mm, Flow Rate: 4.2 l/s)
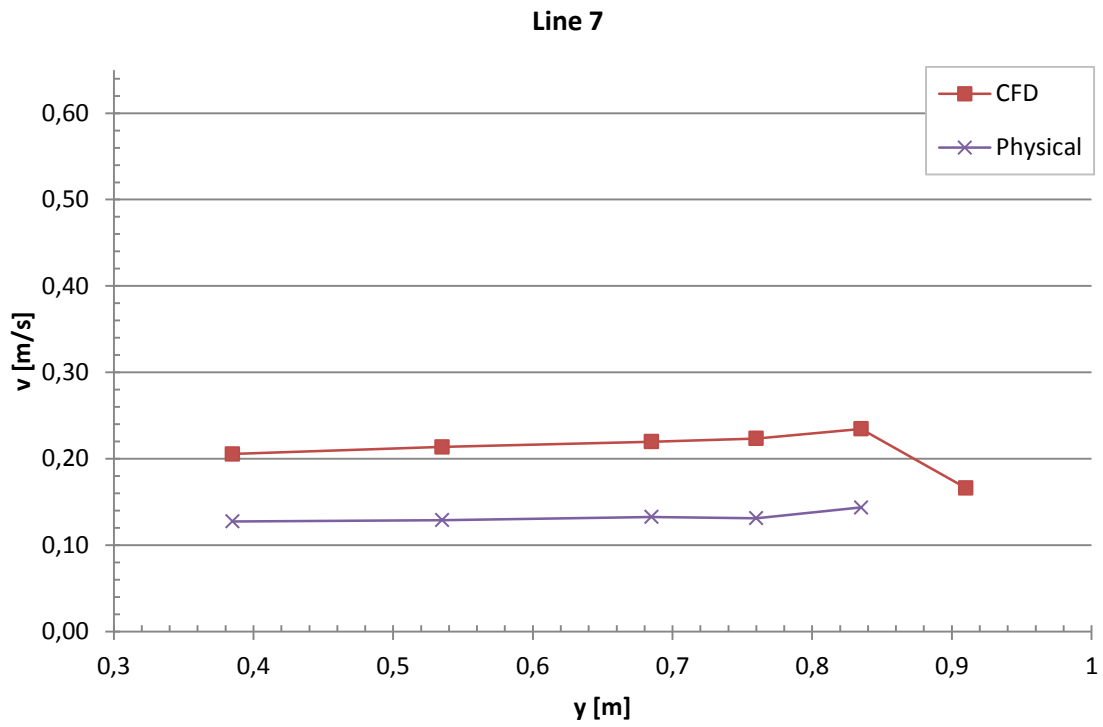
Line 7

Figure 6.7 - Comparison of velocity magnitudes along line 7 (Water Level: 150 mm, Flow Rate: 4.2 l/s)
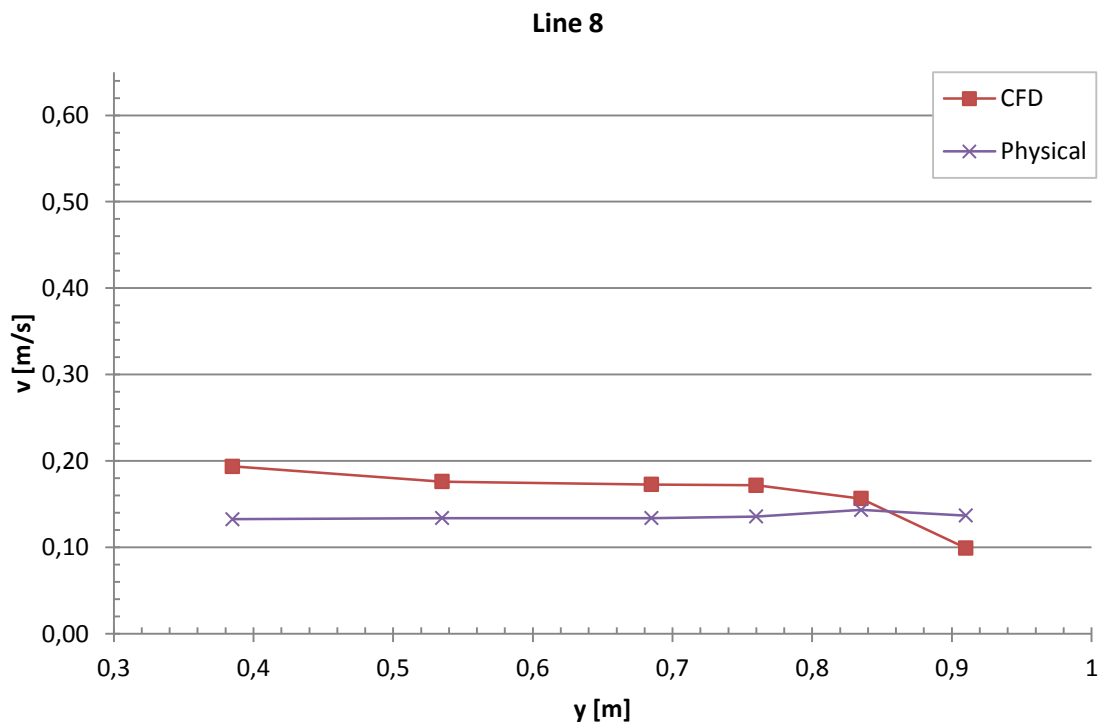
Line 8

Figure 6.8 - Comparison of velocity magnitudes along line 8 (Water Level: 150 mm, Flow Rate: 4.2 l/s)
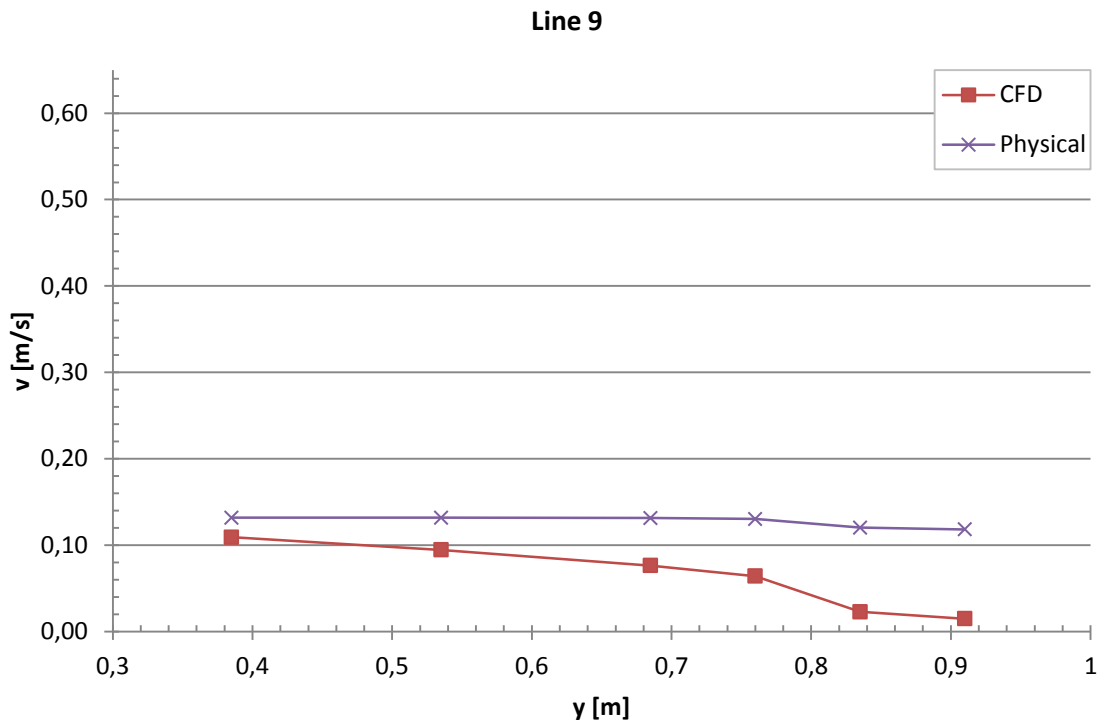
Line 9

Figure 6.9 - Comparison of velocity magnitudes along line 9 (Water Level: 150 mm, Flow Rate: 4.2 l/s)

Inspection of Figures 6.1 to 6.9 above yields the conclusion that the velocity magnitude calculated by the CFD model deviates, sometimes significantly, from what was measured on the physical model, with the above test scenario indicating deviations in both positive and negative directions. The CFD model does exaggerate the trends compared to the physical model, especially in the unsteady, higher velocity regions surrounding the bell mouth.

The CFD model does not always approximate the trend correctly, as can be seen in Figure 6.8 above where the CFD model approximates higher velocities while the physical model indicates a sharp decrease.

In order to compare the quality of the results from the various test scenarios, an indicator value was required. The deviation of the CFD results from the physical model results was used.

The deviation of the individual point velocities (Point Deviation) calculated by the CFD simulation from the point velocities measured by the physical model was calculated in terms of the point velocity magnitudes obtained by the physical model as follows:

$$Point\ Deviation\ (PD)\ [\%] = \left(\frac{V_{CFD} - V_{Physical}}{V_{Physical}}\right) \times 100$$

This gives the deviation of each point, where after the calculated values of all 49 point deviations within one test scenario were averaged to provide an overall indicator, namely the Test Mean Deviation, which is defined as follows:

$$Test\ Mean\ Deviation\ [\%] = \frac{\sum_{i=1}^{49} PD_i}{49}$$

The test mean deviations for each of the scenarios will be presented in Table 10 below, resulting in an overall indicator of the comparison.

Table 10 - Test Mean Deviation for each of the 8 test scenarios

Q [l/s]	Water Level [mm]		
	235	190	150
8.6	54.4	31.8	-
4.2	65.3	-29.1	13.4
2.4	56.9	35.4	5.9

Inspection of Table 10 yields the conclusion that the test mean deviation decreases with a decreasing water level. This increase in accuracy of the CFD model with the decrease in water level could be due to the reduced available area for rotational flows, therewith simplifying the flow field. Alternatively or additionally the location of the measurement points with respect to the shape of the velocity profiles could also result in differences.

Table 10 also shows that for each flow rate, as the water level decreases and the approach flow velocity increases, the test mean deviation decreases indicating an improved approximation of the point velocities.

The test scenario with a water level of 190 mm and a flow rate of 4.2 l/s is the only test scenario that resulted in a negative test mean deviation, indicating that the physical model velocities were on average higher than the CFD model velocities. The graphs for this particular scenario can be seen in Appendix D or on the attached DVD.

6.3   Photographs vs. Vector Plots

The qualitative analysis of the CFD model was carried out by means of comparing vector plots with photographs taken of the flow characteristics in the physical model as well as general observations made while carrying out the physical model tests.

A plot of the velocity vectors from the CFD model for the test scenario of a 235 mm water level and an 8.6 l/s flow rate, as was shown in Figure 3.24, compared well to observations made for the location of the vortex structure. This is a highly unsteady process and the vortices tend to move around continuously, however the location predicted by the CFD model is in the region where majority of the significant vortices develop.

A method to visualize the flow characteristics around the bell mouth was found by using an LED torch with a modified lens to illuminate glass micro balloons in the flow and a camera with a slow shutter speed, as previously mentioned. Three of the photographs taken will be discussed here as they best show the complex and interesting nature of the flow structure surrounding the bell mouth.

Figures 6.10 to 6.12 include photographs of fine tracer particles in the flow, and viewing on the printed media may be difficult, therefore it is advised that the reader consult the electronic media attached to this thesis.

Figure 6.10 provides the comparison of a wall attached vortex, on the right hand side wall (looking downstream from the head box), between the physical and CFD models. The rotation in the CFD model is in the opposite direction in this instance, but it must be kept in mind that the flow in these regions are of a highly unsteady nature, as can be seen in the videos of this same frame which can be seen on the electronic media previously mentioned. The size of the region of rotation is similar and the location fairly accurately predicted. As

mentioned before, the unsteady nature of this region indicates that the vortices are constantly moving.
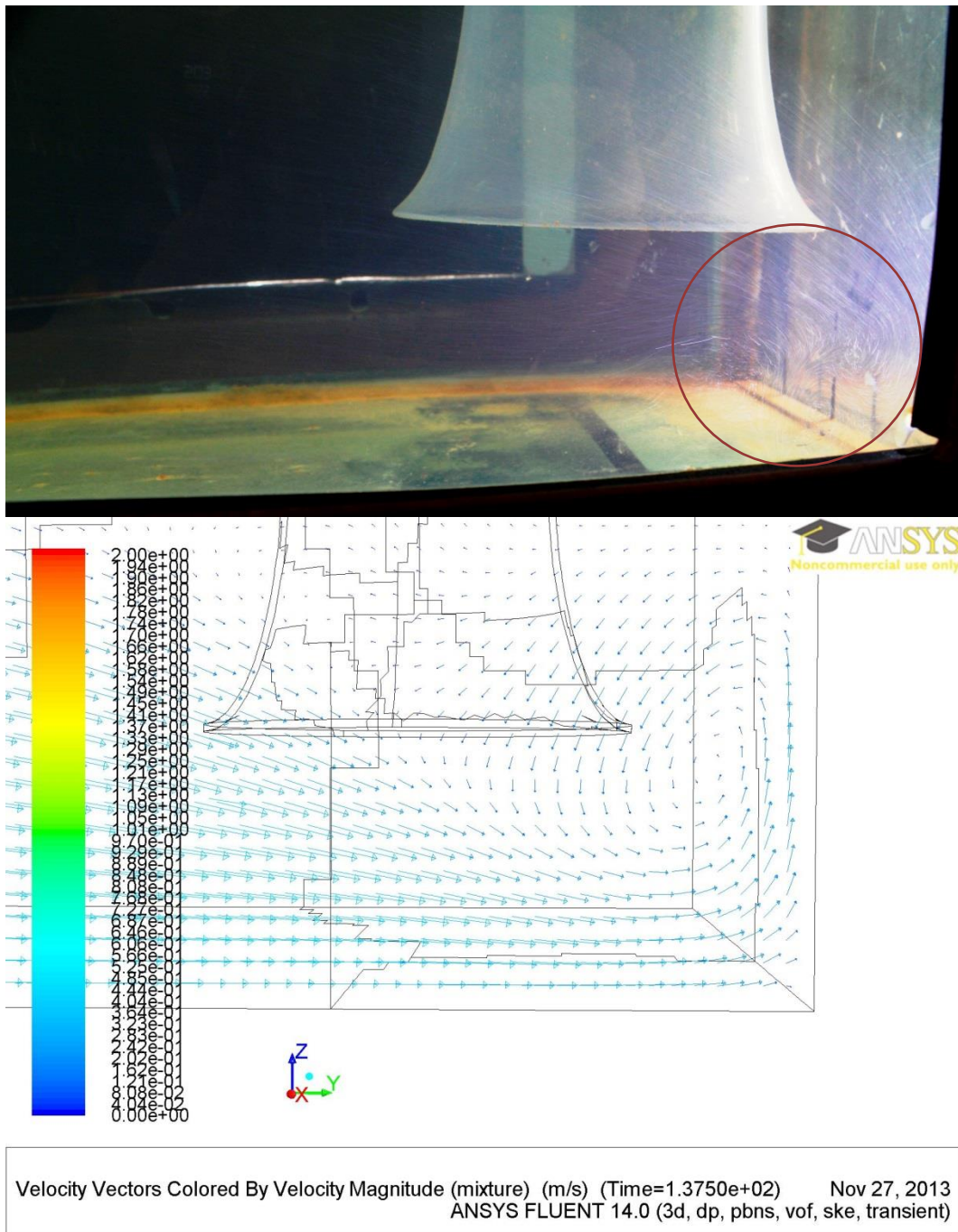
Figure 6.10 - Comparison of side wall vortex (Water Level: 190 mm, Flow Rate: 8.6 l/s)

Figure 6.11 shows the joining of two main flow streams as they enter the bell mouth, which causes a region of high rotational flow. The location of the side wall vortex in Figure 6.10 is

in this region. The CFD model simulates this occurrence in a similar way, and provides more insight as to the details of the flow patterns.
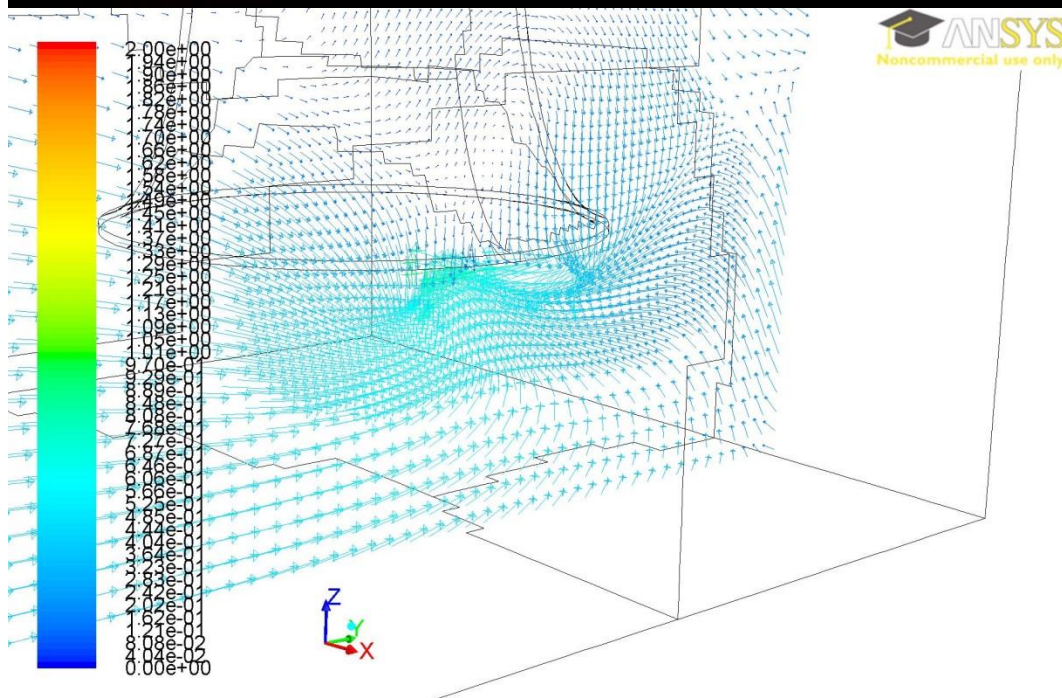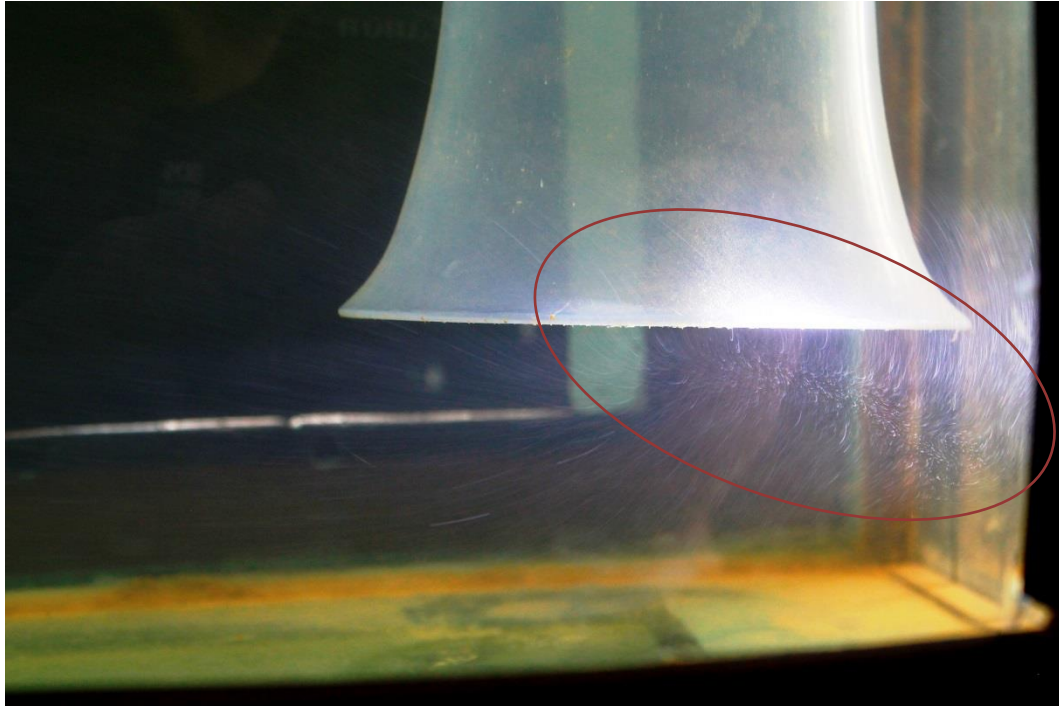
Velocity Vectors Colored By Velocity Magnitude (mixture) (m/s) (Time=1.3750e+02)   Nov 27, 2013
ANSYS FLUENT 14.0 (3d, dp, pbns, vof, ske, transient)

Figure 6.11 - Comparison of joining flow streams (Water Level: 190 mm, Flow Rate: 8.6 l/s)

Similar to Figure 6.10, Figure 6.12 shows the same vortex action on the opposite side wall.
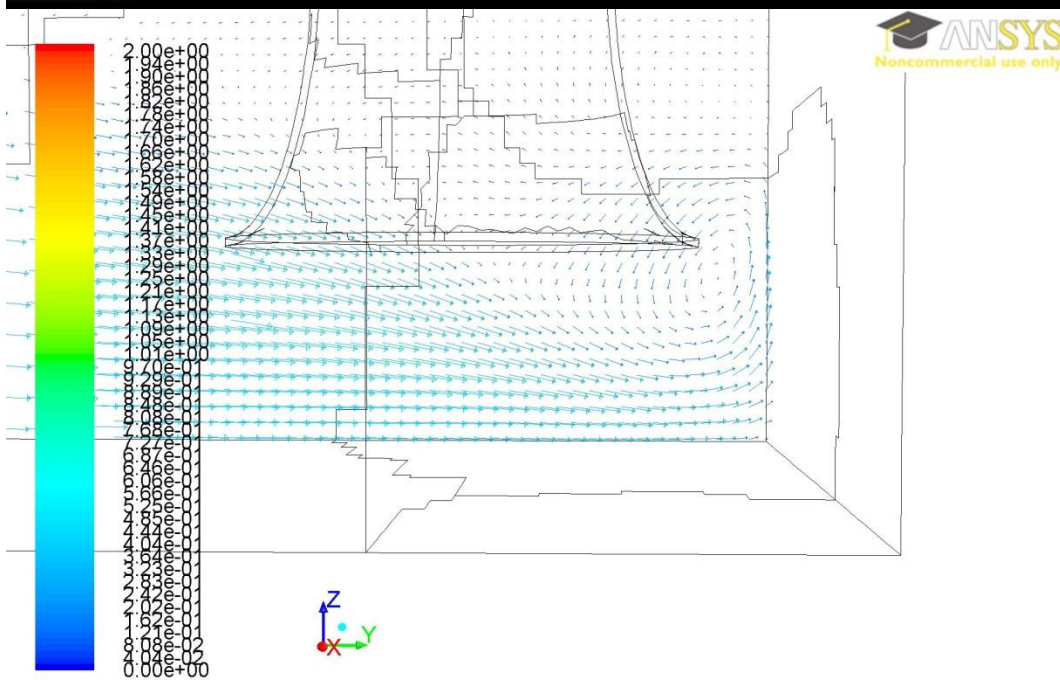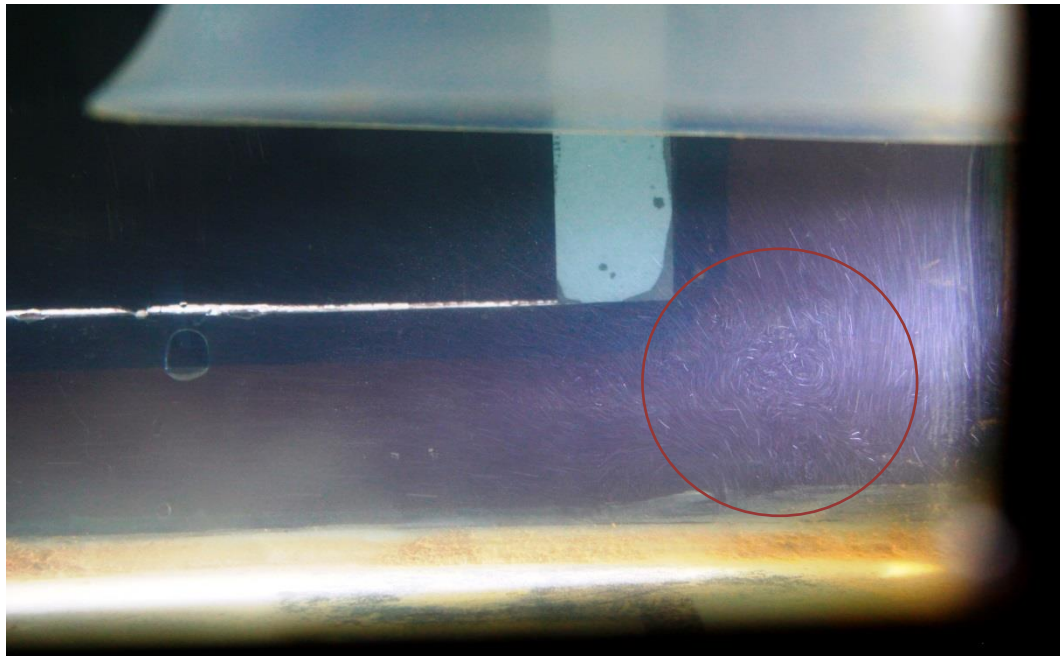
Velocity Vectors Colored By Velocity Magnitude (mixture) (m/s) (Time=1.3750e+02)   Nov 27, 2013
ANSYS FLUENT 14.0 (3d, dp, pbns, vof, ske, transient)

Figure 6.12 - Comparison of side wall vortex on opposite side wall (Water Level: 190 mm, Flow Rate: 8.6 l/s)

6.4   Conclusions

The comparison of the velocity magnitudes along 9 lines was carried out and a single test scenario was shown. The remainder of results from the test scenarios can be seen in summary form in Appendix D or on the attached electronic media. Furthermore the comparison of the general flow conditions in the sump was compared by means of photographs and vector plots. These images can also be seen on the attached electronic media in order to obtain a clearer image.

The quantitative comparison using the point velocity magnitudes indicate that the CFD simulation is still some way from a complete design tool in the configuration tested. That being the transient implicit volume of fluid model solved with the PISO algorithm in ANSYS Fluent 14.0. The 150 mm water level, 4.2 l/s flow rate case shown indicates a low overall average deviation of 13.4 % using the average of all the point velocity deviations. Some instances had overall positive deviations as large as 65.3% and others negative as low as -29.1%.

The test mean deviation indicated that at lower water levels, the CFD approximated the point velocities with higher accuracy. This could be due to the reduced area available for rotational flows and the change in relative location of the point velocities with respect to the variation in the flow profile due to the lower water level.

The qualitative comparison between the photographs or observations and the vector plots from the CFD indicate a good approximation of the flow field. Although the direction and degree of rotation may not be the same, the flow field is well approximated in terms of the type of disturbances or flow characteristics. The joining of the two main flow fields alongside the entrance to the bell mouth can be well visualized.

Overall the CFD model represents the flow field well, although the velocity magnitudes are rather far off in certain cases, sometimes by as much as 100 % for individual points. The conclusion to this thesis will present more thoughts as to the applicability of CFD as a design tool in pump intake design.

7. CONCLUSIONS

The study was carried out to validate a 3 dimensional Computational Fluid Dynamics (CFD) model of a simple pump sump with a vertical outlet pipe, with the use of the CFD model as a design tool to replace or reduce the frequency of hydraulic model studies.

Physical Model

The flow conditions in the physical model were greatly improved with the few simple modifications and the despiked velocity data was of good quality. However the velocity data from the physical model was not validated as the ADV was the only available instrument.

The photographs identified areas of high rotational flow, both on and below the surface with the use of the illuminated glass micro-balloons as flow tracers being invaluable in the identification of the complex flow fields.

Computational Fluid Dynamics Model

The CFD model was solved in the transient state in ANSYS Fluent 14.0 and was run as an implicit multiphase model. The simulation provided a large amount of data, which would not be attainable by hydraulic model studies. The averaged point velocity data, contour and vector plots, pathlines, animations and surface monitors provided detail insight in to the complexity of the flow in the sump. The surface monitor used for the calculation of air entrainment did not converge, however this can be expected due to the time dependant nature of the vortex action. The volumes of air entrainment were within the acceptable limits for safe operation, as stated by Knauss (1987), but the unavailability of an instrument to measure this value on the physical model meant that these results cannot be validated, therefore a suitable means of determining the level of critical submergence by the volume of air entrained is not available in this study. The time-averaged point velocity and the vector plots were then used for comparison to the physical model. Additionally the CFD model provided results relating to the pressure distribution in the bell mouth which could be of interest in future research.

Comparison of the Physical and Computational Fluid Dynamics Model

The averaged point velocity data and photographs vs. vector plots were compared yielding the conclusion that the CFD model simulates the general complexities of the flow field well, the tendencies along the lines plotted in the results were predicted well albeit sometimes exaggerated, but the averaged velocity data showed fluctuating deviations for the various test scenarios run. The vector plots compared well to the photographs in terms of the type of flow characteristics, with the direction or rotation sometimes opposite. The time dependency of the flow characteristics must be kept in mind when judging the comparison due to their unsteady nature.

Can this particular CFD model be used to take the place of hydraulic model studies in the design of pump intakes?

This CFD model as used in this study was not yet able to predict the velocities with an acceptable degree of accuracy and consistency. It could be used for qualitative studies and comparison of designs as qualitatively it models the flow field well.

8. RECOMMENDATIONS

The velocity data obtained from the ADV needs to be validated by means of non-obtrusive velocity measurement techniques, such as Laser Doppler Anemometry, Laser Doppler Velocimetry or Particle Image Velocimetry. Additionally these methods can provide plots very similar to the results obtained from the CFD simulation, allowing an improved comparison. The flow rate should be logged to allow for a complete overview of variation in velocities.

The volume of air entrained in the physical model needs to be measured to allow for accurate validation of the results obtained by the surface monitor in the CFD simulation.

The turbulence on the inflow was estimated to be fairly low and the simulation was run with a turbulence intensity of 10%. Measurement of the flow profiles and turbulence intensity in the physical model for use as input in the CFD model would be ideal, but a sensitivity analysis on the level of turbulence intensity specified on the inlet would be valuable.

The CFD model in this study was run in the implicit multiphase state, which increased stability and resulted in shorter running times. However, it couldn't model the 150 mm water level, 8.6 l/s flow rate scenario accurately. The same model was run in the explicit state and the results indicated significant improvement. Time limitations did not allow for it in this study, but the CFD model should be tested in the transient explicit multiphase state for all scenarios in order to obtain truly unsteady results.

The interesting pressure distributions on the inlet to the bell mouth lead to the views that adding inclination to the bell mouth could decrease the loss factors and potentially reducing the disruptions to the flow. It is recommended that various bell mouth inclinations be tested to verify this. Additionally, the testing of different bell mouth designs, with full roundings or a horizontal disk around the entrance to attempt to reduce the disturbances in the flow in close proximity to the lip of the bell mouth would be of value.

9. BIBLIOGRAPHY

ANSYS, 2013. Information available at www.ansys.com, visited 2013.

Blair, P. and Melvin Cahoon, W. 2006. Best Bell. *Race Engine Technology,* September 2006:34-41.

Constantinescu, G.S and Patel, V.C. 1998. Numerical Model for Simulation of Pump-Intake Flow and Vortices. *Journal of Hydraulic Engineering*. February.

Cooper, P., Heald, C.C., Karassik, I.J., Messina, J.P. 2008. *Pump Handbook (Fourth Edition).* McGraw-Hill, Boston.

Desmukh, T.S., and Gahlot, V.K. 2010. Simulation of Flow Through a Pump Sump and its Validation, in *IJRRAS*, 4(1).

Goring, D.G., and Nikora, V.I. 2002. Despiking Acoustic Doppler Velocimeter Data. *Journal of Hydraulic Engineering.* 117-126.

Hoppe, M.M. 2010. *Validated CFD Model for the Verification of the Applicability of CFD in Determining the Critical Submergence for a Geometrically Simple Sump Intake.* Unpublished dissertation. University of Stellenbosch.

Hundley, K. 2011. *Modelling of a Pump Intake with a Single-Phase CFD Model*. Unpublished master's thesis. University of Stellenbosch.

Kleynhans, S.H. 2012. *Physical Hydraulic Model Investigation of Critical Submergence for Raised Pump Intakes*. Unpublished master's thesis. University of Stellenbosch.

Knauss, J. (ed.). 1987. *Swirling Flow Problems at Intakes.* A.A. Balkema. Rotterdam.

Li, S., Silva, J.M., Lai, Y., Weber, L.J. and Patel, V.C. 2006. *Three-dimensional simulation of flows in practical water-pump intakes*. Journal of Hydroinformatics, 8.2, 111-123.

Lohrmann, A., Cabrera, R. and Kraus, N.C. 1994. Acoustic-doppler Velocimeter (ADV) for Laboratory use, *Fundamentals and advancements in hydraulic measurement and experimentation, Proceedings, Hydraulic Division/ASCE.* 351-365.

Okamura, T., Kamemoto, K. and Matsui, J. 2007. CFD Prediction and Model Experiment on Suction Vortices in Pump Sump, in *The 9th Asian International Conference on Fluid Machinery*. Korea.

Prosser, M.J. 1983. *The hydraulic design of pump sumps and intakes*. Bedford: BHRA Fluid Engineering.

Pump Intake Design. 1998. ANSI/HI 9.8-1998.

Rajendran, V.P., Constantinescu, G.S. and Patel, V.C. 1998. Experiments on Flow in a model Water-Pump Intake Sump To Validate a Numerical Model, in *ASME Fluid Engineering Division Summer Meeting*. Washington.

Rotodynamic pumps – Design of pump intakes – Recommendations for installation of pumps. 2009. PD CEN/TR 13930. January.

Shukla, S.N. and Kshirsagar, J.T. 2008. Numerical Prediction of Air Entrainment in Pump Intakes, in *Proceedings of the Twenty-Fourth International Pump Users Symposium*.

Tokyay, T. and Constantinescu, G. [no date]. *Coherent Structures in Pump-Intake Flows: A Large Eddy Simulation (LES) Study*. University of Iowa.

Versteeg, H.K. and Malalasekera, W. 2007. *An Introduction to Computational Fluid Dynamics, 2nd Edition*. Pearson, Harlow.

Wicklein, E., Sweeney, C., Senon, C., Hattersley, D., Schultz, B. and Naef, R. 2006. Computation Fluid Dynamic Modelling of a Proposed Influent Pump Station, in *WEFTEC .06*. Redmond: ENSR.

APPENDICES

Appendix A – CFD Mesh Settings

Mesh settings used to generate the mesh in ANSYS Meshing.

Defaults	
Physics Preference	CFD
Solver Preference	Fluent
Relevance	54
Sizing	
Use Advanced Size Function	On: Proximity
Relevance Center	Coarse
Smoothing	Medium
Proximity Accuracy	0.5
Num Cells Across Gap	Default (3)
Proximity Size Function Sources	Faces
Proximity Min Size	2.5e-003 m
Max Size	1.e-002 m
Growth Rate	1.0550
Minimum Edge Length	6.e-002 m
Inflation	
Use Automatic Inflation	None
Inflation Option	Smooth Transition
Transition Ratio	0.272
Maximum Layers	5
Growth Rate	1.2
View Advanced Options	No
Assembly Meshing	
Method	CutCell
Feature Capture	Program Controlled
Tessellation Refinement	Program Controlled

Appendix B – Mesh Images

For Water Level 235 mm (Isometric view)
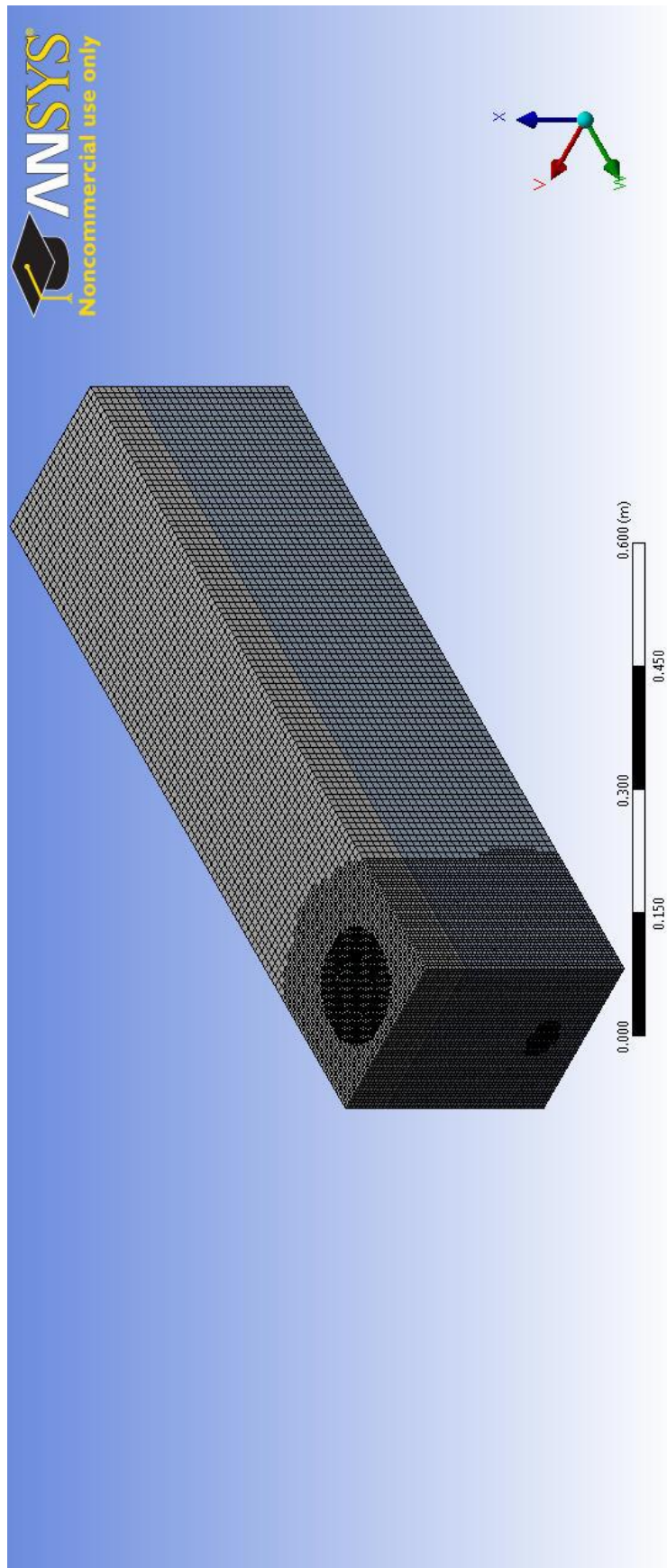
For Water Level 190 mm (Isometric view)
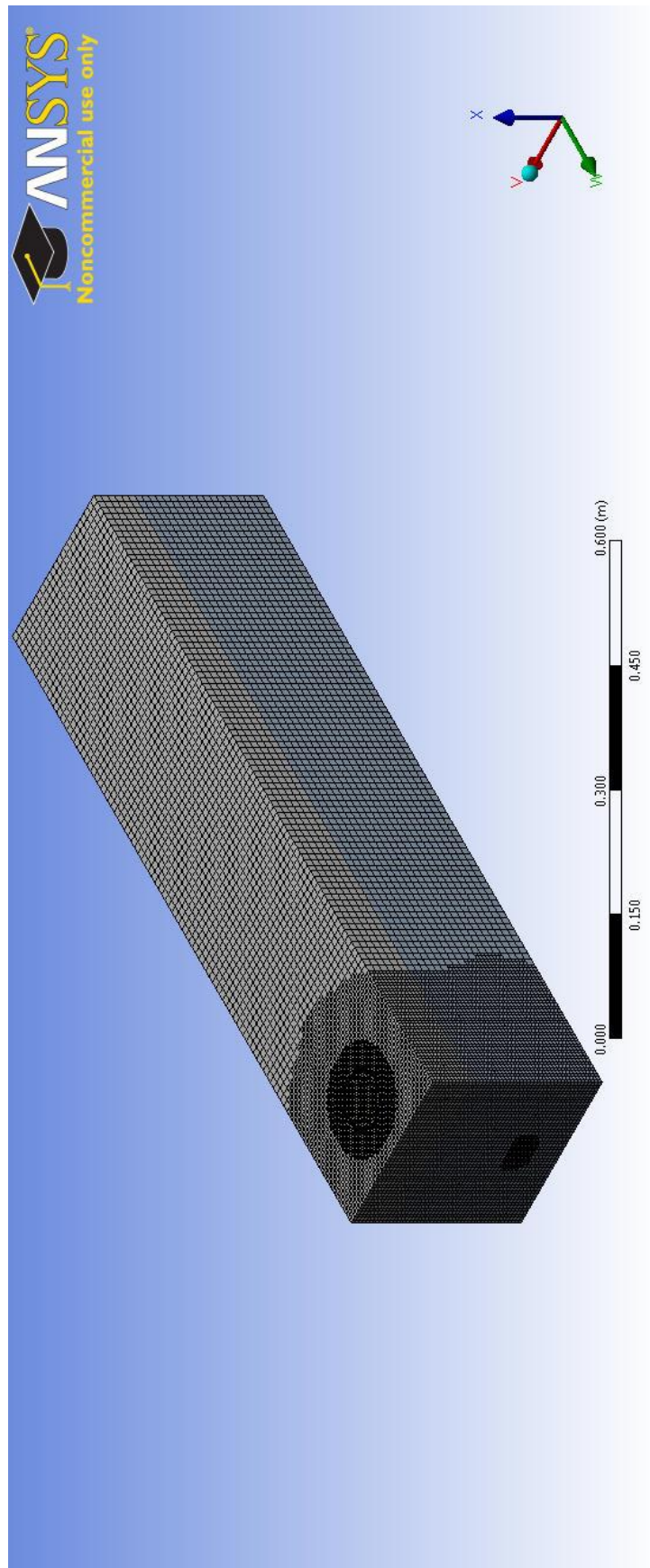
For Water Level 150 mm (Isometric view)
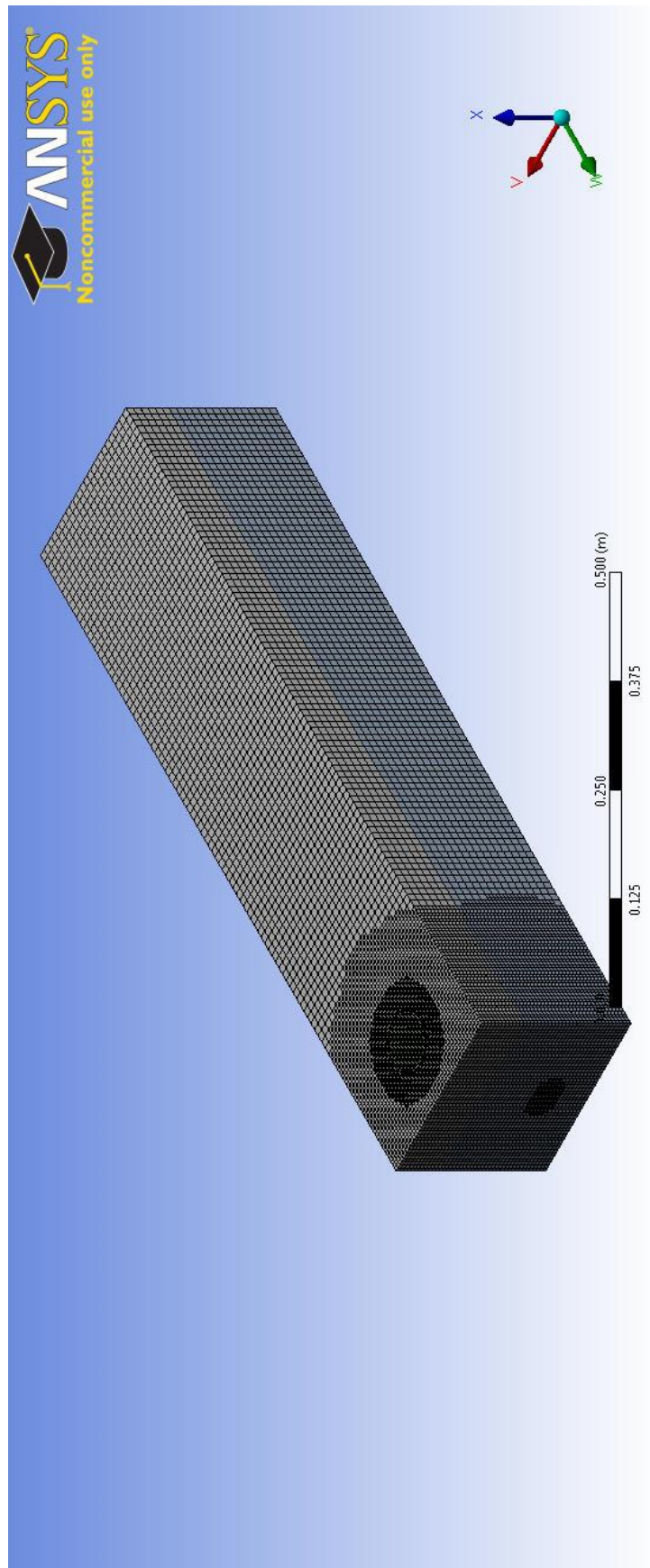
For Water Level 235 mm (Section down centreline)
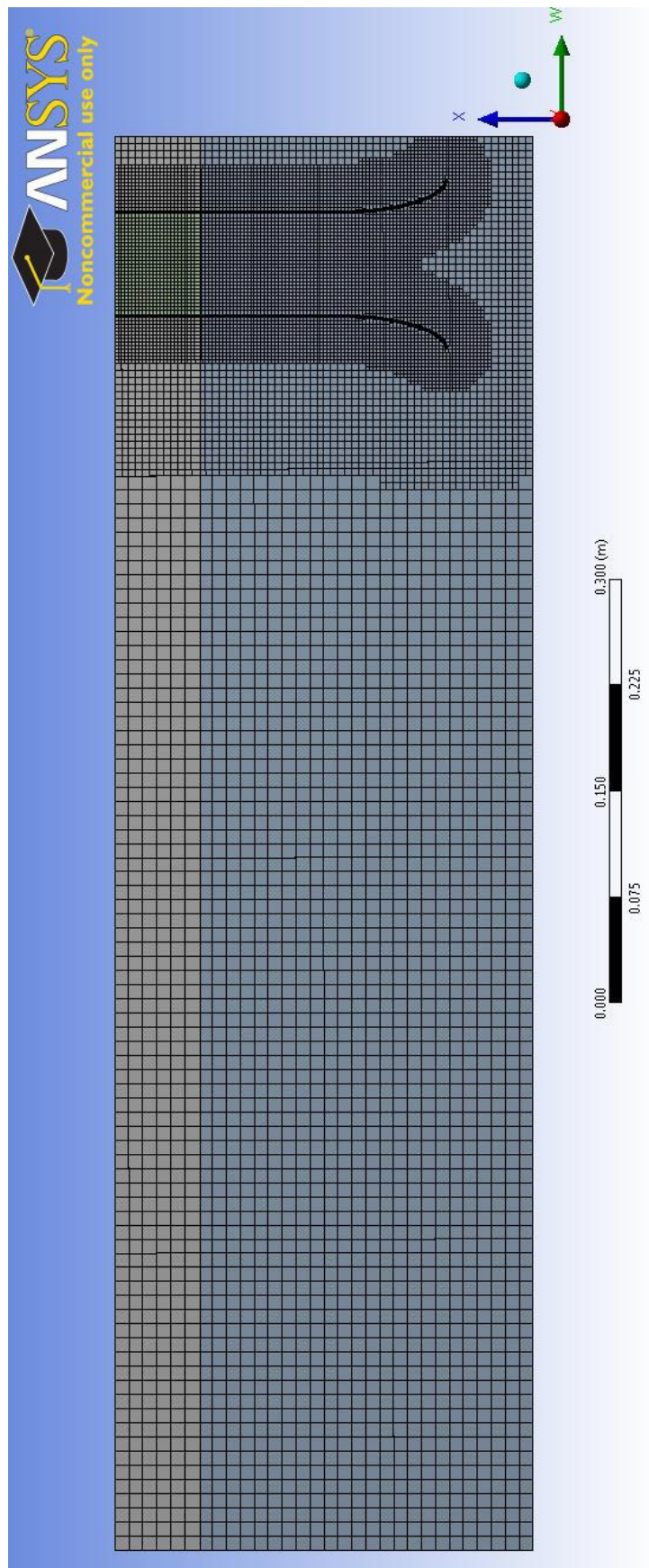
Appendix C – ANSYS Fluent Input Summary

See below summary of input variable as printed from Input Report function in Fluent

FLUENT

Version: 3d, dp, pbns, vof, ske, transient (3d, double precision, pressure-based, VOF, standard k-epsilon, transient)

Release: 14.0.0

Title:

Models

Model	Settings
Space	3D
Time	Unsteady, 2nd-Order Implicit
Viscous	Standard k-epsilon turbulence model
Wall Treatment	Standard Wall Functions
Heat Transfer	Disabled
Solidification and Melting	Disabled
Species	Disabled
Coupled Dispersed Phase	Disabled
NOx Pollutants	Disabled
SOx Pollutants	Disabled
Soot	Disabled
Mercury Pollutants	Disabled

Material Properties

   Material: water-liquid (fluid)

Property	Units	Method	Value(s)
Density	kg/m3	constant	998.2
Cp (Specific Heat)	j/kg-k	constant	4182

Thermal Conductivity   w/m-k   constant 0.6

Viscosity   kg/m-s   constant 0.001003

Molecular Weight   kg/kgmol   constant 18.0152

Thermal Expansion Coefficient 1/k   constant 0

Speed of Sound   m/s   none   #f

Material: air (fluid)

  Property   Units   Method   Value(s)

  Density   kg/m3   constant 1.225

  Cp (Specific Heat)   j/kg-k   constant 1006.43

  Thermal Conductivity   w/m-k   constant 0.0242

  Viscosity   kg/m-s   constant 1.7894e-05

  Molecular Weight   kg/kgmol   constant 28.966

  Thermal Expansion Coefficient 1/k   constant 0

  Speed of Sound   m/s   none   #f

  Material: aluminum (solid)

  Property   Units   Method   Value(s)

  Density   kg/m3   constant 2719

  Cp (Specific Heat)   j/kg-k   constant 871

  Thermal Conductivity w/m-k   constant 202.4

Cell Zone Conditions

  Zones

    name   id   type

    ----

    air   3   fluid

water   4   fluid

Setup Conditions

air

Condition	Value

Material Name	water-liquid
Specify source terms?	no
Source Terms	()
Specify fixed values?	no
Local Coordinate System for Fixed Velocities	no
Fixed Values	()
Frame Motion?	no
Relative To Cell Zone	-1
Reference Frame Rotation Speed (rad/s)	0
Reference Frame X-Velocity Of Zone (m/s)	0
Reference Frame Y-Velocity Of Zone (m/s)	0
Reference Frame Z-Velocity Of Zone (m/s)	0
Reference Frame X-Origin of Rotation-Axis (m)	0
Reference Frame Y-Origin of Rotation-Axis (m)	0
Reference Frame Z-Origin of Rotation-Axis (m)	0
Reference Frame X-Component of Rotation-Axis	0
Reference Frame Y-Component of Rotation-Axis	0
Reference Frame Z-Component of Rotation-Axis	1
Reference Frame User Defined Zone Motion Function	none
Mesh Motion?	no
Relative To Cell Zone	-1
Moving Mesh Rotation Speed (rad/s)	0
Moving Mesh X-Velocity Of Zone (m/s)	0
Moving Mesh Y-Velocity Of Zone (m/s)	0

Moving Mesh Z-Velocity Of Zone (m/s)   0

Moving Mesh X-Origin of Rotation-Axis (m)   0

Moving Mesh Y-Origin of Rotation-Axis (m)   0

Moving Mesh Z-Origin of Rotation-Axis (m)   0

Moving Mesh X-Component of Rotation-Axis   0

Moving Mesh Y-Component of Rotation-Axis   0

Moving Mesh Z-Component of Rotation-Axis   1

Moving Mesh User Defined Zone Motion Function   none

Deactivated Thread   no

LES zone?   no

Laminar zone?   no

Set Turbulent Viscosity to zero within laminar zone?   yes

Embedded Subgrid-Scale Model   0

Momentum Spatial Discretization   0

Cwale   0.325

Cs   0.1

Porous zone?   no

Porosity   1

Interfacial Area Density (1/m)   1

Heat Transfer Coefficient (w/m2-k)   1

water

   Condition   Value

   Material Name   water-liquid

   Specify source terms?   no

   Source Terms   ()

   Specify fixed values?   no

   Local Coordinate System for Fixed Velocities   no

   Fixed Values   ()

   Frame Motion?   no

Relative To Cell Zone   -1

Reference Frame Rotation Speed (rad/s)   0

Reference Frame X-Velocity Of Zone (m/s)   0

Reference Frame Y-Velocity Of Zone (m/s)   0

Reference Frame Z-Velocity Of Zone (m/s)   0

Reference Frame X-Origin of Rotation-Axis (m)   0

Reference Frame Y-Origin of Rotation-Axis (m)   0

Reference Frame Z-Origin of Rotation-Axis (m)   0

Reference Frame X-Component of Rotation-Axis   0

Reference Frame Y-Component of Rotation-Axis   0

Reference Frame Z-Component of Rotation-Axis   1

Reference Frame User Defined Zone Motion Function   none

Mesh Motion?   no

Relative To Cell Zone   -1

Moving Mesh Rotation Speed (rad/s)   0

Moving Mesh X-Velocity Of Zone (m/s)   0

Moving Mesh Y-Velocity Of Zone (m/s)   0

Moving Mesh Z-Velocity Of Zone (m/s)   0

Moving Mesh X-Origin of Rotation-Axis (m)   0

Moving Mesh Y-Origin of Rotation-Axis (m)   0

Moving Mesh Z-Origin of Rotation-Axis (m)   0

Moving Mesh X-Component of Rotation-Axis   0

Moving Mesh Y-Component of Rotation-Axis   0

Moving Mesh Z-Component of Rotation-Axis   1

Moving Mesh User Defined Zone Motion Function   none

Deactivated Thread   no

LES zone?   no

Laminar zone?   no

Set Turbulent Viscosity to zero within laminar zone?   yes

Embedded Subgrid-Scale Model   0

Momentum Spatial Discretization   0

Cwale   0.325

Cs   0.1

Porous zone?   no

Porosity   1

Interfacial Area Density (1/m)   1

Heat Transfer Coefficient (w/m2-k)   1

Boundary Conditions

  Zones

    name   id   type

    ----

    airinlet   7   outlet-vent

    wall-air   8   wall

    wall-water   9   wall

    inlet   10   velocity-inlet

    pressureoutlet 11   pressure-outlet

    wall-air.1   12   wall

    wall-water.1   15   wall

  Setup Conditions

    airinlet

      Condition   Value

      Gauge Pressure (pascal)   0

      Backflow Direction Specification Method   1

      Coordinate System   0

      X-Component of Flow Direction   1

      Y-Component of Flow Direction   0

Z-Component of Flow Direction   0

X-Component of Axis Direction   1

Y-Component of Axis Direction   0

Z-Component of Axis Direction   0

X-Coordinate of Axis Origin (m)   0

Y-Coordinate of Axis Origin (m)   0

Z-Coordinate of Axis Origin (m)   0

Turbulent Specification Method   3

Backflow Turbulent Kinetic Energy (m2/s2)   1

Backflow Turbulent Dissipation Rate (m2/s3)   1

Backflow Turbulent Intensity (%)   0.99999998

Backflow Turbulent Length Scale (m)   1

Backflow Hydraulic Diameter (m)   0.2

Backflow Turbulent Viscosity Ratio   10

is zone used in mixing-plane model?   no

Radial Equilibrium Pressure Distribution   no

Loss Coefficient   ((polynomial normal-velocity 0))

wall-air

Condition   Value

Enable shell conduction?   no

Wall Motion   0

Shear Boundary Condition   0

Define wall motion relative to adjacent cell zone?   yes

Apply a rotational velocity to this wall?   no

Velocity Magnitude (m/s)   0

X-Component of Wall Translation   1

Y-Component of Wall Translation   0

Z-Component of Wall Translation   0

Define wall velocity components?   no

X-Component of Wall Translation (m/s)   0

Y-Component of Wall Translation (m/s)   0

Z-Component of Wall Translation (m/s)   0

Wall Roughness Height (m)   0

Wall Roughness Constant   0.5

Rotation Speed (rad/s)   0

X-Position of Rotation-Axis Origin (m)   0

Y-Position of Rotation-Axis Origin (m)   0

Z-Position of Rotation-Axis Origin (m)   0

X-Component of Rotation-Axis Direction   0

Y-Component of Rotation-Axis Direction   0

Z-Component of Rotation-Axis Direction   1

X-component of shear stress (pascal)   0

Y-component of shear stress (pascal)   0

Z-component of shear stress (pascal)   0

Fslip constant   0

Eslip constant   0

Specularity Coefficient   0

wall-water

Condition   Value

Enable shell conduction?   no

Wall Motion   0

Shear Boundary Condition   0

Define wall motion relative to adjacent cell zone?   yes

Apply a rotational velocity to this wall?   no

Velocity Magnitude (m/s)   0

X-Component of Wall Translation   1

Y-Component of Wall Translation   0

Z-Component of Wall Translation   0

Define wall velocity components?   no

X-Component of Wall Translation (m/s)   0

Y-Component of Wall Translation (m/s)   0

Z-Component of Wall Translation (m/s)   0

Wall Roughness Height (m)   0

Wall Roughness Constant   0.5

Rotation Speed (rad/s)   0

X-Position of Rotation-Axis Origin (m)   0

Y-Position of Rotation-Axis Origin (m)   0

Z-Position of Rotation-Axis Origin (m)   0

X-Component of Rotation-Axis Direction   0

Y-Component of Rotation-Axis Direction   0

Z-Component of Rotation-Axis Direction   1

X-component of shear stress (pascal)   0

Y-component of shear stress (pascal)   0

Z-component of shear stress (pascal)   0

Fslip constant   0

Eslip constant   0

Specularity Coefficient   0

inlet

Condition   Value

Velocity Specification Method   2

Reference Frame   0

Velocity Magnitude (m/s)   0.1525

Supersonic/Initial Gauge Pressure (pascal)   0

Coordinate System   0

X-Velocity (m/s)   0

Y-Velocity (m/s)   0

Z-Velocity (m/s)   0

X-Component of Flow Direction   1

Y-Component of Flow Direction   0

Z-Component of Flow Direction   0

X-Component of Axis Direction   1

Y-Component of Axis Direction   0

Z-Component of Axis Direction   0

X-Coordinate of Axis Origin (m)   0

Y-Coordinate of Axis Origin (m)   0

Z-Coordinate of Axis Origin (m)   0

Angular velocity (rad/s)   0

Turbulent Specification Method   3

Turbulent Kinetic Energy (m2/s2)   1

Turbulent Dissipation Rate (m2/s3)   1

Turbulent Intensity (%)   9.9999998

Turbulent Length Scale (m)   1

Hydraulic Diameter (m)   0.16

Turbulent Viscosity Ratio   10

is zone used in mixing-plane model?   no

pressureoutlet

Condition   Value

Gauge Pressure (pascal)   -3468

Backflow Direction Specification Method   1

Coordinate System   0

X-Component of Flow Direction   1

Y-Component of Flow Direction   0

Z-Component of Flow Direction   0

X-Component of Axis Direction   1

Y-Component of Axis Direction   0

Z-Component of Axis Direction   0

X-Coordinate of Axis Origin (m)   0

Y-Coordinate of Axis Origin (m)   0

Z-Coordinate of Axis Origin (m)   0

Turbulent Specification Method   3

Backflow Turbulent Kinetic Energy (m2/s2)   1

Backflow Turbulent Dissipation Rate (m2/s3)   1

Backflow Turbulent Intensity (%)   9.9999998

Backflow Turbulent Length Scale (m)   1

Backflow Hydraulic Diameter (m)   0.072

Backflow Turbulent Viscosity Ratio   10

is zone used in mixing-plane model?   no

Radial Equilibrium Pressure Distribution   no

wall-air.1

Condition   Value

Enable shell conduction?   no

Wall Motion   0

Shear Boundary Condition   0

Define wall motion relative to adjacent cell zone?   yes

Apply a rotational velocity to this wall?   no

Velocity Magnitude (m/s)   0

X-Component of Wall Translation   1

Y-Component of Wall Translation   0

Z-Component of Wall Translation   0

Define wall velocity components?   no

X-Component of Wall Translation (m/s)   0

Y-Component of Wall Translation (m/s)   0

Z-Component of Wall Translation (m/s)   0

Wall Roughness Height (m)   0

Wall Roughness Constant   0.5

Rotation Speed (rad/s)   0

X-Position of Rotation-Axis Origin (m)   0

Y-Position of Rotation-Axis Origin (m)   0

Z-Position of Rotation-Axis Origin (m)   0

X-Component of Rotation-Axis Direction   0

Y-Component of Rotation-Axis Direction   0

Z-Component of Rotation-Axis Direction   1

X-component of shear stress (pascal)   0

Y-component of shear stress (pascal)   0

Z-component of shear stress (pascal)   0

Fslip constant   0

Eslip constant   0

Specularity Coefficient   0

wall-water.1

Condition   Value

Enable shell conduction?   no

Wall Motion   0

Shear Boundary Condition   0

Define wall motion relative to adjacent cell zone?   yes

Apply a rotational velocity to this wall?   no

Velocity Magnitude (m/s)   0

X-Component of Wall Translation   1

Y-Component of Wall Translation   0

Z-Component of Wall Translation   0

Define wall velocity components?   no

X-Component of Wall Translation (m/s)   0

Y-Component of Wall Translation (m/s)   0

Z-Component of Wall Translation (m/s)   0

Wall Roughness Height (m)   0

Wall Roughness Constant   0.5

Rotation Speed (rad/s)   0

X-Position of Rotation-Axis Origin (m)   0

Y-Position of Rotation-Axis Origin (m)   0

Z-Position of Rotation-Axis Origin (m)   0

X-Component of Rotation-Axis Direction   0

Y-Component of Rotation-Axis Direction   0

Z-Component of Rotation-Axis Direction   1

X-component of shear stress (pascal)   0

Y-component of shear stress (pascal)   0

Z-component of shear stress (pascal)   0

Fslip constant   0

Eslip constant   0

Specularity Coefficient   0

Solver Settings

  Equations

   Equation   Solved

   Flow   yes

   Volume Fraction   yes

   Turbulence   yes

  Numerics

Numeric   Enabled

Absolute Velocity Formulation   yes

Unsteady Calculation Parameters

Time Step (s)   0.025

Max. Iterations Per Time Step   20

Relaxation

Variable   Relaxation Factor

Pressure   0.3

Density   0.80000001

Body Forces   0.80000001

Momentum   0.7

Volume Fraction   0.44999999

Turbulent Kinetic Energy   0.8

Turbulent Dissipation Rate   0.8

Turbulent Viscosity   0.80000001

Linear Solver

                Solver   Termination Residual Reduction

Variable   Type   Criterion   Tolerance

Pressure   V-Cycle   0.1

X-Momentum   Flexible 0.1   0.7

Y-Momentum   Flexible 0.1   0.7

Z-Momentum   Flexible 0.1   0.7

Volume Fraction   Flexible 0.1   0.7

Turbulent Kinetic Energy   Flexible 0.1   0.7

Turbulent Dissipation Rate Flexible 0.1   0.7

Pressure-Velocity Coupling

```
Parameter              Value

---------------------------------

Type                   PISO

Skewness-Neighbour Coupling   yes

Skewness Correction        1

Neighbour Correction       1
```

Discretization Scheme

```
Variable               Scheme

-----------------------------------------------

Pressure               Body Force Weighted

Momentum               Second Order Upwind

Volume Fraction        Second Order Upwind

Turbulent Kinetic Energy    Second Order Upwind

Turbulent Dissipation Rate   Second Order Upwind
```

Solution Limits

```
Quantity               Limit

--------------------------------------

Minimum Absolute Pressure      1

Maximum Absolute Pressure      5e+10

Minimum Temperature        1

Maximum Temperature        5000

Minimum Turb. Kinetic Energy    1e-14

Minimum Turb. Dissipation Rate   1e-20

Maximum Turb. Viscosity Ratio    100000
```
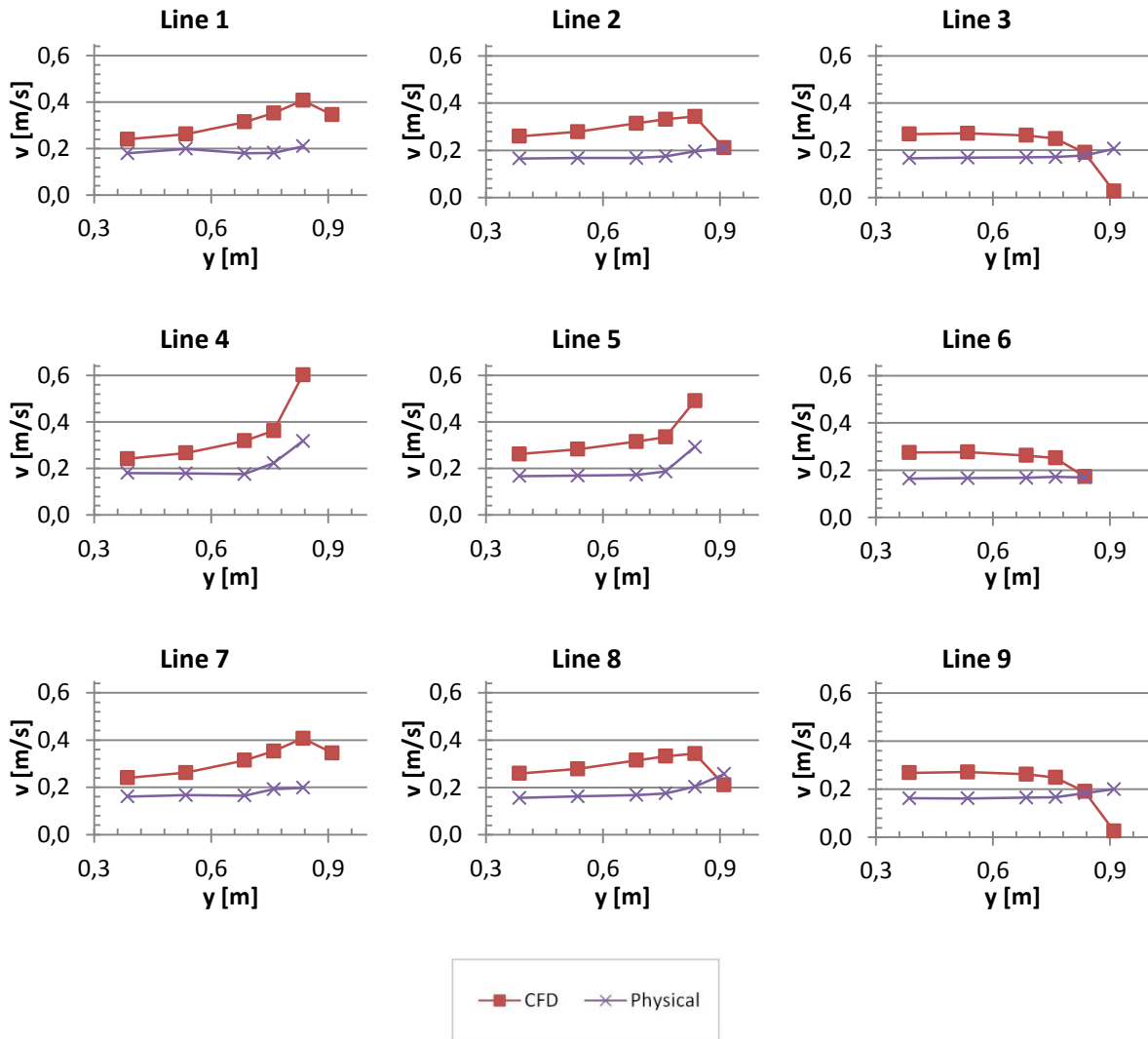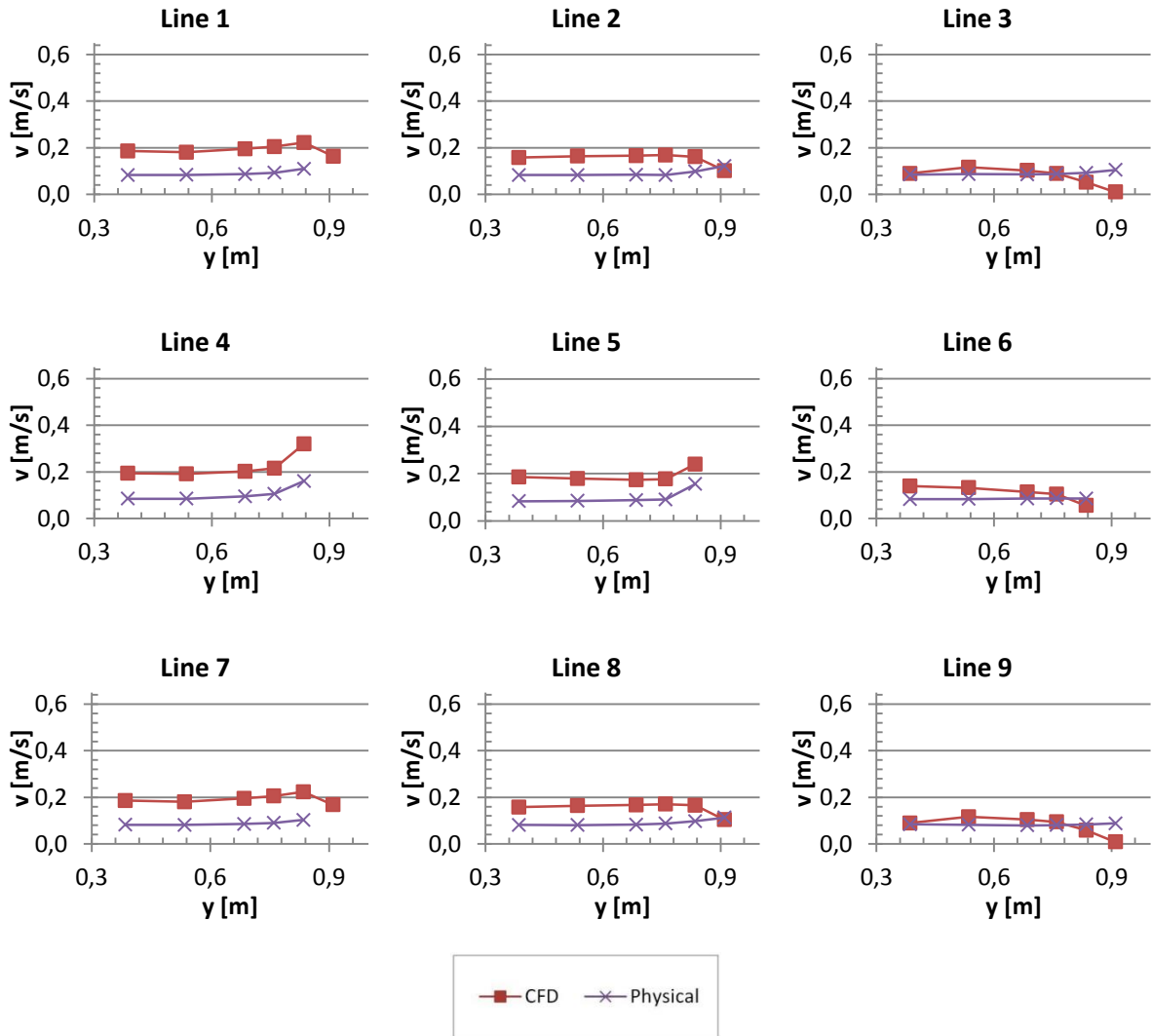
Appendix D – Comparison Graphs of Velocity Magnitude

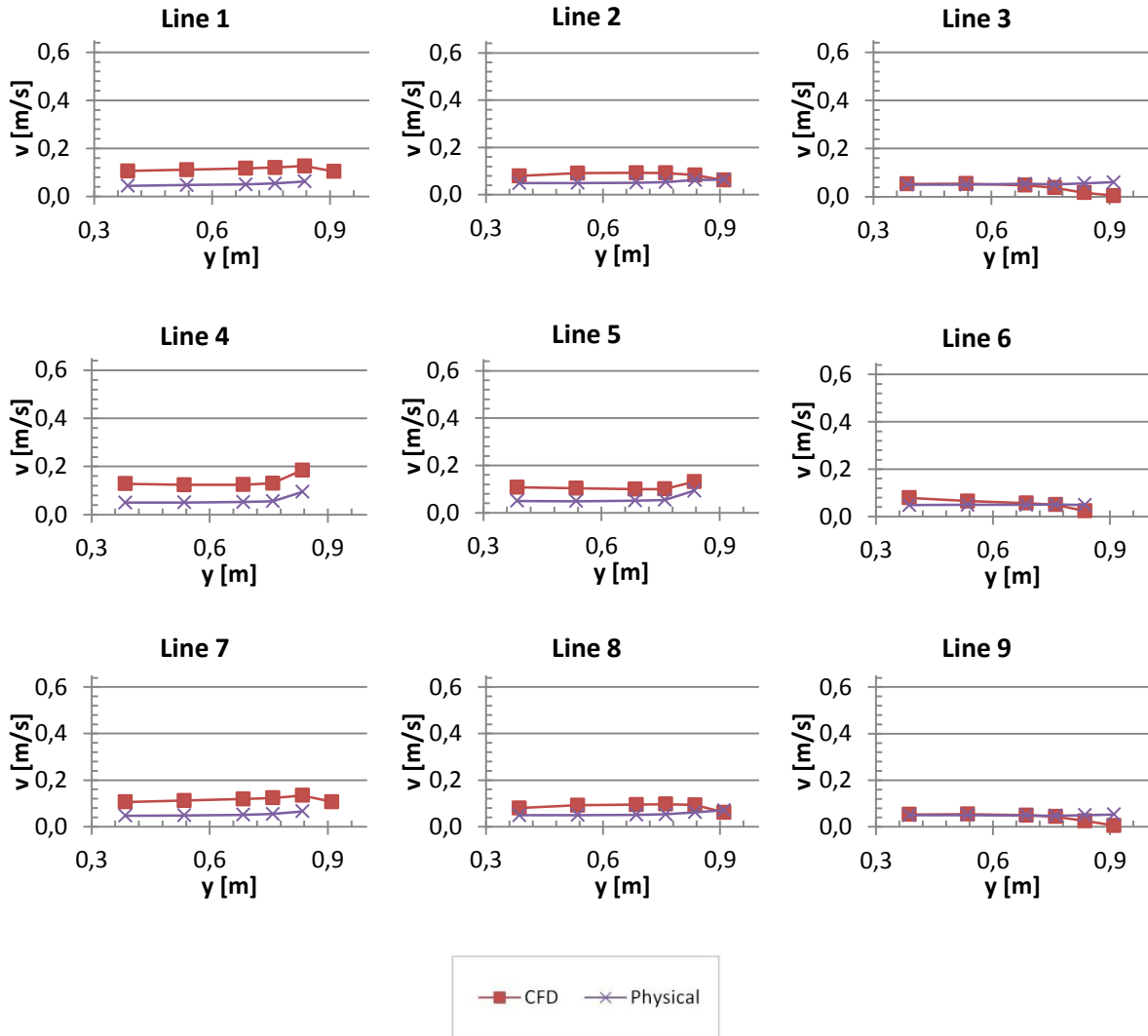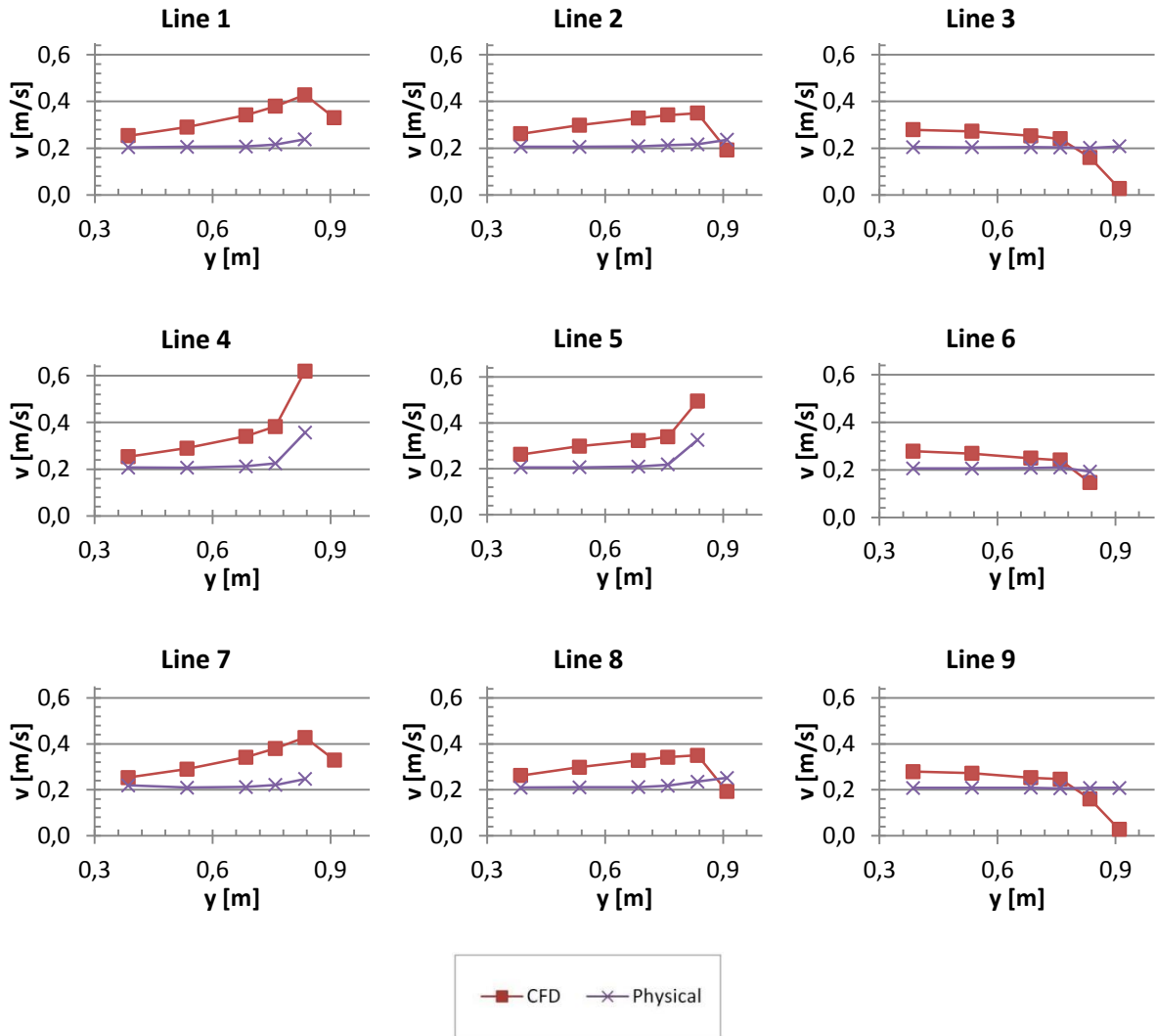CFD vs. Physical Velocity Magnitude along Lines as Specified in Figure 4.1
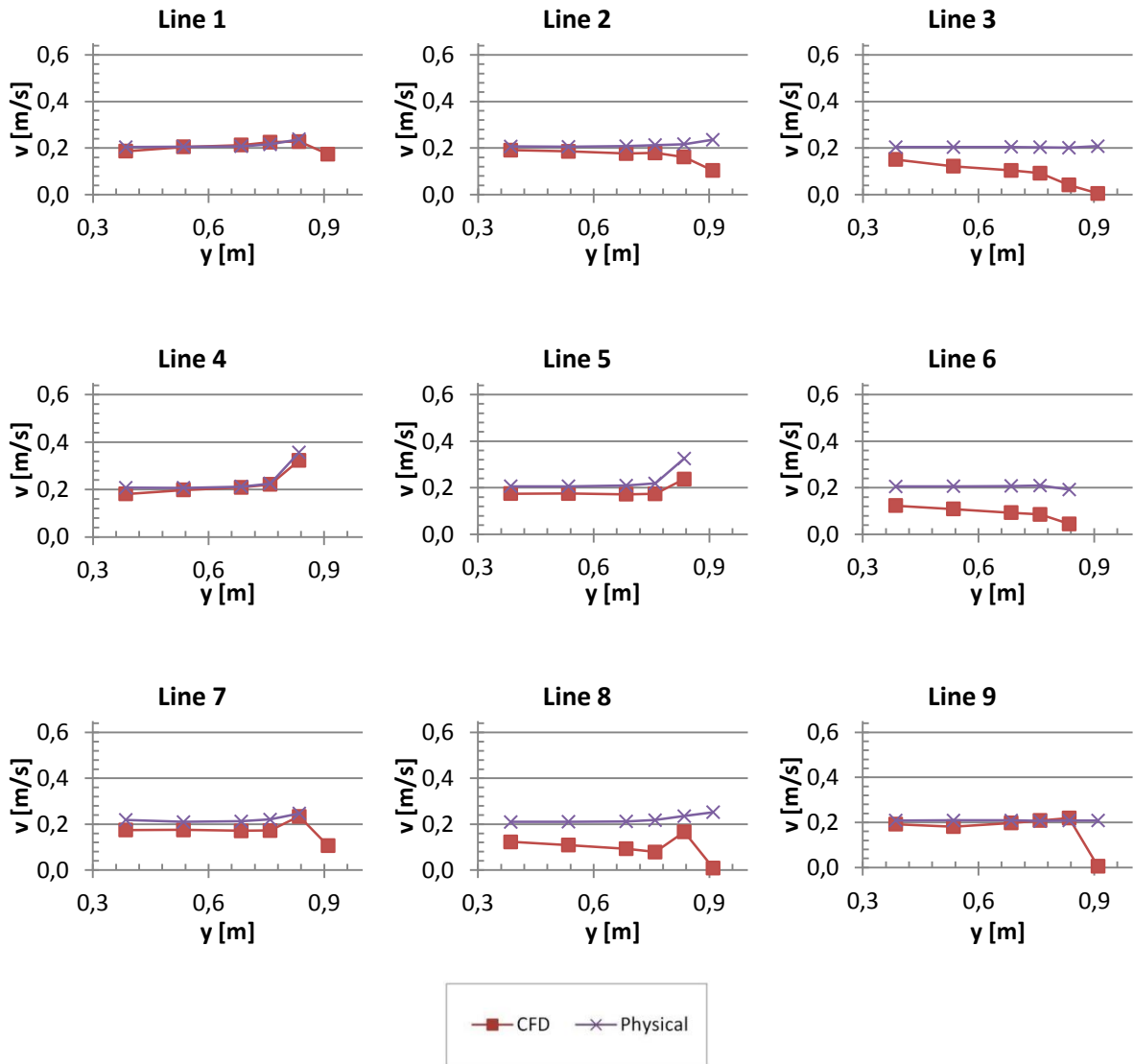
235 mm - 8.6 l/s

235 mm – 4.2 l/s

Line 1

Line 2

Line 3

Line 4

Line 5

Line 6

Line 7

Line 8

Line 9

CFD   Physical

235 mm – 2.4 l/s

Line 1

Line 2

Line 3

Line 4

Line 5

Line 6

Line 7
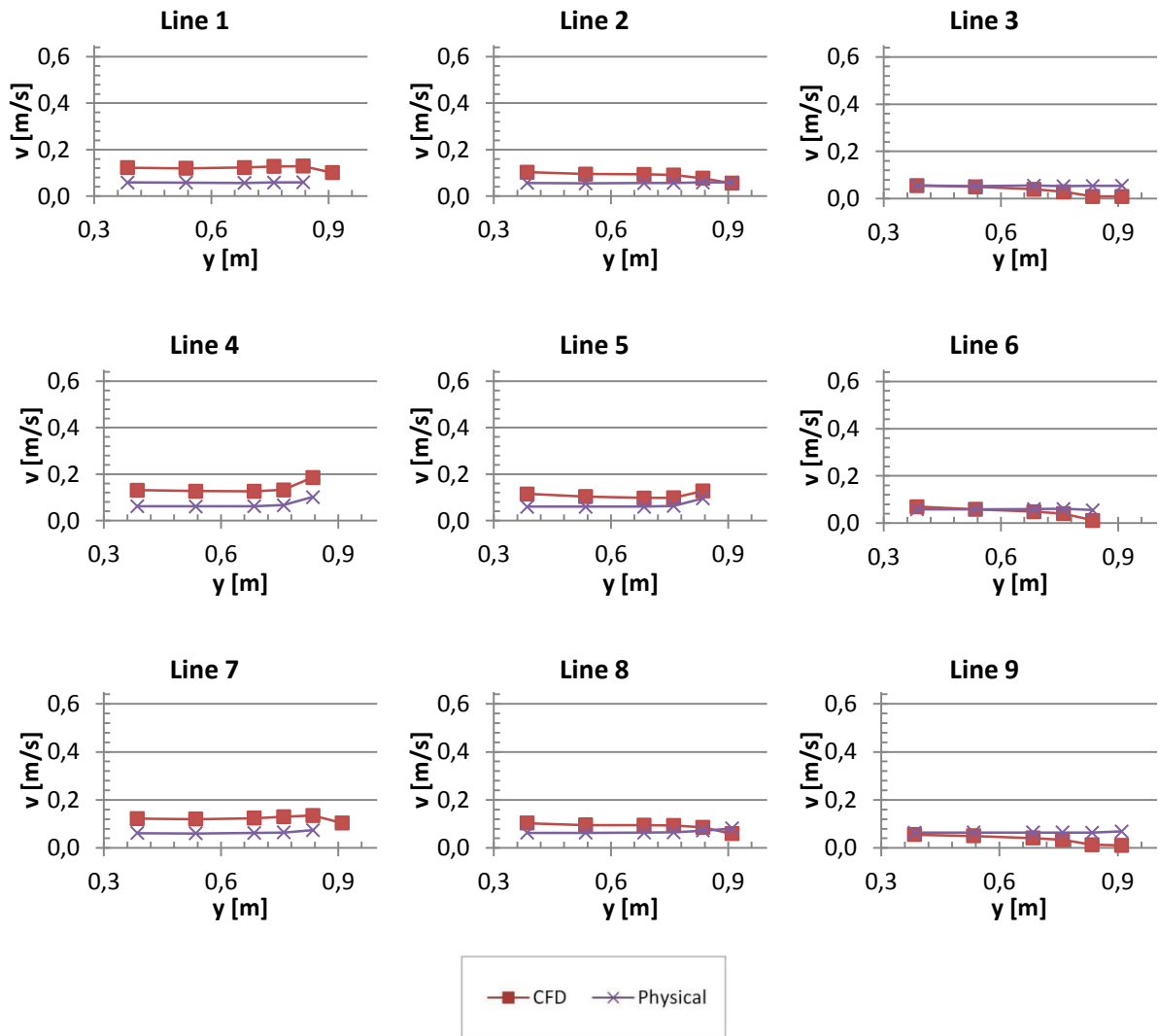

Line 8

Line 9
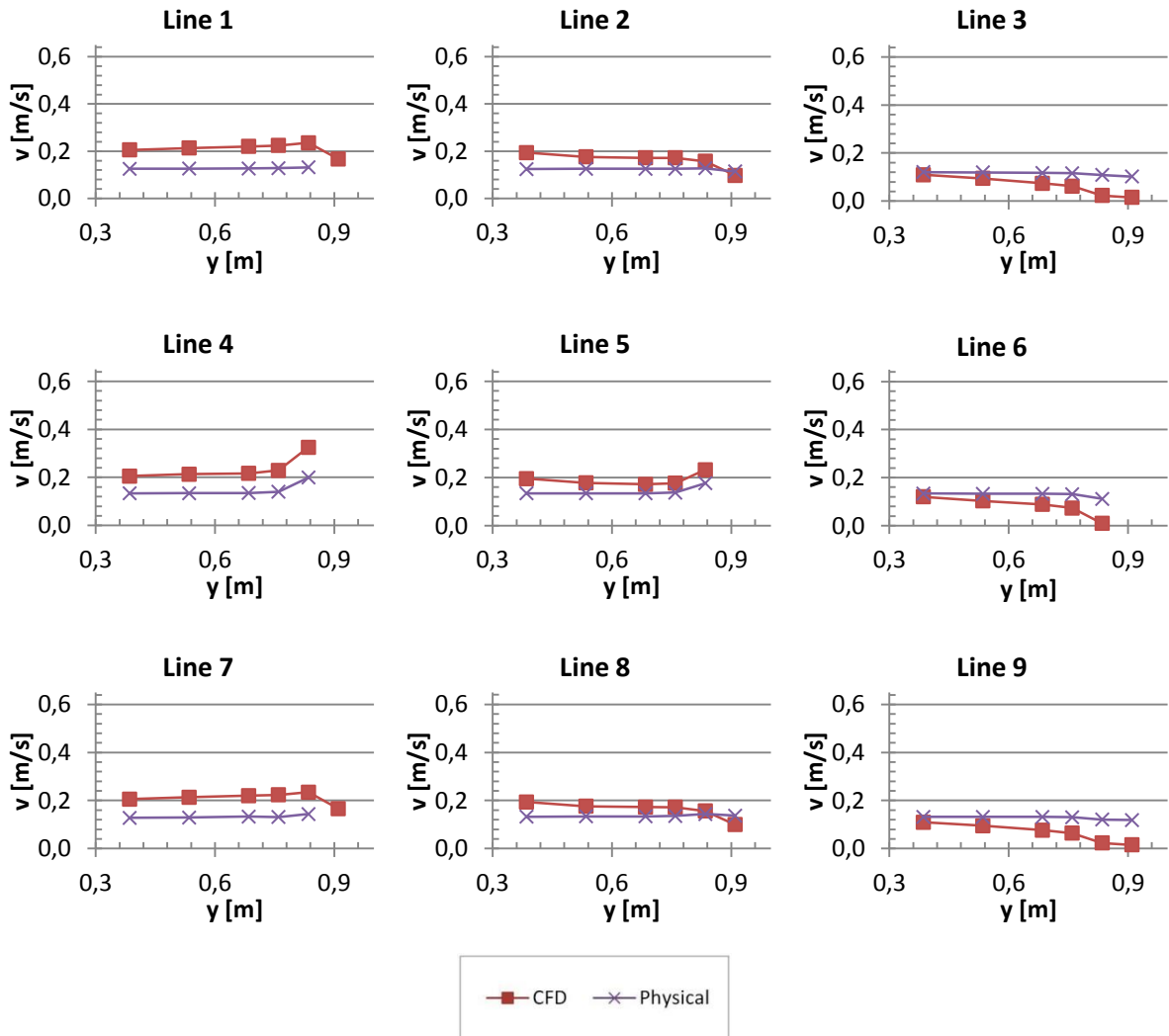

CFD   Physical

190 mm – 8.6 l/s

190 mm - 4.2 l/s

190 mm – 2.4 l/s

150 mm – 4.2 l/s

150 mm – 2.4 l/s

Line 1

Line 2

Line 3

Line 4

Line 5

Line 6

Line 7

Line 8

Line 9

CFD   Physical